CEDR

Conférence Européenne des Directeurs des Routes

Conference of European Directors of Roads

Pavement LCM

Report on durability data analysis

Deliverable D4.1

June 2021

University of Nottingham UK | CHINA | MALAYSIA

vti

VILNIAUS GEDIMINO TECHNIKOS UNIVERSITETAS SAPERE AUDE

Project Nr. 128556

Project acronym: PavementLCM

Project title:

Life Cycle Management of Green Asphalt Mixtures and Road Pavements

Deliverable D4.1 – Report on durability data analysis

Start date of project: 01.10.2018

End date of project: 30.06.2021

Author(s) of this deliverable:

Björn Kalman, VTI, Sweden

Abubeker Ahmed, VTI, Sweden

Jiqing Zhu, VTI, Sweden

Luis Neves, UNOT, UK

Mohammad Shafiqur Rahman, VTI, Sweden

Olle Eriksson, VTI, Sweden

Rita Kleizienė, VGTU, Lithuania

Tony Parry, UNOT, UK

CONTACTS

Björn Kalman *bjorn.kalman@vti.se*

Davide Lo Presti *davide.lopresti@unipa.it* *davide.lopresti@nottingham.ac.uk* *(coordination)*

Executive summary

The goal with this deliverable is to provide an assessment of the expected lifetimes for existing surface courses and for new, and potentially greener, mixes.

The durability assessments are based on lab test results, accelerated load tests, lifetime expectancies of reference materials in different countries and the spectra of distress modes limiting the service life in different countries. In the weighted assessment, the latter parts, the lifetime expectancies, and typical distress modes for different countries were gathered through a questionnaire directed to local experts.

The underlying assumption in using lab test results and accelerated load tests results to estimate the lifetime of a surface mix are that there are correlations between the lab tests and the field performance. If such correlations have been proven in the past, it is not certain that such a correspondence will be valid for new materials.

Each part in the weighted assessment brings its own uncertainty into the total uncertainty in the estimate. In the durability assessments for the new mix the judgment from one local expert, or in some case the judgments of two local experts, have been used for each country. If several experts' opinions are available Bayesian inference theory can be used to account for the combined uncertainty. An example of how Bayesian inference theory can be used to calculate uncertainty in the lifetime distributions when combining estimates from different sources and experts is given in Chapter 3.3 and an Excel spreadsheet template for doing such an analysis is provided separately.

The assessments of the expected lifetimes will thus be encumbered with uncertainty that is difficult to evaluate. However, the more informed an assessment is the better it is assumed to be. A field study of the new mixes on many different road sections will give the ultimate answer how the lifetime distributions differ from the lifetime distributions of the regular road surfacings.

In the literature review of durability for the reference mixes there were marked differences between the estimated service lives for different countries and between different sources for the same type of surface course. Service life based on historical data should not be disputed numbers. In Chapter 3.2 we provide an example how service life distributions could be modelled using a Weibull distribution with increasing failure rate with time. Historical survival data has two types of events and each event has an event time. An event is a case if the time for end of life is observed. If rather the time at end of study is observed the subject is still alive, the event is known as censoring. Censored observations contain partial information about the survival time even though end of live is not observed. Survival analysis methods properly take care of both the complete information in the cases and the partial information in the censored observations. Analytical expressions for the service lives opens the possibility to take into account the uncertainty in the lifetimes in the LCA.

The laboratory studies included tests for ageing of loose mix in an oven at 86 °C for one and two weeks; binder recovery and analysis of softening point and shear modulus; water sensitivity using a moisture induced stress test protocol; cyclic indirect stiffness modulus test; shear modulus test. The accelerated load test used a circular road simulator and both unaged and aged mixes were tested in the ALT using both elevated temperatures and freeze-thaw cycles with water sprayed on the surface to cover different types of climate conditions.

To summarize the outcome of the experimental studies the new mixes were classified as performing better or worse than the reference mix in each study using a scale with five levels from - - to ++ where - - and - indicates much worse and worse performance

compared to the reference mix respectively. = indicates equal performance to the reference mix and + and ++ indicates better or much better performance. The compilations are presented in the tables below.

Relative performance of new SMA mixes compared to the reference SMA16 mix. The relative performance is indicated with - -, -, =, +, ++ where - - and - indicates much worse and worse, = indicates equal performance and + and ++ indicates better or much better performance.

	Test	SMA11 10%RA	SMA11 40%RA	SMA8 60% RA
Climate	Water sensitivity/MIST	=	=	=
Ageing	Short and long term oven ageing	+ +	+ +	- -
Traffic	ALT / CRS	= ravelling = rutting = cracking = friction	= ravelling - rutting = cracking = friction	= ravelling - rutting = cracking = friction
Traffic/aging	ALT / CRS aged material	= ravelling = rutting + cracking = friction	= ravelling = rutting + cracking = friction	= ravelling = rutting - cracking = friction
Traffic/climate	ALT / CRS Water sensitivity and freeze-thaw cycles	=	=	- aged material
Traffic	Stiffness modulus / road structure performance	+	=	-
Traffic	Shear modulus / rutting	+ +	=	+

Relative performance of new PA mixes compared to the reference PA16 mix (ZOAB+). The relative performance is indicated with - -, -, =, +, ++ where - - and - indicates much worse and worse, = indicates equal performance and + and ++ indicates better or much better performance.

	Test	Fibra 1 / PA8	Fibra 3 / PA8 panacea	Fibra 4 / PA8 aramid
Climate	Water sensitivity/MIST	=	=	=
Ageing	Short and long term oven ageing	=	- -	- -
Traffic	ALT / CRS	+ ravelling + rutting + cracking + friction	= ravelling = rutting = cracking + friction	= ravelling = rutting = cracking + friction
Traffic/aging	ALT / CRS aged material	- - ravelling + rutting = cracking + friction	- - ravelling + rutting = cracking + friction	- - ravelling + rutting = cracking + friction
Traffic/climate	ALT / CRS Water sensitivity and freeze-thaw cycles	=	=	=
Traffic	Stiffness modulus / road structure performance	-	=	=
Traffic	Shear modulus / rutting	/	+	+

The questionnaire survey among experts revealed that they agree that the service life of a surface course with will only change approximately by 10% (5-15 %) if the traffic volume deceases by 25% for a high-volume road. This has the implication that one should interpret any accelerated load test with care since there is only a weak correlation between the number of loadings in the field and the service life of a surface course in general. Other factors such as climate and ageing have a considerable impact on the service life as well.

The questionnaire provided both the typical distress modes for different road surface mixes in their country and the average lifetime to be expected for the reference mixes in the country. The spectra of typical distress modes triggering resurfacing for SMA and porous asphalt in different countries is shown in the tables below:

Distresses likely to trigger resurfacing of high-volume roads with for SMA16 (or SMA11, or SMA11 10%RA). ++ indicates that the distress is likely cause for resurfacing operations. + indicates that the distress is somewhat likely cause for resurfacing operations.

	Denmark	Sweden 1	Sweden 2	Germany	Norway	Lithuania
Answers valid for NMAS	11	16	16	11	16	11
Fretting	++	++			+	++
Ravelling	+	++			+	++
Rutting	+	++	++		++	
Road wear		++			+	
Low friction	+			++		++
Cracking (not specified)		+		++		++
Transverse cracking						
Longitudinal cracking		+			+	++
Edge cracking					+	+
Block cracking						+
Alligator cracking		+				+
Other						+

Distresses likely to trigger resurfacing of high-volume roads with PA16 (or PA11). ++ indicates that the distress is likely cause for resurfacing operations. + indicates that the distress is somewhat likely cause for resurfacing operations.

	Sweden 1	Sweden 2	Netherlands	Germany
Answers valid for NMAS	16	16	16	11
Fretting	++			
Ravelling	++		++	++
Rutting		++		
Road wear	++	++		
Low friction				
Cracking (not specified)				
Transverse cracking				
Longitudinal cracking				
Edge cracking				
Block cracking				
Alligator cracking				
Other			+	

Estimated average lifetimes in years for SMA mixes on high-volume roads in years. The average lifetime for the reference SMA16 was the stated lifetime in the survey.

Country\Mix	SMA16 (reference)	SMA11 10% RA	SMA11 40% RA	SMA8 60% RA
Denmark	14	15	14	12
Sweden & Norway	9	10	9	8
Germany & Lithuania	15	16	15	13

Estimated lifetimes for PA mixes on high-volume roads in years.

Country\Mix	PA16 (ZOAB+) (reference)	PA8 (Fibra 1)	PA8 panacea (Fibra 3)	PA8 aramid (Fibra 4)
Sweden, Netherlands and Germany	12*	11	10	10

***)** There is a considerable difference in the experience of the average lifetime for a PA16 in the questionnaire. 12 years was used as a reasonable estimate for the lifetime for the reference.

For future research projects we suggest that a thorough analysis of historical survival data in each country is done. This analysis could both be used as means in itself to have analytical expressions of the survival distributions and as a starting point for analyzing the causes for the variations.

List of Tables

List of Figures

Abbreviations

ALT – Accelerated load test

CEDR – Conference of European Directors of Roads

CRS – Circular Road Simulator

MPD – Mean Profile Depth

MPH – Mean Profile Height (defined in an analogues way as MPD but taking the average maximum depth instead average maximum height of the profile)

PA - Porous Asphalt

PMB - Polymer Modified Bitumen

RA – Reclaimed Asphalt

SMA - Stone Mastic Asphalt

Table of content

1 Introduction

National Road Authorities in Europe have an increasing interest in implementing sustainability assessment of roads. Service life is a critical parameter in any lifecycle calculation. The lifetime distributions for often used road surface mixes varies across Europe. Even within a country, the distribution varies with local conditions and with the type of road and traffic volume. The objective of this study is to estimate the relative service life expectancy for new types of mixes compared to regular products under in different countries. The objective is also to show how to estimate the uncertainty in the durability.

2 Goal and Scope

The goal with this deliverable is to provide the PavementLCM Sustainability Assessment Framework with an assessment of the expected lifetime for existing surface courses and for new, and potentially greener, mixes.

For the well-known materials a literature review covers the range of estimated life-times across Europe. A questionnaire is used to further research the variation of expected lifetimes and variability of lifetimes. A case study to analyse actual survival data from one region were launched to demonstrate the variation of lifetime distributions with traffic volume.

The lifetime distributions were also calculated based on the experts' opinion expressed in the questionnaire and Bayesian inference theory.

A major part of this deliverable is devoted to the durability testing of proven and new experimental surface mixes. Tools to evaluate the relative performances was both standard laboratory procedures such as studying the water sensitivity, characterizing the mechanical properties mixes and more elaborate accelerated environmental and load tests. The latter tests included simulated ageing of the mixes and an accelerated load test with a circular road simulator.

The goal was to pinpoint potentially weakness or strengths of the new mixes compared to the well-known mixes.

A questionnaire was used to gather information regarding dominate distress modes for different types of mixes in different countries and the expected effect of different conditions such as traffic volume and climate factors on the durability of the reference materials. This information was further used to make the final assessment of the expected service lives for the new mixes in different countries in Europe.

3 Durability datasets review

3.1 Literature data on durability for reference mixes

OECD conducted a survey in beginning of 21st century regarding surfacing practices of highly trafficked pavements (> 10 000 ADT, and more than 15 % heavy trucks) (Christensen & et al., 2005). The expected service lives of surface courses in a selection of European countries are presented in Table 3-1.

Table 3-1. Expected service lives for surfacing on high volume roads in the heavy vehicle lane (Christensen & et al., 2005).

Country	Expected service life, surfacing	Typical surfacing	AADT (k)	ESALs (millions)	% heavy traffic
Denmark	14	SMA	60	5	8
France	8	-	25	-	19
Finland	5	-			
Netherlands	9	PA	55	36	17
Norway	5	SMA			
Poland	10	SMA	20	14	20
Portugal	15	SMA	11	19	15
Sweden	9	SMA	13	25	10
UK	9	SMA	111	106	15

In 2007 EAPA issued a technical document regarding long-life asphalt pavements (EAPA, 2007) where their experts have estimated the durability of different road surfacing based on best practice placed on properly built high volume roads and properly built secondary roads, see Table 3-2. For high volume roads the expected durability in the European countries was on average 20 years with a 15% percentile of 14 years and an 85% percentile of 25 years. On secondary roads the expected durability in the European countries was also on average 20 years with a 15% percentile of 16 years and an 85% percentile of 25 years.

For porous asphalt surfacing on high volume roads the expected durability in the European countries was on average 10 years with a 15% percentile of 8 years and an 85% percentile of 14 years

Table 3-2. EAPA estimated average durability in European context for SMA and PA

Mix type	Average durability High volume road	15 % percentile High volume road	85 % percentile High volume road	Average durability Secondary road	15 % percentile Secondary road	85 % percentile Secondary road
SMA	**20**	14	25	**20**	16	25
PA	**10**	8	14			

In 2016 PIARC conducted an analysis of service lives for road surfacing (Briessinck, Moffatt, Perveneckas, & Seiler, 2016) based on questionnaires. The reported expected service lives of road surfacing for a selection of European countries are presented in Table 3-3.

Table 3-3. Expected service life of wearing courses for high volume roads in Europe.

Country	Expected service life
France	**12**
Germany	**18-20**
Lithuania	**10-15**
Poland	**20**
Portugal	**20**
Switzerland	**20**

Comparing the results from the three studies indicates that there are large differences between the expected service life not only between countries but also between different surveys. A part of the differences in the results could be traced back to how the questions have been asked i.e., if the respondents are reporting the median actual service life or if it is the service life of the best performing roads. For example, Poland reports a service life of 10 years in the heavy traffic lane in the OECD study and 20 years in the PIARC study. Likewise, France reports a service life of 8 years in the heavy traffic lane and 16 years in the fast lane in the OECD study while in the PIARC study the expected service life is in between – 16 years.

Since service life is a key property in any LCA it is of high importance to study the actual historic records of service life in different settings. How this can be done is demonstrated in the next section with data from a county in Sweden. In this case study we have tested a Weibull distribution. The distribution takes only positive real values and is often used for describing distribution of lifetimes especially for skewed data set. Another distribution that might fit the survival data is the Log-normal distribution. We have also tried to fit data to log-normal distribution but for the particular data set used in the case study it seems that the Weibull distribution gives a better fit to the data. Analytical expressions for the service lives opens the possibility to take into account the uncertainty in the lifetimes in the LCA.

3.2 Case study of analysis of lifetime distribution

Weibull distribution can be used to model the lifetime (time to failure) if the failure rate is proportional to a power of time. In the special case of a constant failure rate, the Weibull distribution becomes identical to an exponential distribution. Failure rate decreasing with time is possible to model with Weibull distribution but not likely for pavements. The longer a pavement has survived the more likely it becomes that new paving is needed the following year. A Weibull distribution with increasing failure rate therefore seems suitable for modelling pavement lifetime.

Survival data has two types of events and each event has an event time. An event is a case if the time for end of life is observed. If rather the time at end of study is observed, or some other event that is not end of life while the subject is still alive, the event is known as sensoring. Sensored observations contain partial information about the survival time though end of live is not observed. Survival analysis methods properly take care of both the complete information in the cases and the partial information in the sensored observations.

In this study, survival times of SMA pavements layers after 1 Jan 1980 in Östergötland, Sweden was analysed. More than 95% of SMA sections in Östergötland have a nominal maximum aggregate size of 16 mm. The data consists of 4190 homogenous sections of varying length (12 to 8184 m). The number of observations (observed pavement layers) are 6699 of which there are 3918 cases and 2781 sensored layers. The rate and the change in rate over time are assumed to depend on AADT class. The classes and a summary of number of observations are shown in Table 3-4.

Table 3-4. Number of sections and events in different AADT classes

AADT class	AADT	# sections	# events	# sensored	# cases
1	AADT ≤ 1000	133	140	19	121
2	1000 < AADT ≤ 2000	455	571	190	381
3	2000 < AADT ≤ 4000	1204	1589	778	811
4	4000 < AADT ≤ 8000	1429	2277	996	1281
5	8000 < AADT ≤ 12000	472	950	369	581
6	12000 < AADT ≤ 16000	463	1091	407	684
7	16000 < AADT	34	81	22	59

Analyses are done separately for each AADT class. Data are weighted such that longer sections has higher weight in the analyses, proportional to length in Table 3-5 and in Figure 3-1 to Figure 3-7. In the empirical Kaplan-Meier approach, this is achieved by repeating the data according to the length of the section while in the Weibull analysis this is done by using weighted maximum likelihood estimation. Table 3-5 shows estimated median survival time with Kaplan-Meier approach followed by estimated median and mean survival time assuming that the lifetime has Weibull distribution. All numbers rounded to integers.

Table 3-5. Measures of central tendency of survival time in days (and years) for different AADT classes

AADT class	Median survival (Kaplan-Meier)	Median survival (assuming Weibull)	Mean survival (assuming Weibull)
1	1103 (3,0)	1562 (4,3)	1805 (4,9)
2	3132 (8,6)	2390 (6,5)	2896 (7,9)
3	4054 (11,1)	3777 (10,3)	4217 (11,6)
4	3994 (10,9)	3585 (9,8)	3800 (10,4)
5	2946 (8,1)	2784 (7,6)	2855 (7,8)
6	2313 (6,3)	2331 (6,4)	2357 (6,5)
7	2270 (6,2)	2469 (6,8)	2632 (7,2)

The results are shown graphically in Figure 3-1 to Figure 3-7 with Kaplan-Meier curve as black lines on the upper half of the figure. This is an empirical estimate without an assumption of any underlying distribution which looks like an irregular staircase. The parameters of the Weibull distribution are also estimated and the survival curve based on the estimated parameters is added as a black curve to the Kaplan-Meier plot. They are in most cases similar, showing that an assumption of an underlying Weibull distribution is not obviously wrong. The largest deviation is seen for AADT < 1000. The estimated survival density based on Weibull distribution is shown on the lower half of the figure. Pavement dates are not nearly continuous in time because paving in large scale is not done in winter, causing a slight approximation in the Weibull approach. The horizontal scale is in days since pavement date with grey vertical lines for every 5th year.

As seen in the density functions and Kaplan-Meier curves shown in Figure 3-1 to Figure 3-7, the density functions (survival distribution functions) are typically broad. For example, the bottom 10 % least performing roads in AADT class 3 were replaced within three years and the top 10 % survived 17 years.

The median survival time reaches a maximum for roads in the AADT class 3 and then gradually decreases with increasing traffic. This could probably be explained by the fact that rutting partially caused by studded tires is a major cause for maintenance measures in Sweden. The road wear caused by studded tires is mitigated by using aggregates with lower tendency to be crushed by studs for high volume roads compared to the aggregates used for low volume roads. The decrease in survival time is not inversely proportional to the traffic volume.

The median survival time in AADT class 3 and class 4 which represents 60% of the observations, is 10 years. The mean median survival time for all AADT classes weighted by the number of observations is 9 years which is the same average survival time reported in the OECD report (Christensen & et al., 2005) for Sweden.

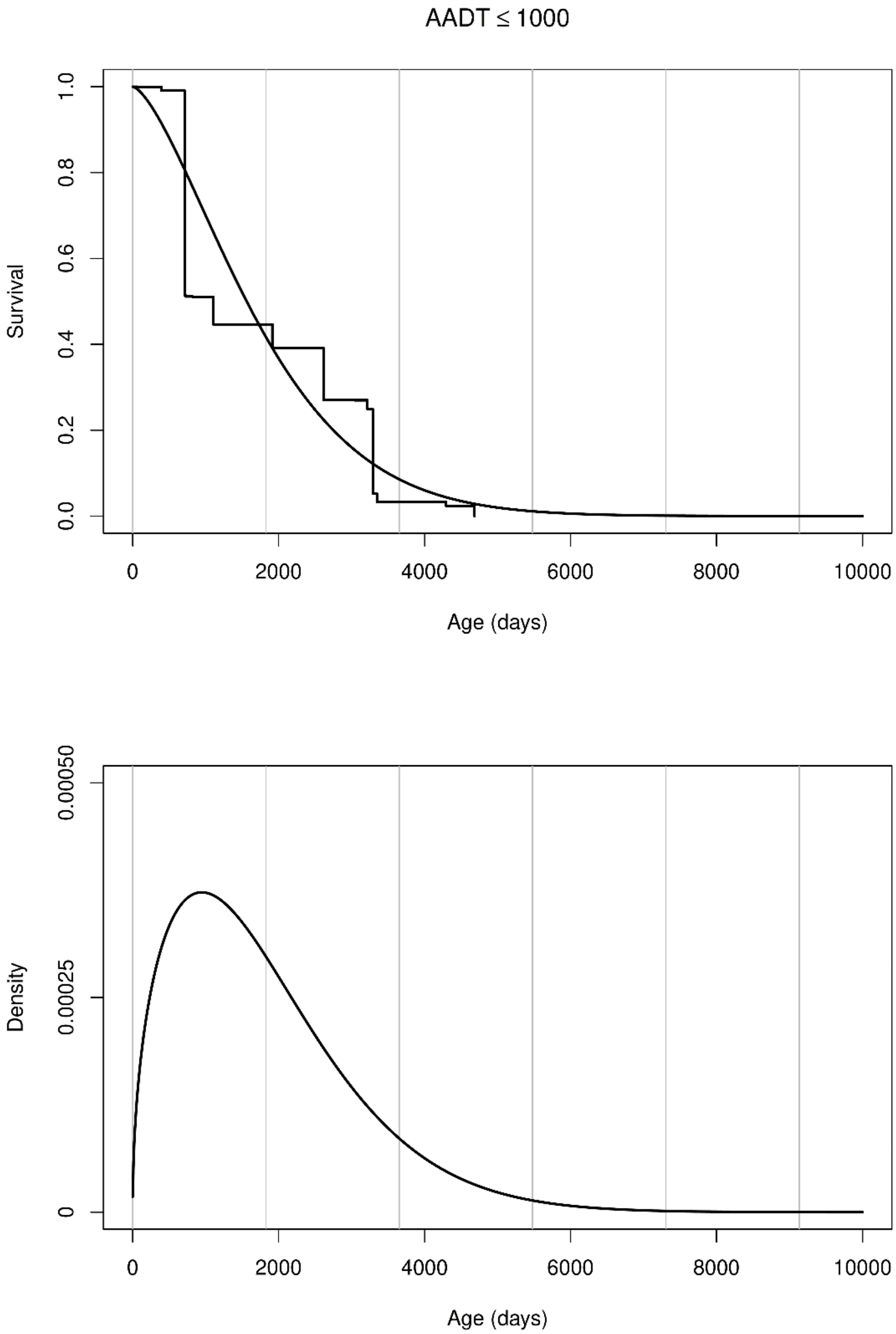

Figure 3-1. Survival function and lifetime density function, AADT < 1000

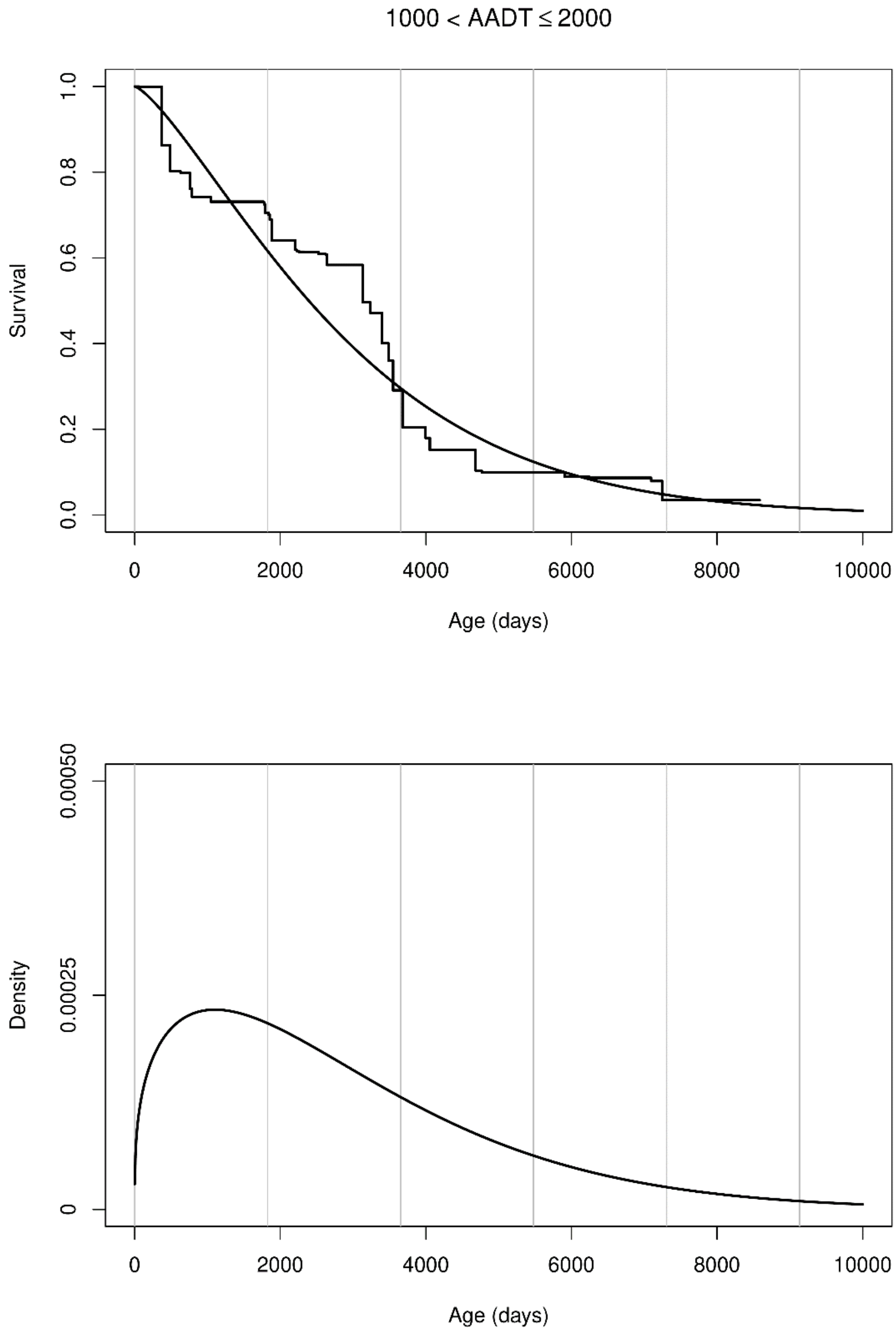

Figure 3-2. Survival function and lifetime density function, 1000 < AADT ≤ 2000

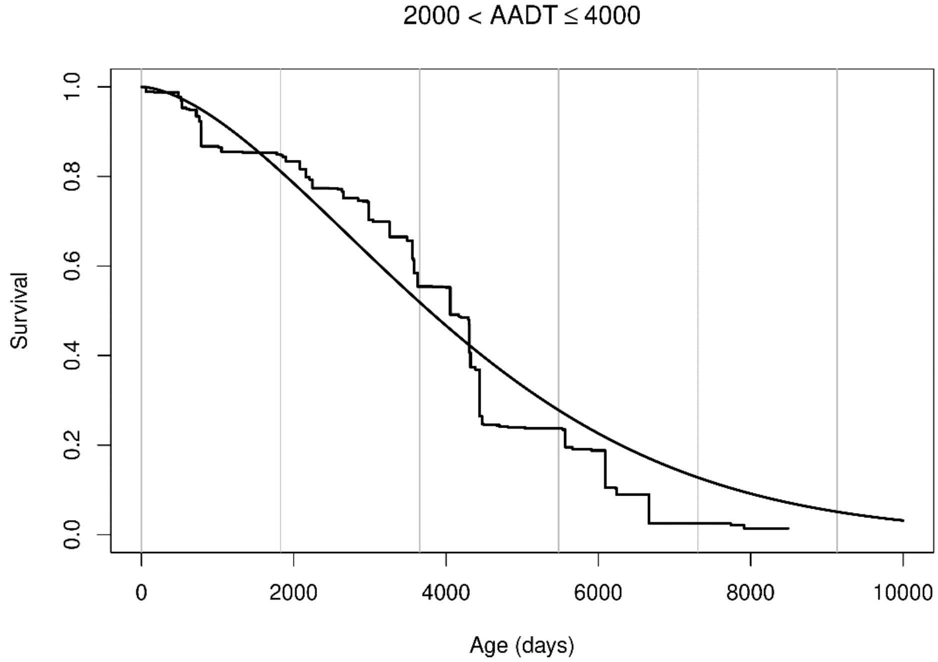

2000 < AADT ≤ 4000
Survival
0.0
0.2
0.4
0.6
0.8
1.0
0
2000
4000
6000
8000
10000
Age (days)

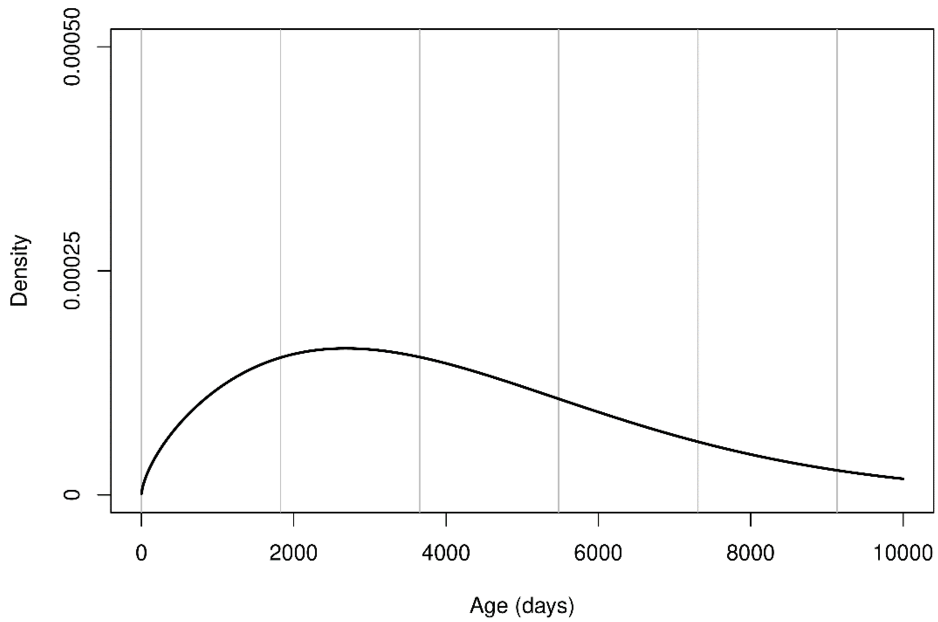

Density
0
0.00025
0.00050
0
2000
4000
6000
8000
10000
Age (days)

Figure 3-3. Survival function and lifetime density function, 2000 < AADT ≤ 4000

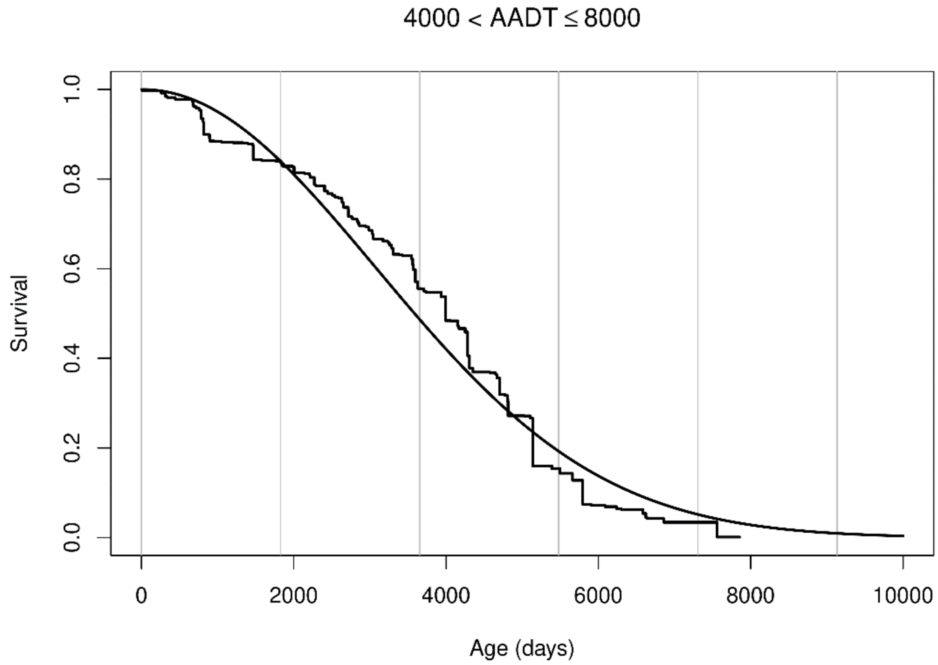

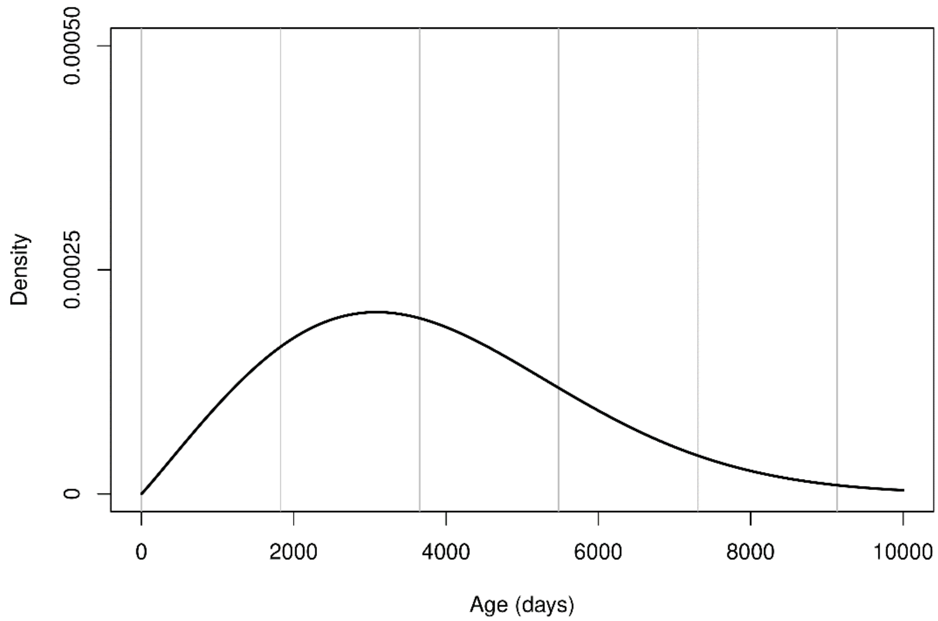

Figure 3-4. Survival function and lifetime density function, 4000 < AADT ≤ 8000

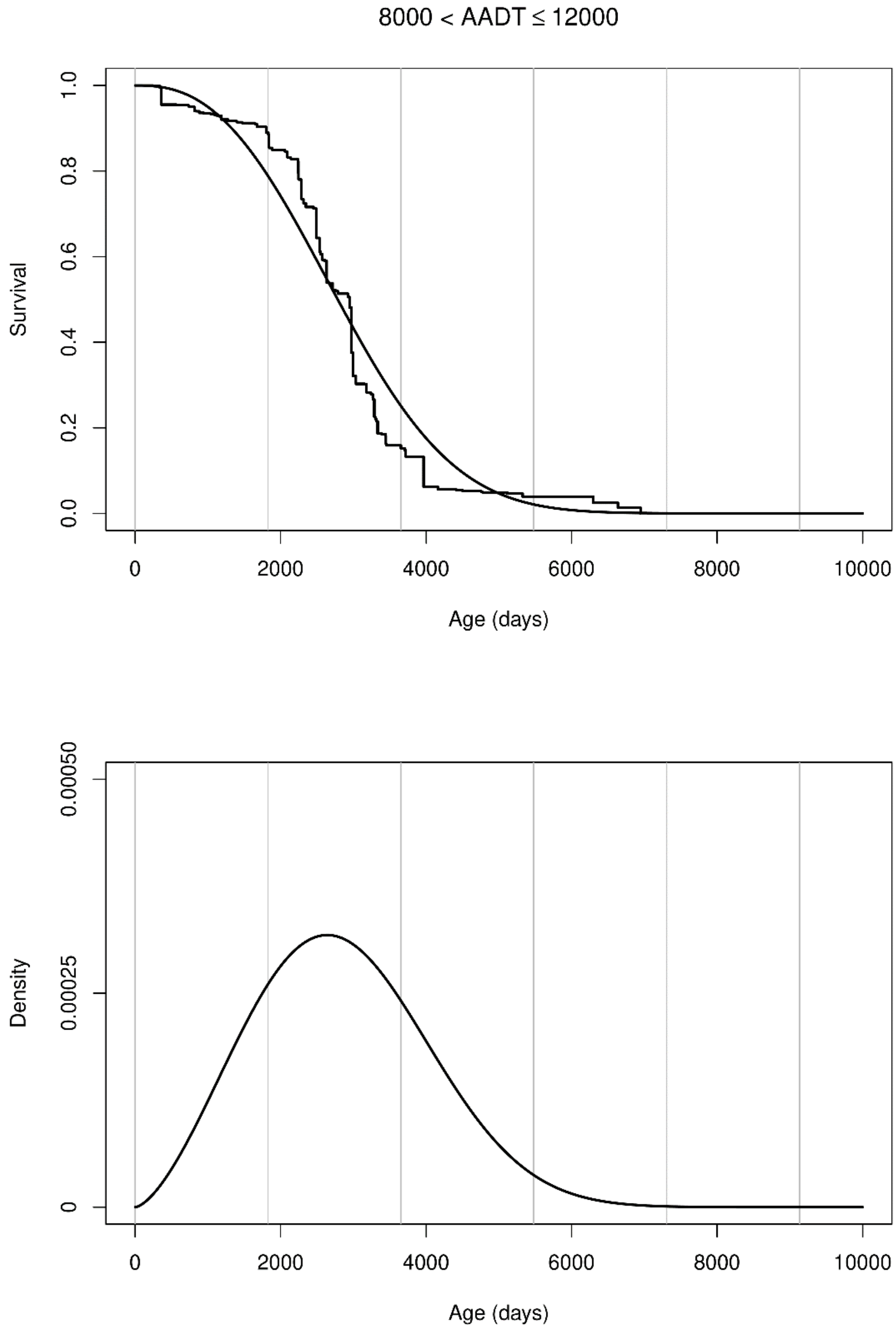

Figure 3-5. Survival function and lifetime density function, 8000 < AADT ≤ 12000

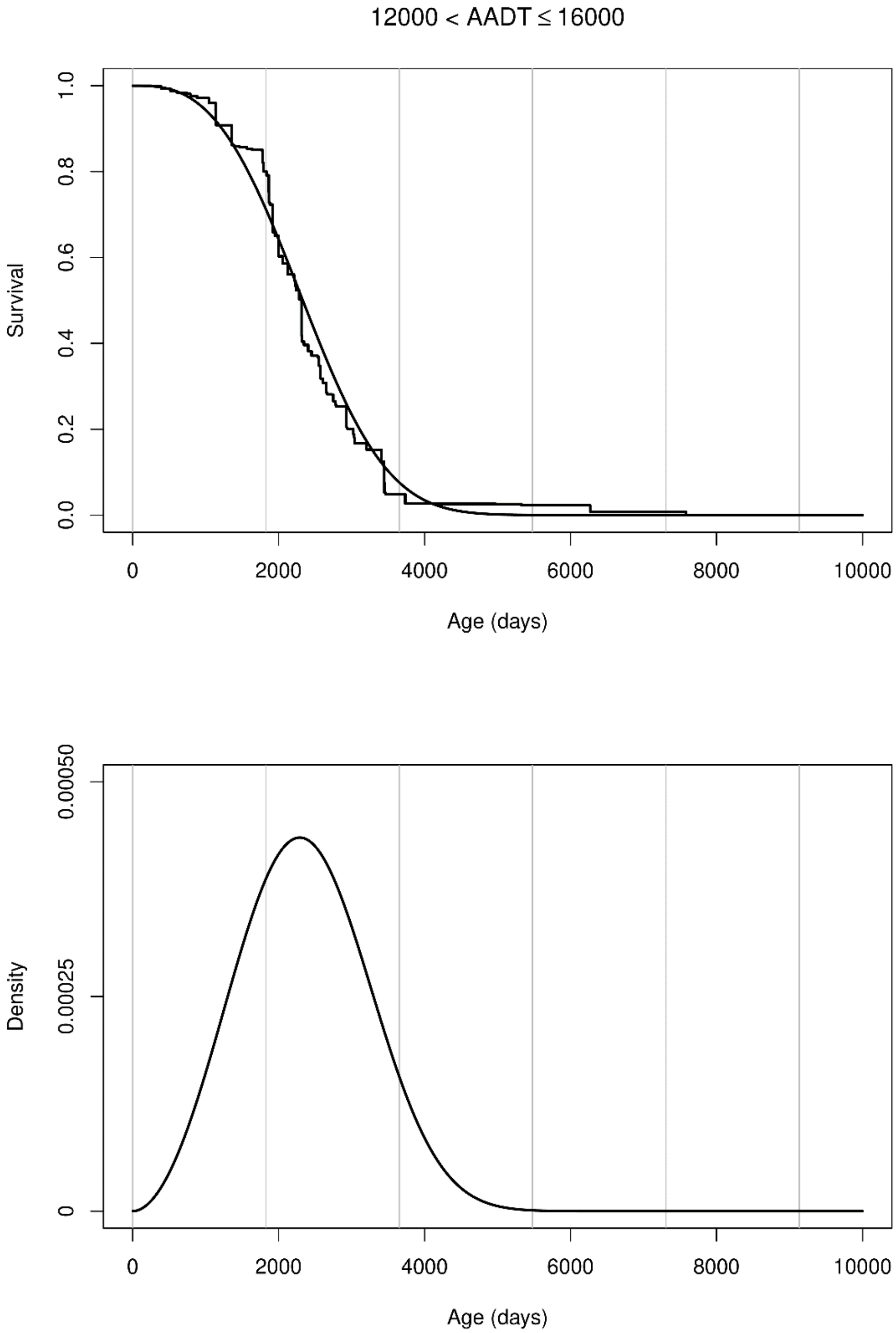

Figure 3-6. Survival function and lifetime density function, 12000 < AADT ≤ 16000

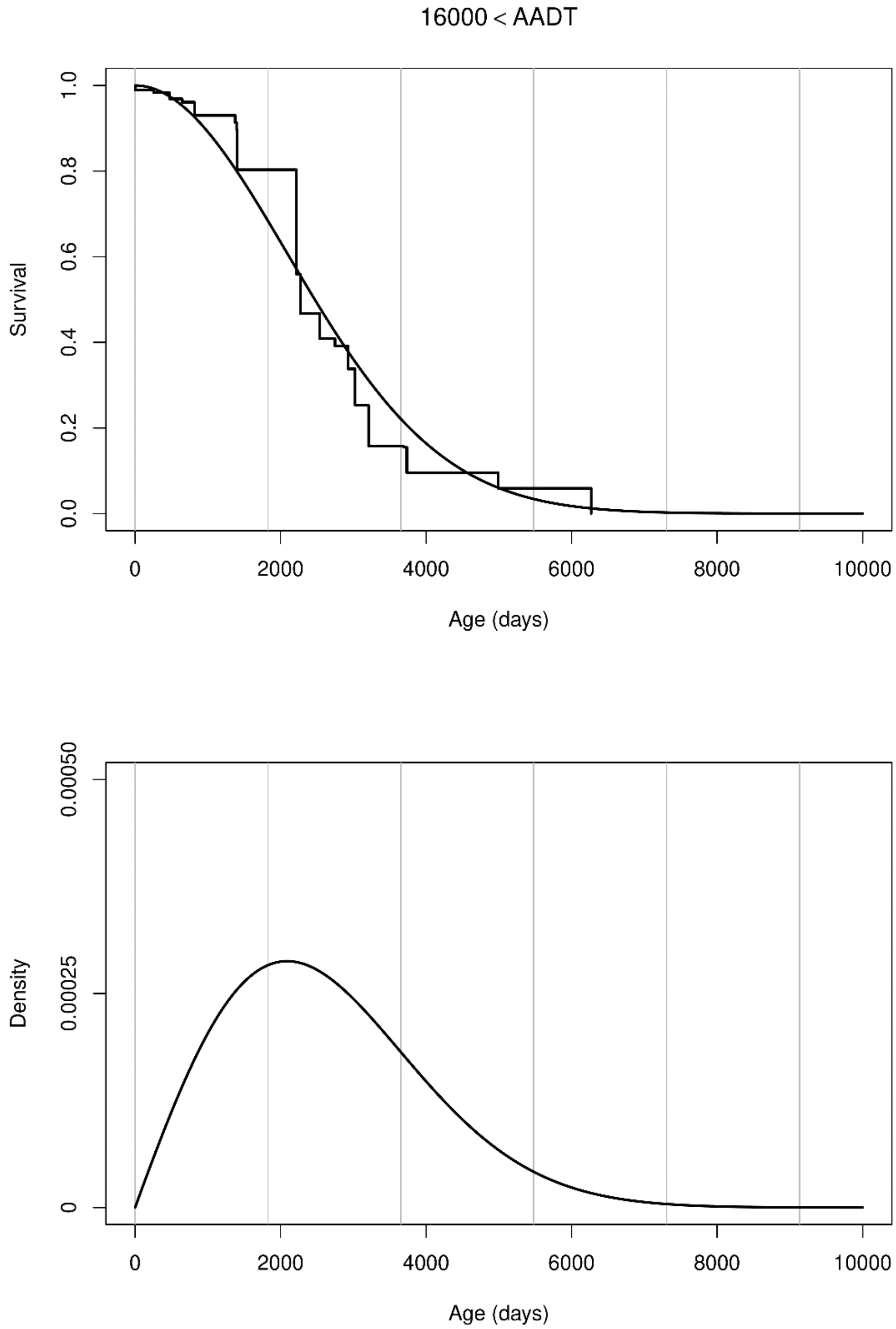

Figure 3-7. Survival function and lifetime density function, 16000 < AADT

3.3 Lifetime distributions estimated from expert judgments.

In the 3rd CEDER PavementLCM workshop experts' opinions on the service lives of wearing courses in Europe was gathered and the results is presented in Deliverable D2.1 (Jiménez del Barco Carrión, Buttitta, Neves, & Lo Presti, 2021). The result is also presented in Table 3-6 and Table 3-7 below.

Table 3-6. Durability estimates for SMA16 used in high traffic roads

Expert	Expected durability (years)	Worst case durability (years)	Best case durability (years)
1	15	12	25
2	10	4	20
3	10	3	12
4	15	10	17
5	7	4	12

Table 3-7. Durability estimates for PA16 used in high traffic roads

Expert	Expected durability (years)	Worst case durability (years)	Best case durability (years)
1	10	7	14
2	6	3	10
3	17	7	-
4	9	5	12

When analysing the durability of pavements based on experts' judgement, there are fundamentally two sources of uncertainty (Kiureghian & Ditlevsen, 2009). On the one hand, what is often denoted as aleatory uncertainty is associated with natural variations in durability of pavements due to local conditions, foundations, quality of construction, traffic and loads, amongst other factors. This means that amongst all pavements built in the future, there will be variations in durability that can only be predicted from a statistical viewpoint. This source of uncertainty is intrinsic to the problem and, can usually, not be reduced with better information or more reliable models. On the other hand, the present estimates are based on experts' opinion and therefore include a second source of uncertainty (epistemic uncertainty) associated with the experts' disagreements, the effects of limited sample sizes and local conditions they are familiar with, and their own bias and preconceptions.

Bayesian inference is a suitable tool to account for both types of uncertainty and to develop models that take both into account in a consistent manner. Considering that the durability of pavement surfaces is necessarily positive but that they are associated with large uncertainty, it is reasonable to assume a lognormal distribution to model durability.

The lognormal distribution is characterized by a probability density function (PDF) in the form:

$$\mathrm{f(x)} = \frac{1}{\mathrm{x}\sigma\sqrt{2\pi}} \exp\left(-\frac{(\ln \mathrm{x} - \mu)}{2\sigma^2}\right)$$

Equation 3-1

The parameters of this distribution, μ and σ, can be found, if extensive data exists, using maximum likelihood estimates. However, in the present case, we aim at producing an initial estimate of the distribution based on experts' opinion. Because we have limited data and this includes significant epistemic uncertainty, there is significant uncertainty regarding the parameters of the distribution. To take this into account, we will define durability *D* as a lognormal distribution with mean μ and standard deviation σ defined by normal distributions as:

$$\mathrm{D} \sim \mathrm{Lognormal}\left(\mathrm{N}(\mu_\mu, \sigma_\mu); \mathrm{N}(\mu_\sigma, \sigma_\sigma)\right)$$

Equation 3-2

In this work, the distribution of the mean was estimated based on the experts' opinion regarding the mean durability (see second column of Table 3-6). As such, the mean and the standard deviation of the mean (μ_μ and σ_μ) correspond to the mean and standard deviation of column 2 of Table 3-6. The standard deviation associated with the standard deviation of each expert's durability estimate is computed as:

$$\sigma^{\mathrm{i}} = \frac{D_{sup}^{i} - D_{inf}^{i}}{\Phi^{-1}(0.90) - \Phi^{-1}(0.90)}$$

Equation 3-3

where Φ^{-1} is the inverse standard normal distribution and D_{sup}^{i} and D_{inf}^{i} are the optimistic and pessimistic estimate for expert *i*. From this, the mean and standard deviation of the standard deviation of durability ($\mu_\sigma, \sigma_\sigma$) can be computed directly as:

$$\mu_\sigma = \sum_{i=1}^{N} \frac{\sigma_i}{N}$$

Equation 3-4

$$\sigma_\sigma = \sqrt{\frac{\sum_{\mathrm{i}=1}(\sigma_{\mathrm{i}} - \mu_\sigma)^2}{\mathrm{N}}}$$

Equation 3-5

Once the mean and standard deviation of the distribution parameters of the durability of surfacings are computed, Monte Carlo Simulation can be used to compute the properties of the distribution of the durability. This procedure was implemented in the attached spreadsheet.

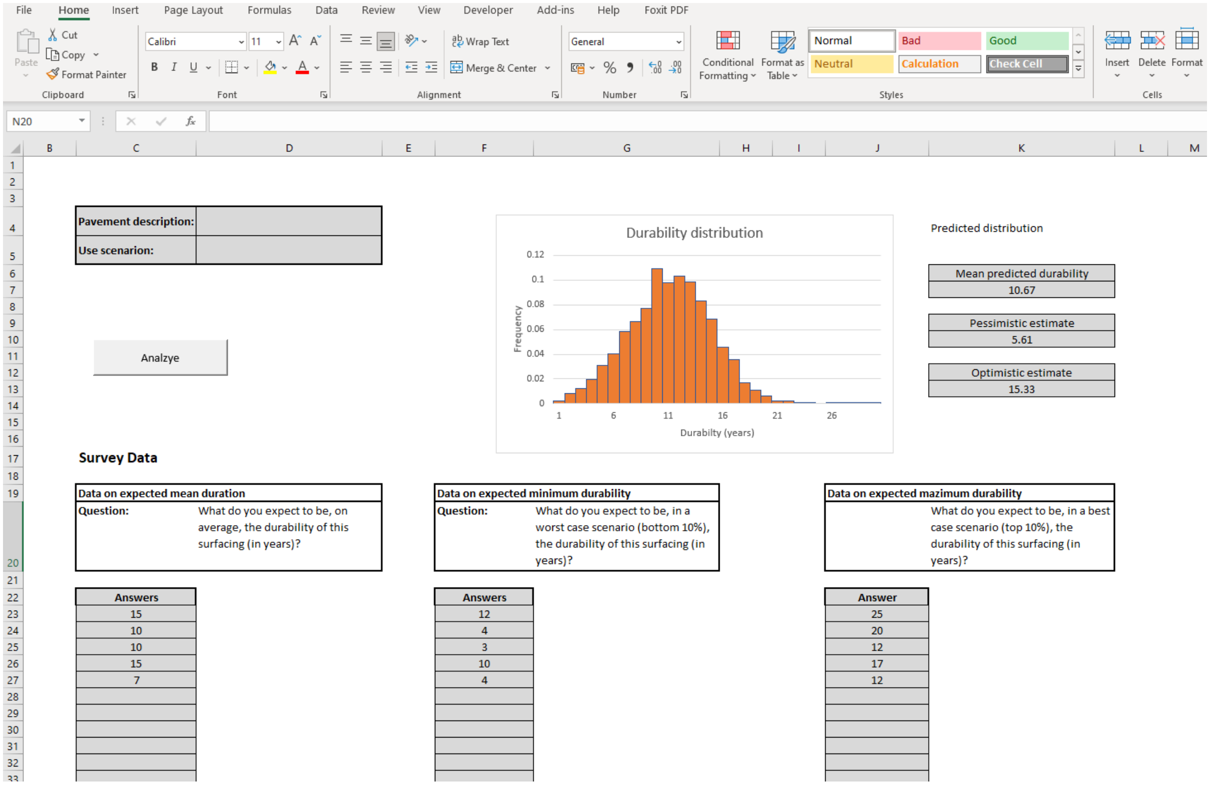

Figure 3-8.Snapshot of the spreadsheet computing the distribution of durability considering the response of five experts.

The predicted durability distribution is shown in Figure 3-9. The mean of the distribution is equal to 10.6 years, whereas the estimated worst- and best-case scenario durability are 5.7 and 15.5 years, respectively.

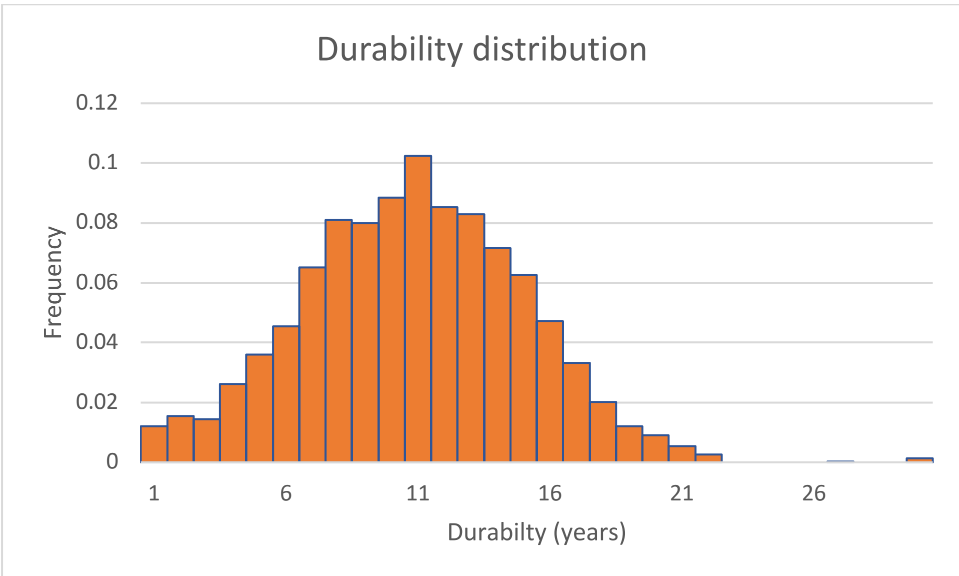

Figure 3-9. Predicted distribution of the durability of SMA16

The estimates of durability of PA16 can be computed in a similar manner, resulting in the probability distribution presented in Figure 3-10. The mean of the distribution is equal to 10.2 years, whereas the estimated worst- and best-case scenario durability are 4.9 and 15.6 years, respectively. These results show that, although the mean estimate varies only 4%, the pessimistic estimate varies 15%, as a result of the greater uncertainty associated with PA16.

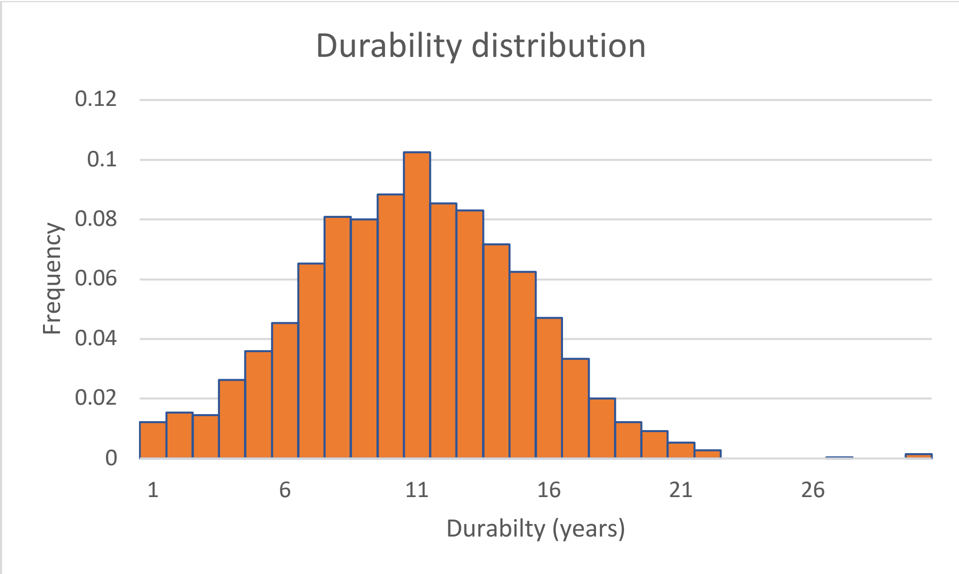

Figure 3-10. Predicted distribution of the durability of PA16

4 Materials

4.1 Stone Mastic Asphalt

Four stone mastic asphalt were used in the study.

SMA 16

SMA 11 10% RA

SMA 11 40% RA

SMA 8 60% RA

The reference mix was a SMA 16 70/100 with 6,2% binder. The mix was produced in a plant in Sweden. The aggregate was granite from Styvinge in Östergötland. 0,4% cellulose fibers and 0,3% Wetfix BE was added to the mix. Air voids in Marshall compacted specimens was 2,7%.

Two SMA 11 mixes came from plants in Denmark.

The first mix was a SMA 11 40/60 with 5,8% binder. The aggregate was approximately 70 % Hyperit, 20 % Labradorit and 10 % granite from the RA. 1,5 % reactive filler and 1,25% limestone filler was used together with 0,35% Viatorp 66. The mix was produced in Hjallerup. Air voids in Marshall compacted specimens was 2,1 - 2,6%.

The second mix was a SMA 11 with 40 % RA in the mix. This was also produced in a plant.

The last SMA was a SMA 8 50/70 with 60 % RA in the mix. It was produced in the lab. The RA collected from a plant was split into two fractions with a 4 mm sieve. A sieve and binder analysis were made of each fraction. The binder content in the fraction larger than 4 mm was 6,78% and had a penetration value of 18 x 10^{-1} mm and a softening point of 65,4 °C. For the other fraction, the binder content was 3,85% and the penetration value was 15 x 10^{-1} mm and a softening point of 68,6 °C.

The 50/70 binder added to produce the SMA 8 60% RA had a softening point of 51,0 °C. 33,4% of the aggregate in the mix were from the larger fraction of the RA and 26,5% of the aggregate in the mix were from the smaller fraction of RA. 54% of the binder in the final mix originated from the RA. To compensate/rejuvenate for the hardened binder in the RA, 0,53% of a VMA additive was used (8,7% of the total binder content) as described in AllBack2Pave (Wellner et al., 2015). 0,5% of cellulose fibres were used in the mix. The added aggregate was a granite from Skärlunda in Östergötland.

4.2 Porous Asphalt

Four porous asphalt mix were used in the study they are designated as

PA 16 or ZOAB+

PA 8 or Fibra 1

PA 8 Panacea or Fibra 3

PA 8 Aramid or Fibra 4

The PA 16 70/100 with a binder content of 5,5 % was produced in the laboratory based the mix detailed by Zhang (Zhang, Anupam, Scarpas, & Kasbergen, 2018). All coarse granite aggregates 2 – 16 mm were washed and came from Skärlunda in Östergötland. Sand 0,063 – 2 mm came from Baskarp. Filler content (Wigro 60K) in the aggregate was 4,7 %. 0,3 % cellulose fibres were added to the mix.

The Fibra mixes were produced in a plant in Netherlands for the Fibra project.

Fibra 1: Is the standard PA 8 mixture for two layers porous asphalt in the Netherlands. The binder is a SBS polymer modified bitumen

Fibra 3: A PA 8 mixture made with 70/100 bitumen and panacea fibres

Fibra 4: A PA 8 mixture made with 70/100 bitumen and aramid fibres

4.3 Density and compaction

The maximum density for the mixes is shown in Table 4-1.

Table 4-1. Maximum density of mixes in g/cm^{-3}

SMA 16	SMA 11 10 % RA	SMA 11 40 % RA	SMA 8 60 % RA	PA 16	Fibra 1	Fibra 3	Fibra 4
2,486	2,642	2,624	2,410	2,418	2,505	2,489	2,488

Specimens were prepared in the laboratory using the Marshal compaction method, EN 12697-30. The size of the cylindrical specimens was 100 mm in diameter and 40 mm in thickness. The air voids of the specimens were determined in accordance with the European standards EN 12697-6 and EN 12697-8, respectively.

The air voids in Marshall compacted specimens is shown in Table 4-2.

Table 4-2. Air void ratio and densities of Marshall compacted specimens.

	SMA 16	SMA 11 10 % RA	SMA 11 40 % RA	SMA 8 60 % RA	PA 16	Fibra 1	Fibra 3	Fibra 4
Air void ratio	1,8 %	1,6 %	0,9 %	0,8 %	13,4 %	23,9 %	22,4 %	22,6 %
Density (g/cm^{-3})	2,441	2,600	2,599	2,392	2,093	1,906	1,931	1,927

These air voids contents/densities were subsequently used as target values for gyratory compacted samples used for shear modulus testing and for plates produced in a frame using a roller compactor. In the latter case the total air void target of the plate was 1 % higher than air void ratio in the Marshall specimen since the experience is that the density of the plate is slightly lower at the outer rim of the plate compared to the central part of the plate. By slightly reducing the amount of material in the frame the central part reaches the same air void ratio as Marshall compacted specimens.

4.4 Ageing procedure

It is widely thought that ageing of the binder in a pavement layer could have a detrimental effect on the performance of the mix in some. Extensive ageing makes bituminous binders hard and brittle. To what extent the progressive hardening of the binder is a limiting factor for a asphalt layer service life depends on the mix type and the structural properties of the road. To simulate the ageing and to be able to test the mixes in a hardened state we used oven ageing of the loose mixes to simulate the ageing that occurs during service. Oven ageing of loose mix has been used to simulate field ageing has been used in the past for example in (Mollenhauer, Mouillet, Pierard, Tusar, & Gabet, 2012) & (De la Roche C. et al., 2009). We followed these examples and aged loose mix in a tray at approximately 86 °C for seven and fourteen days. The temperature fluctuated in the oven between 84 and 88 °C. These aged mixes are called short- and long-term aged mixes, which should not be confused with the short-term ageing occurring at production of the mix or long-term ageing of binder using a pressure ageing vessel, PAV. The aged batches of the mixes were used together with the un-aged material in the accelerated test.

4.5 Binder recovery and characterization

Binder recovery was conducted for all the prepared asphalt mixtures, before and after ageing in laboratory. The obtained binders were experimentally characterized with different test methods. This section describes these methods and discusses the test results.

4.5.1 Test methods

The binder recovery was performed according to EN 12697-3:2013+A1:2018. Dichloromethane was used as the solvent. During the first phase of the distillation, the oil bath temperature was 85 °C and the applied pressure was 85 kPa. During the second phase, the temperature was 150 °C and pressure was 2,0 kPa. No extra phase was needed for the binder recovery. Totally 24 different binders were obtained.

The obtained binders were thereafter tested for the Ring and Ball softening point according to EN 1427:2015. Water was used as the bath liquid for the determinations below 80 °C while glycerol was used for the determinations above 80 °C. According to EN 1427:2015, there is an approximately 4 °C difference when a given bitumen is tested in the different baths. The test result is usually higher in a glycerol bath than in a water bath.

Furthermore, the obtained binders were tested for the complex shear modulus G* and phase angle δ in the linear viscoelastic region with a dynamic shear rheometer (DSR) according to EN 14770:2012. Temperature sweep was conducted at 10 rad/s with a 6 °C interval up to 82 °C. The plate-plate geometry of 25 mm diameter and 1 mm gap was used for the DSR measurement.

4.5.2 Ring and Ball softening point

Results of the Ring and Ball softening point tests are listed in Table 4-3 and presented in Figure 4-1. In the tables and figures and in the following discussion the term “original” does not denote the original state of the binder but rather the state of the binder recovered from the mix. Thus, some hardening of the binder has occurred during production of the mixes and after storage in ambient temperature. Furthermore, it should be noted that the measurements for recovered binders from long-term aged PA8 panacea, long-term aged PA8 aramid and long-term aged SMA8 60% RA VMA reached the maximum temperature capacity of the testing equipment. Thus, no values were obtained for the softening point for these mixes after long term aging.

The test results show that the softening point of binder increases after ageing of the asphalt mixture. The longer the ageing conditioning lasts, the more it increases after the ageing. This means that the ageing hardens and stiffens binders. However, the sensitivity of different asphalt mixtures to ageing is different. For example, the change of SMA11 40% RA in softening point was relatively small after ageing, but the changes of PA8 panacea and PA8 aramid were relatively high. This could be explained by the PA gradation (making porous structure thus better accessibility to air) and smaller aggregate size (thus larger specific surface area) of PA8 panacea and PA8 aramid. The effects of additives in these two asphalt mixtures were nearly the same but it could not be known exactly how the additives affect the softening point change only with these test results.

The use of PMB in PA8 resulted in relatively high softening point of the binder in freshly mixed asphalt mixture and, furthermore, made the mixture more resistant to ageing. In addition, the incorporation of reclaimed asphalt materials could lead to relatively high softening point of the recovered binder, for example in SMA8 60% RA VMA, and to certain extent make the asphalt mixture less sensitive to ageing. On the other hand, the use of rejuvenating additives can reduce the softening point of recovered binders while their effects on ageing behaviour of the asphalt mixture are expectedly variant-specific.

Table 4-3. Results of the Ring and Ball softening point tests.

Asphalt mixtures	Ageing conditions	Softening point of recovered bitumen (°C)
ZOAB+	Original	56,6
	Short-term aged	66,4
	Long-term aged	87,0
PA8	Original	74,8
	Short-term aged	91,5
	Long-term aged	106,5
PA8 panacea	Original	59,6
	Short-term aged	87,0
	Long-term aged	>115,0*
PA8 aramid	Original	60,0
	Short-term aged	86,5
	Long-term aged	>115,0*
SMA16	Original	57,0
	Short-term aged	72,8
	Long-term aged	109,5
SMA11 40% RA	Original	57,6
	Short-term aged	64,4
	Long-term aged	75,2
SMA8 60% RA VMA	Original	66,8
	Short-term aged	74,6
	Long-term aged	>115,0*
SMA11 10% RA	Original	64,0
	Short-term aged	72,4
	Long-term aged	84,5

* These measurements reached the maximum temperature capacity of the testing equipment.

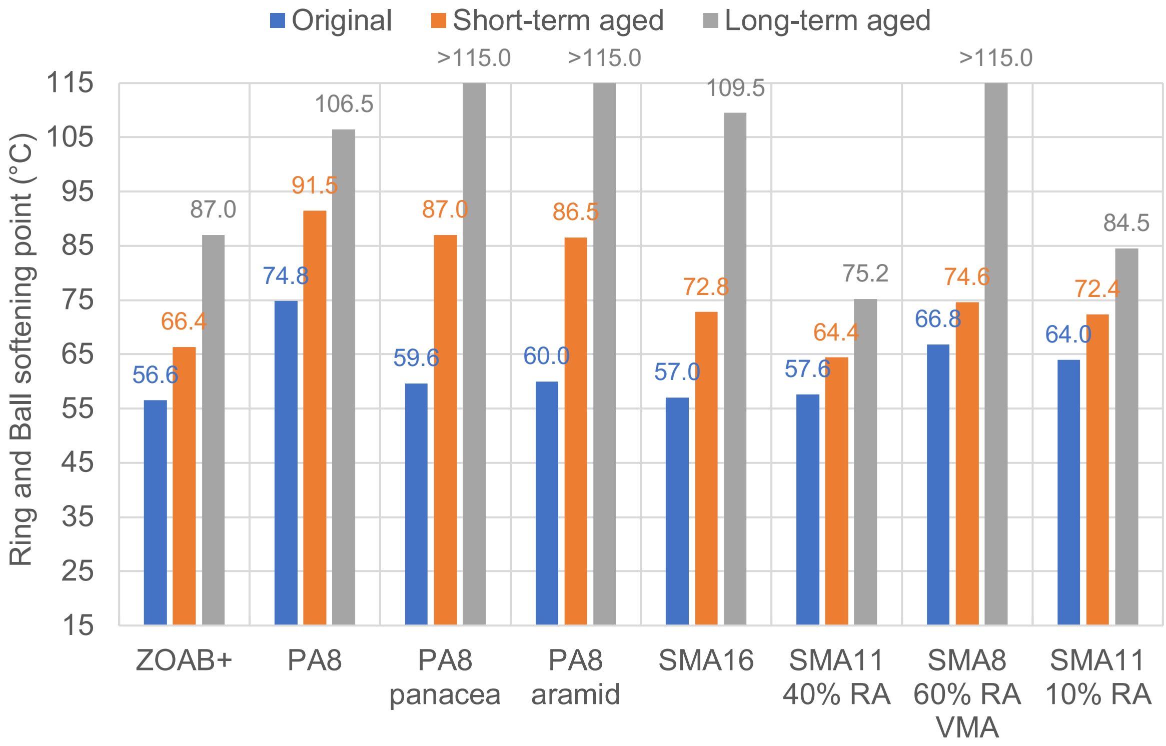

Figure 4-1. Bar chart of the Ring and Ball softening point test results.

4.5.3 DSR temperature sweep

The DSR temperature sweep results at 10 rad/s are shown in Figure 4-2 through Figure 4-5. As the temperature rises, the complex shear modulus G* (vertical axis on the right) of the recovered binders decreases. In other words, the binders soften as they warm up. Meanwhile, for almost all the recovered binders (except those from PA8), the phase angle δ (vertical axis on the left) increases as the temperature rises. This means that the binders become more viscous and less elastic at a higher temperature. The recovered binders from PA8, however, showed almost constant phase angle at 10 rad/s and the tested temperatures, which is a sign for that PMB is used in the asphalt mixture. The modification with polymer made the binder still very elastic even at a relatively high temperature.

Furthermore, the DSR temperature sweep results indicate the effects of asphalt mixture ageing on binder properties. For all recovered binders, the complex shear modulus G* increases after ageing of the asphalt mixture while the phase angle δ decreases. The longer the ageing conditioning lasts, the more G* increases and δ decreases after the ageing. This means that the ageing hardens binders and makes them less viscous. A shifting effect can be observed for both the G* and δ curves towards higher temperatures after ageing of the asphalt mixture, without significantly changing the shape of curves.

However, the sensitivity of different asphalt mixtures to ageing is different. This is to say that the recovered binders behave differently in terms of how much their curves are shifted after the ageing. For example, the curves of PA8 panacea and PA8 aramid (Figure 4-3) are much more towards higher temperatures after the ageing compared to the curves of SMA11 40% RA (Figure 4-5). Having very similar softening point results, the recovered binders from PA8 panacea and PA8 aramid show very similar DSR results as well.

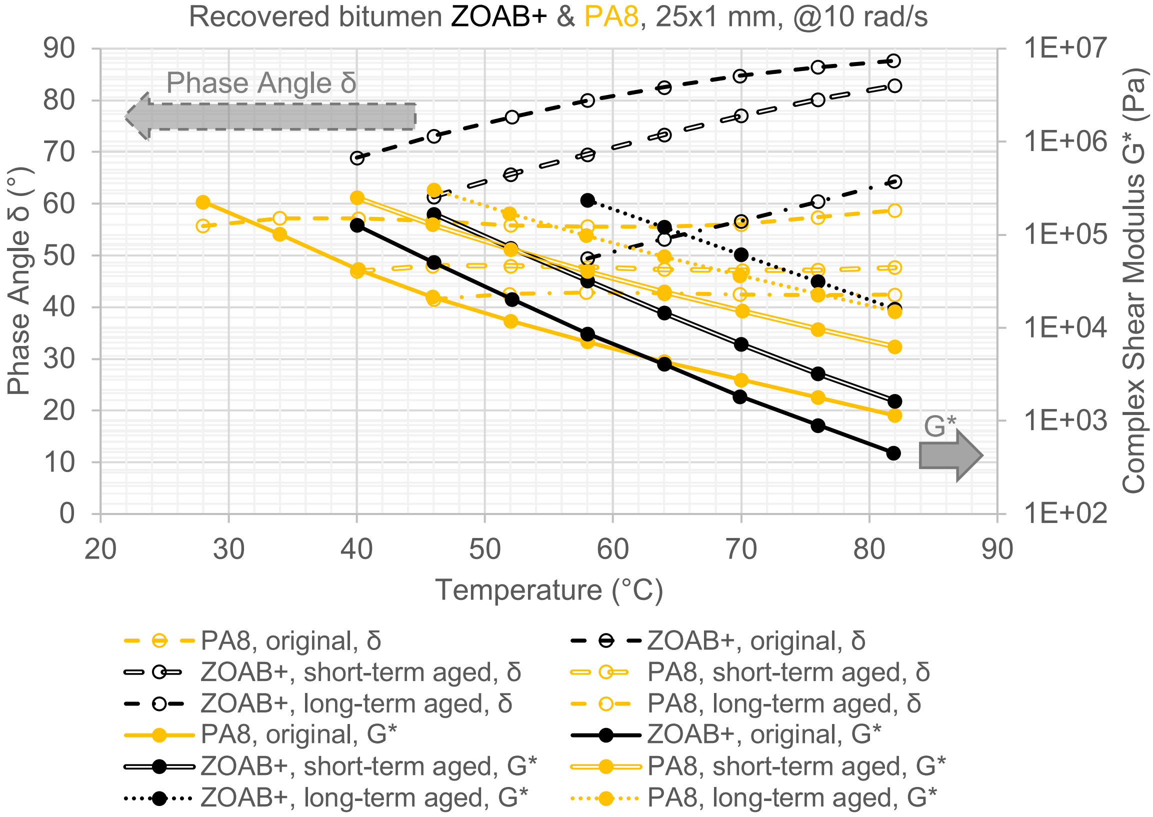

Recovered bitumen ZOAB+ & PA8, 25x1 mm, @10 rad/s
Phase Angle δ
G*
Phase Angle δ (°)
Complex Shear Modulus G* (Pa)
Temperature (°C)
0
10
20
30
40
50
60
70
80
90
1E+02
1E+03
1E+04
1E+05
1E+06
1E+07
20
30
40
50
60
70
80
90
PA8, original, δ
ZOAB+, original, δ
ZOAB+, short-term aged, δ
PA8, short-term aged, δ
ZOAB+, long-term aged, δ
PA8, long-term aged, δ
PA8, original, G*
ZOAB+, original, G*
ZOAB+, short-term aged, G*
PA8, short-term aged, G*
ZOAB+, long-term aged, G*
PA8, long-term aged, G*

Figure 4-2. Temperature sweep of recovered bitumen from ZOAB+ and PA8.

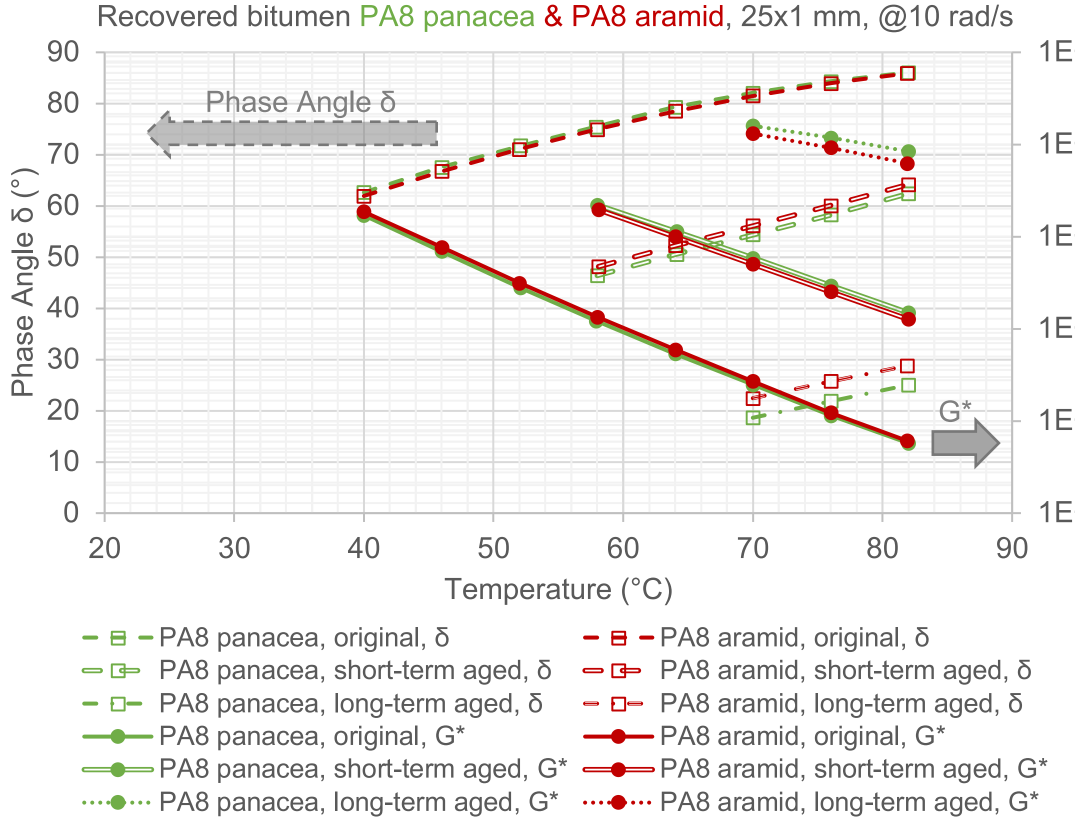

Figure 4-3. Temperature sweep of recovered bitumen from PA8 panacea and PA8 aramid.

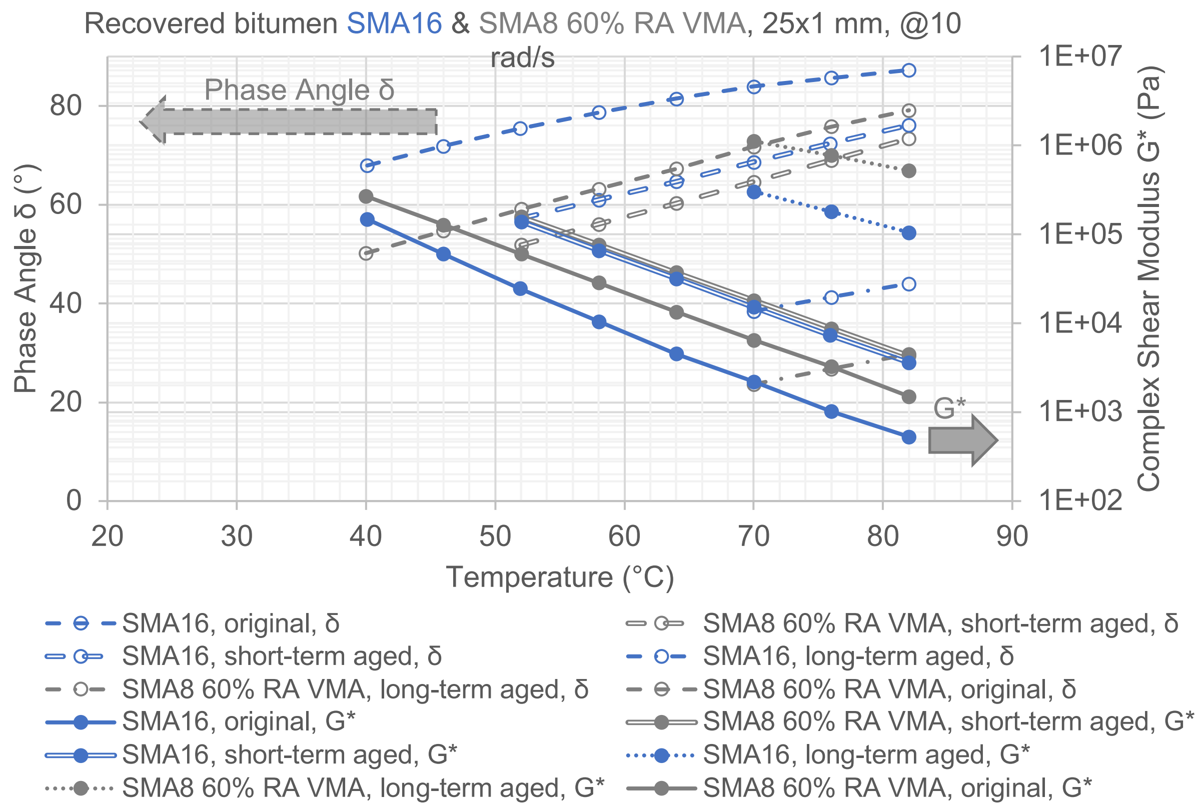

Figure 4-4. Temperature sweep of recovered bitumen from SMA16 and SMA8 60% RA VMA.

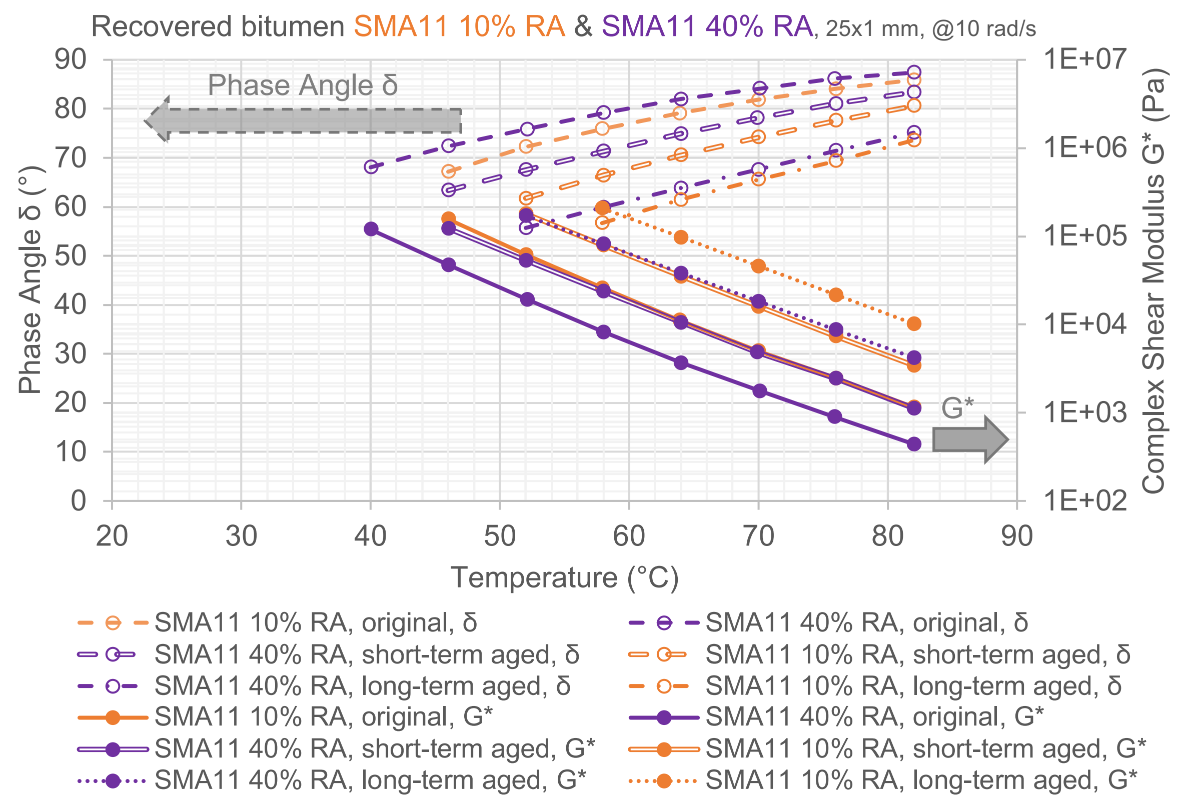

Figure 4-5. Temperature sweep of recovered bitumen from SMA11 10% RA and SMA11 40% RA.

To more explicitly compare the different ageing conditions and different materials, a few parameters were calculated based on the DSR temperature sweep results at 10 rad/s, including the binder performance grading (PG) high-temperature rutting parameter $G^*/\sin\delta$ at 70 °C and the increasingly popular BTSV ("Bitumen-Typisierungs-Schnell-Verfahren" in German, Binder-Fast-Characterization-Test in English) parameters. In the Superpave PG system, $G^*/\sin\delta$ is used to regulate the high-temperature rutting performance of binders. It was derived from the loss compliance J" to limit the non-recoverable strain (Petersen, et al., 1994). This parameter works quite well for neat bitumen but is known being inadequate in describing and predicting PMB's resistance to permanent deformation (Subhy, 2017). In this study, the values of $G^*/\sin\delta$ were calculated at 70 °C, which would be very close to the PG high-temperature grade of most binders in the original asphalt mixtures.

The calculation results of $G^*/\sin\delta$ at 70 °C and 10 rad/s are listed in Table 4-4 and presented in Figure 4-6. The bar chart (Figure 4-6) displays a very similar pattern as the results of softening point (Figure 4-1). Thus, $G^*/\sin\delta$ is plotted against the softening point in Figure 4-7. It should be noted that the softening point results in Figure 4-7 are normalised to water bath. This is to say that 4 °C is subtracted from the softening point values determined in the glycerol bath while the values determined in water bath remain the same. The normalisation is to ensure a uniform basis for the comparison and analysis. Additionally, those binders whose softening point was not exactly obtained, are not included in Figure 4-7.

Table 4-4. G*/sinδ of recovered bitumen at 70 °C and 10 rad/s.

Asphalt mixtures	Ageing conditions	G*/sinδ of recovered bitumen @70 °C (Pa)
ZOAB+	Original	1,84E+03
	Short-term aged	6,85E+03
	Long-term aged	7,33E+04
PA8	Original	3,34E+03
	Short-term aged	2,07E+04
	Long-term aged	5,40E+04
PA8 panacea	Original	2,50E+03
	Short-term aged	7,17E+04
	Long-term aged	4,99E+06
PA8 aramid	Original	2,72E+03
	Short-term aged	6,06E+04
	Long-term aged	3,44E+06
SMA16	Original	2,22E+03
	Short-term aged	1,63E+04
	Long-term aged	4,88E+05
SMA11 40% RA	Original	1,77E+03
	Short-term aged	4,97E+03
	Long-term aged	1,97E+04
SMA8 60% RA VMA	Original	6,83E+03
	Short-term aged	2,01E+04
	Long-term aged	2,78E+06
SMA11 10% RA	Original	5,08E+03
	Short-term aged	1,66E+04
	Long-term aged	5,01E+04

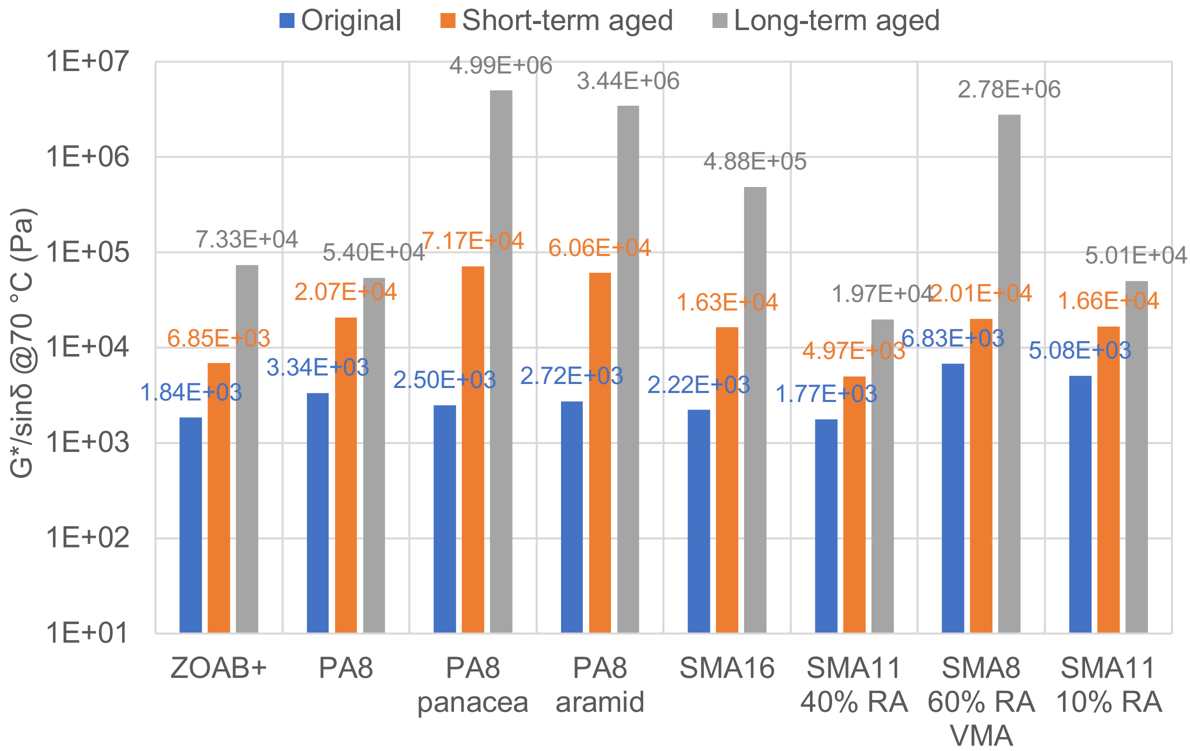

Figure 4-6. Bar chart of G*/sinδ at 70 °C and 10 rad/s.

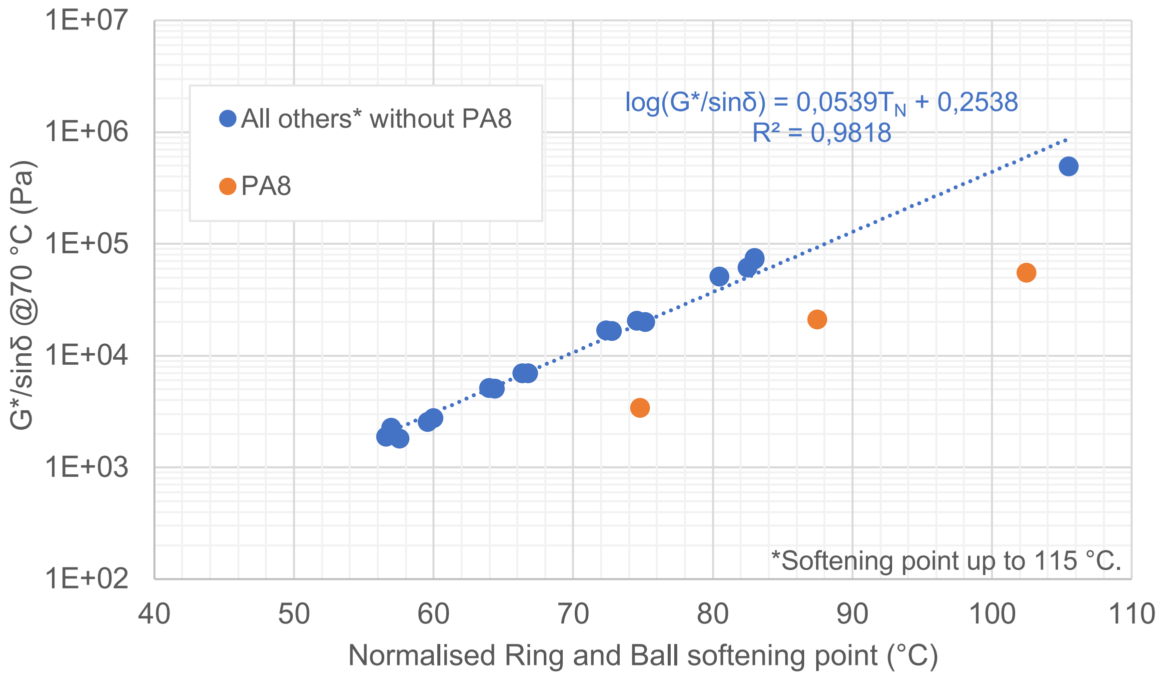

Figure 4-7. Relationship between G*/sinδ at 70 °C (10 rad/s) and the softening point normalised to water bath.

Figure 4-7 indicates that, for all binders except those from PA8, there is a very clear positive linear correlation between log(G*/sinδ) and the softening point. The distinction of PA8 binders is expectedly due to the use of PMB in the asphalt mixture. The polymer modification resulted in relatively high softening point of the binder. The stiffening effect of ageing on the PMB binder, however, could still be seen in the test results. It seems that the asphalt mixture with PMB is more resistant to ageing (namely smaller change in G*/sinδ after ageing) than those of the same gradation type.

For all other binders except those from PA8, the G*/sinδ results lead to similar conclusions as for the softening point. The G*/sinδ value of binder increases after ageing of the asphalt mixture. The longer the ageing conditioning lasts, the more it increases after the ageing. The G*/sinδ results also indicate that the sensitivity of different asphalt mixtures to ageing is different. For example, the changes of SMA11 40% RA and SMA11 10% RA in G*/sinδ were relatively small after ageing, but the changes of PA8 panacea and PA8 aramid were relatively big. The PA gradation and smaller aggregate size of PA8 panacea and PA8 aramid could probably explain this.

The BTSV method (Schrader & Wistuba, On the use of a novel Binder-Fast-Characterization-Test, 2019; Alisov, Riccardi, Schrader, Cannone Falchetto, & Wistuba, 2020) is developed as an alternative test to evaluate the high-temperature properties of bitumen with DSR. This method is based on the identified phenomenon that, at 10 rad/s, the most common bituminous binders tend to reach the G* level of 15 kPa at their respective softening point (Ring & Ball method). A temperature sweep at 10 rad/s with DSR can thus help to determine the iso-modulus temperature (T_{BTSV}, indicating the binder stiffness/hardness) and phase angle (δ_{BTSV}, reportedly indicating the degree of modification) corresponding to the G* of 15 kPa. These parameters reflect the softening state of bitumen and therefore can be used to characterize the bitumen behaviour at high temperatures. This test has been successfully used in Germany to replace the traditional Ring & Ball method and has been standardized as the German technical standard FGSV 720 “AL DSR-Prüfung (BTSV)”. According to the related research on rejuvenating and recycling the reclaimed asphalt pavement (Walther, et al., 2019; Schrader J. , Wistuba, Cannone Falchetto, Riccardi, & Alisov, 2020), the BTSV protocol is even effective for evaluating different rejuvenators and determining the rejuvenator’s proportions.

Based on the DSR temperature sweep results presented above, the BTSV method was employed to analyse the recovered binders in this study. In principle, it was logarithmic interpolation that was applied for G* to determine T_{BTSV} at which G* is equal to 15 kPa at 10 rad/s (linear interpolation for temperature). Due to the extremely high stiffness of some binders recovered from long-term aged asphalt mixtures, however, a part of the determinations was by extrapolation. The corresponding δ_{BTSV} (phase angle at T_{BTSV}) was determined as well by either linear interpolation or extrapolation. The BTSV analysis results are listed in Table 4-5 and presented in Figure 4-8 and Figure 4-9.

Table 4-5. BTSV analysis of recovered bitumen (G*=15 kPa @10 rad/s).

Asphalt mixtures	Ageing conditions	T_{BTSV} (°C)	δ_{BTSV} (°)
ZOAB+	Original	54,2	77,9
	Short-term aged	63,8	73,2
	Long-term aged*	82,6	64,7
PA8	Original	49,6	56,2
	Short-term aged	70,2	47,1
	Long-term aged*	82,0	42,4
PA8 panacea	Original	56,4	74,5
	Short-term aged	81,9	62,4
	Long-term aged*	153,1	62,6
PA8 aramid	Original	57,2	74,4
	Short-term aged	80,6	63,2
	Long-term aged*	138,5	58,1
SMA16	Original	55,5	77,3
	Short-term aged	70,0	68,7
	Long-term aged*	103,9	54,0
SMA11 40% RA	Original	53,8	76,8
	Short-term aged	61,4	73,3
	Long-term aged	71,6	68,6
SMA8 60% RA VMA	Original	63,2	66,7
	Short-term aged	71,6	65,8
	Long-term aged*	134,8	55,5
SMA11 10% RA	Original	61,8	78,0
	Short-term aged	70,5	74,5
	Long-term aged	78,9	71,4

* These determinations were by extrapolation, while the others were by interpolation.

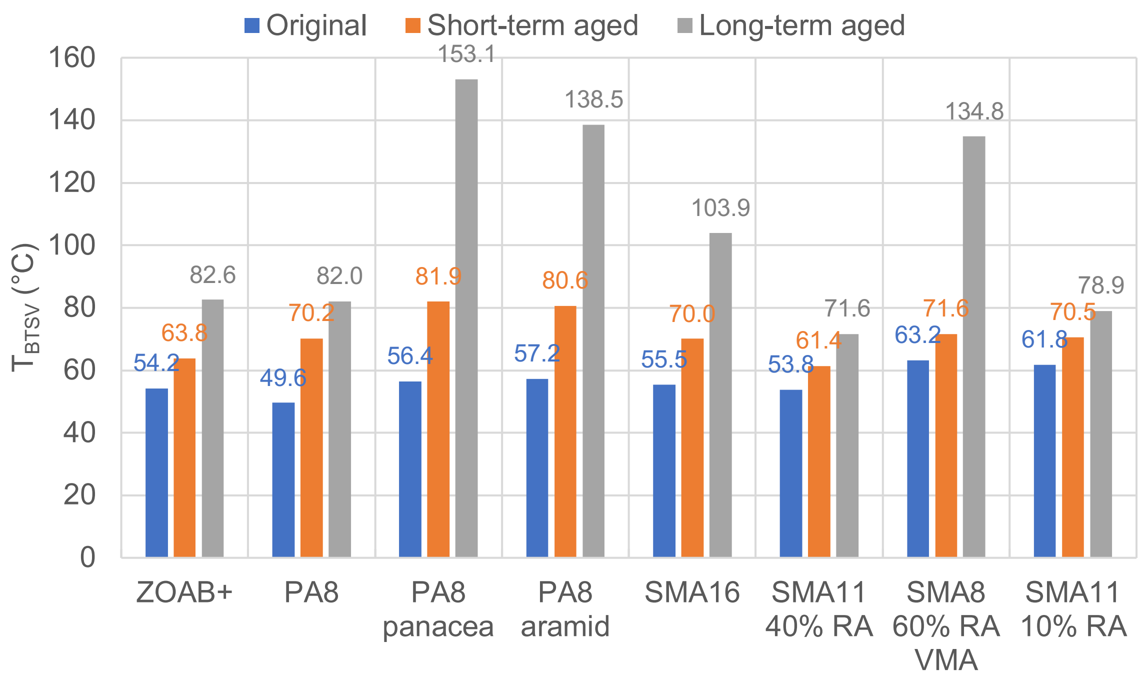

Figure 4-8. Bar chart of the BTSV parameter T_{BTSV}.

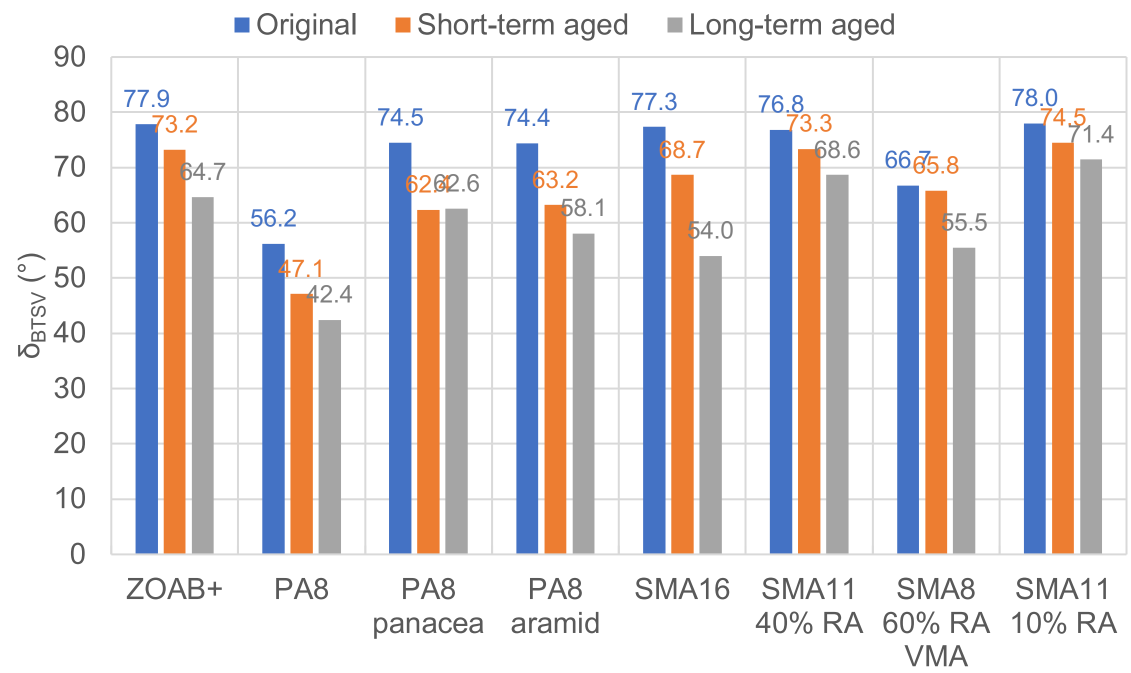

Figure 4-9. Bar chart of the BTSV parameter δ_{BTSV}.

The bar chart of T_{BTSV} (Figure 4-8) also displays a very similar pattern as the results of softening point (Figure 4-1) and G*/sinδ (Figure 4-6). As the T_{BTSV} of a neat bitumen is known to be very close to its softening point, T_{BTSV} is firstly plotted against the softening point in Figure 4-10. The softening point results are normalised to water bath and only those binders with exactly determined softening point are included in Figure 4-10.

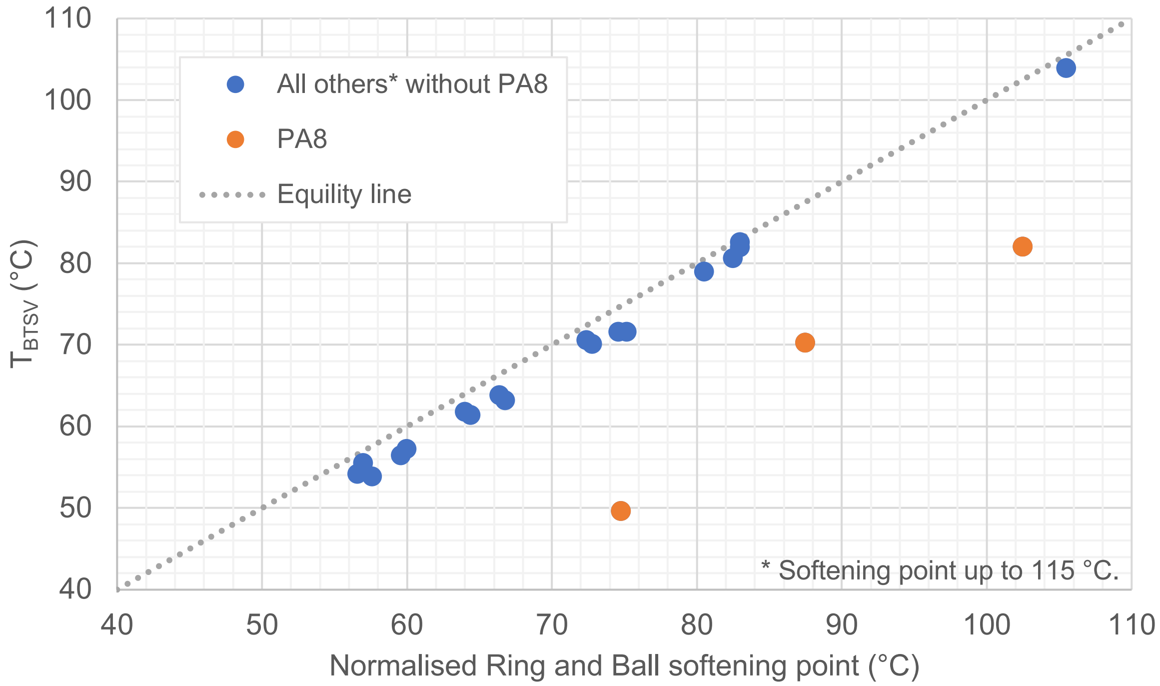

Figure 4-10. Relationship between T_{BTSV} and the softening point normalised to water bath.

Figure 4-10 indicates that, for all binders except those from PA8, the T_{BTSV} is very close to the softening point. The distinction of PA8 binders is expectedly due to the use of PMB in the asphalt mixture. PMB usually shows a lower G* value than neat bitumen at the softening point (Alisov, Riccardi, Schrader, Cannone Falchetto, & Wistuba, 2020; Fan, Lin, Wei, Zhang, & Wang, 2014; Zhu, Lu, Langfjell, & Gudmarsson, 2021). When the *G** level for neat bitumen (15 kPa) is used to determine the T_{BTSV}, this temperature tends to underestimate the softening point of PMB. However, the stiffening effect of ageing on the PMB binder could still be seen in the BTSV analysis results. For all other binders except those from PA8, the T_{BTSV} results lead to same conclusions as for the softening point (Section 4.5.2).

The next step is to analyse the relationship between T_{BTSV} and G*/sinδ at 70 °C. Figure 4-11 presents the plot of T_{BTSV} against G*/sinδ at 70 °C and 10 rad/s. All binders are included in the plot, even the hardest after long-term ageing of the asphalt mixture. It indicates that there is a very clear positive linear correlation between T_{BTSV} and log(G*/sinδ). This is valid for all binders, including those from PA8. Since T_{BTSV} is based on a constant G* level (15 kPa at 10 rad/s) and the value of G*/sinδ depends largely on the G* value (sinδ affecting only limitedly) as well, it is not a surprise that a clear correlation could be seen between them. A remaining question to be answered, however, is what T_{BTSV} can indicate more than G*/sinδ in terms of binder performance, especially for PMBs. This question could not be answered in this study, due to the limited number of PMB, among others.

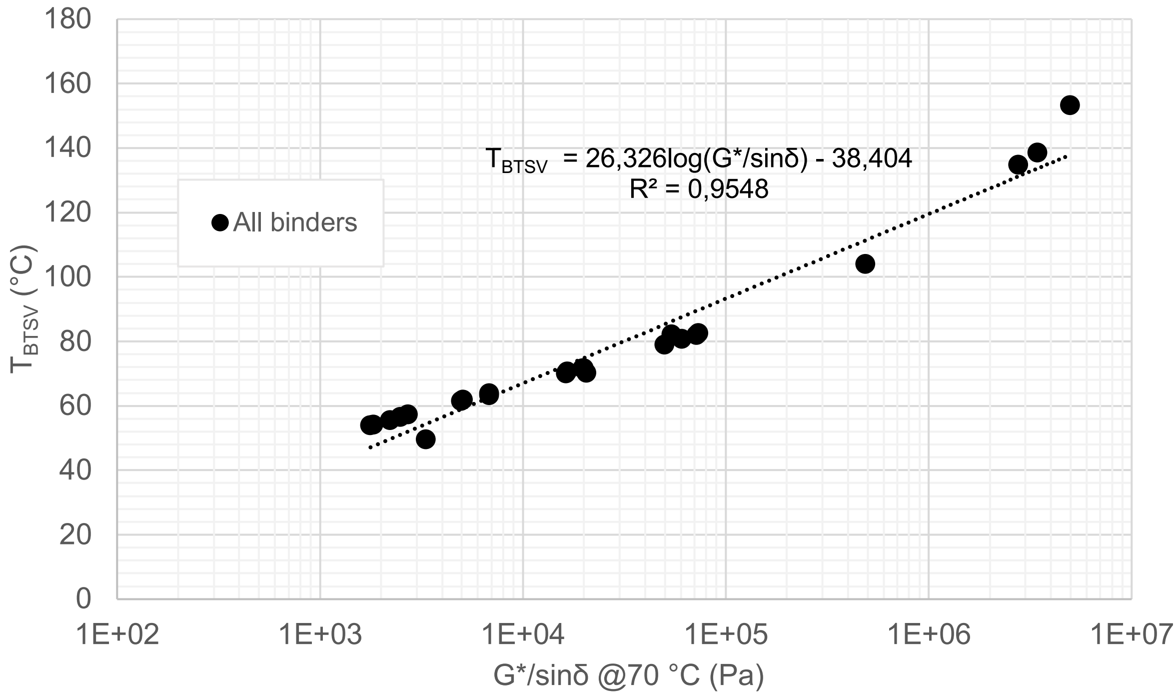

Figure 4-11. Relationship between T_{BTSV} and G*/sinδ at 70 °C (10 rad/s).

Another parameter from the BTSV analysis is the δ_{BTSV}. The analysis results in Figure 4-9 show that δ_{BTSV} of binder decreases after ageing of the asphalt mixture. The longer the ageing conditioning lasts, the more it decreases after the ageing. This means that the ageing makes binders less viscous at the G* level of 15 kPa (10 rad/s). However, the sensitivity of different asphalt mixtures to ageing is different. For example, the changes of SMA11 40% RA and SMA11 10% RA in δ_{BTSV} were relatively small after ageing, compared to the other asphalt mixtures. Additionally, the δ_{BTSV} values of asphalt mixtures were already different before any ageing. The values of original PA8 and SMA8 60% RA VMA were lower than the others. The use of PMB in PA8 resulted in relatively low δ_{BTSV} of the binder in freshly mixed asphalt mixture while the incorporation of reclaimed asphalt materials was probably the reason for the relatively low δ_{BTSV} of binder recovered from original SMA8 60% RA VMA.

4.5.4 Summary

Test results of recovered binders indicate that the ageing of asphalt mixture hardens binders and makes them less viscous. The longer the ageing conditioning lasts, the harder and less viscous binders become after the ageing. However, the sensitivity of different asphalt mixtures to ageing is different. The DSR results suggested a shifting effect for both the G* and δ curves towards higher temperatures after ageing, without significantly changing the shape of curves. In addition, the use of PMB in PA8 resulted in very distinct properties of the recovered binder. The incorporation of reclaimed asphalt materials could lead to harder and less viscous recovered binders. On the other hand, the use of rejuvenating additives can soften the binders while their effects on ageing behaviour of the asphalt mixture are expectedly variant-specific.

4.6 *Water sensitivity. Moisture induced stress test*

4.6.1 Background

Pavements are subjected to various amounts of moisture in different physical states depending on the location and climatic conditions. Moisture in either liquid, vapor or frozen state is one of the major damaging factors and is also one of the most difficult distresses to recognize in asphalt concrete (AC) pavements. Moisture contributes to various forms of damages such as stripping, ravelling, rutting, shoving, cracking and so on (Chen & Huang, 2008; Htet, 2007; Varveri, Avgerinopoulos, & Scarpas, 2015; Showkat & Singh, 2021).

Moisture damage of AC pavements can be divided into long-term damage and short-term damage. Long-term damage is mainly caused by moisture diffusion. Moisture entering through the surface or coming up from the bottom changes the physio-chemical properties of the binder through a molecular or emulsification process (Varveri, Avgerinopoulos, & Scarpas, 2015; Ahmad, Mannan, Islam, & Tarefder, 2018). This reduces the cohesive strength of the binder as well as weakens the adhesive bond between the binder and aggregates. Short-term damage can be attributed to mechanical damage due to pumping action and cyclic pore pressure generation due to the moving traffic load. This causes erosion and accelerates the long-term damage of the AC layer. Generally, moisture damage in AC layers is influenced by the ambient temperature and the magnitude of pore pressure generated by the traffic loading (Varveri, Avgerinopoulos, & Scarpas, 2015; Showkat & Singh, 2021).

For pavement design and maintenance activities, it is essential to evaluate the AC mixtures with respect to moisture damage susceptibility. The test method used for this purpose should be quick and convenient besides being reasonable and rational (Varveri, Avgerinopoulos, & Scarpas, 2015). Some of the test methods used throughout the world are the boiling water (ASTM D3625), static immersion (AASHTO T182), rolling bottle (CEN prEN 12697-11), Tunnicliff and Root conditioning (NCHRP 274), the saturation ageing tensile stiffness (SATS; EN 12697-45), the Hamburg wheel tracking (HWT; AASHTO T234) and the modified Lottman (AASHTO T283) tests (freeze–thaw cycle) (Terrel & Shute, 1989; Chen & Huang, 2008; Varveri, Avgerinopoulos, & Scarpas, 2015). In Europe, the method ‘Determination of the water sensitivity of bituminous specimens (EN 12697-12:2018)’ is used. However, some of the drawbacks of the above-mentioned methods are that these are quite variable and lacks any tight control over the water saturation, the results do not correlate well with field performances, it takes a long time for testing and getting the results and most significantly these methods disregard the pumping action of water and thus do not estimate the short-term damage of AC due to moisture (Varveri, Avgerinopoulos, & Scarpas, 2015). To overcome some of these issues, the moisture induced sensitivity test (MIST) was developed (Mallick, Pelland, & Hugo, 2005; Chen & Huang, 2008; Htet, 2007; Varveri, Avgerinopoulos, & Scarpas, 2015; Showkat & Singh, 2021). It is a relatively quick method that simulates stripping due to repeated pore pressure generation as well as elevated in-service temperatures. The elevated temperature also simulates the long-term damage to some extent (Buchanan & Vernon, 2005; Mallick, Pelland, & Hugo, 2005; Ahmad, Mannan, Islam, & Tarefder, 2018). Hence for this study, the MIST approach was adopted to examine the moisture susceptibility of the AC mixtures under investigation.

4.6.2 Objectives and methodology

The objective of this study was to investigate the moisture susceptibility of eight AC mixtures using the MIST method of moisture conditioning. The specimens of the different AC mixes were tested for stiffness modulus in their initial states and then again after the MIST conditioning. Then the changes in the stiffness modulus values of the specimens due to MIST conditioning were analysed.

4.6.3 Experimental Procedure

4.6.3.1 Tested AC mixes

In this study, eight AC mixes were tested for moisture susceptibility. The specimens were prepared in the laboratory using the Marshal compaction method, EN 12697-30. The size of the cylindrical specimens was 100 mm in diameter and 40 mm in thickness. The bulk densities and air voids of the specimens were determined in accordance with the European standards EN 12697-6 and EN 12697-8, respectively. Three specimens of each mix type were prepared and tested. The designations of the tested mixes and mean values (of three specimens of each mix types) of their bulk densities and air void contents are presented in Table 4-2

4.6.3.2 Stiffness modulus test

The stiffness modulus test was conducted twice on each specimen. First time, the tests were conducted before the MIST conditioning at the initial or reference states of the specimens after submerging the specimens in water at 10°C for about an hour. The reason for submerging the specimens in water was to compare the stiffnesses of the specimens in identical conditions before and after the MIST conditioning. Previous experiences have shown that the initial stiffness of the specimens may not be the same in dry versus wet conditions. Each of the specimens was tested for the second time after the MIST conditioning in a similar manner. The stiffness modulus tests were conducted in indirect tension mode and in accordance with the method prescribed by the European Standard EN 12697-26. The tests were performed at 10°C. The indirect tensile test apparatus is shown in Figure 4-12. Indirect tensile test apparatus. Figure 4-12.

Figure 4-12. Indirect tensile test apparatus.

4.6.3.3 MIST conditioning

The MIST is an accelerated moisture conditioning method under cyclic pore pressure generation. It was designed to simulate the stripping mechanisms due to water under repeated traffic loading and elevated in place temperatures. Tests can be conducted on both compacted laboratory specimens and core drilled field samples in relatively short times (< 24 hours). In the MIST equipment, shown in Figure 4-13, the temperature, pressure and number of cycles are adjustable. It is an automated and sensors monitored process. The conditioning is done inside a cylindrical sample chamber (up to 3 samples can be conditioned at a time). The device includes a hydraulic pump and piston mechanism. It cyclically adds and relieves pressure inside the sample chamber through a bladder inside the sample tank. The test is performed at elevated temperatures to further accelerate the potential long-term damage. The test involves placing a specimen inside the sample chamber, filling the chamber with water, closing the sample chamber lid and starting the test. The machine automatically heats up the water/specimen and starts cycling (to the desired temperature, pressure and number of cycles).

The MIST conditioning method is standardized by the ASTM D7870/D7870M−20. However, for this study, a customised approach was followed. The MIST conditioning was conducted at 40°C, at 0.28 MPa (40 psi) pressure for 12000 cycles. The temperature was set lower than the ASTM standard’s recommendation to avoid any deformation of the specimens due to the combined effect of elevated temperature and high pressure. The number of cycles was chosen to be higher (12000 vs 3500) to compensate for the lower temperature and to detect any significant impact of moisture since the specimens were water resistant (Ahmad, Mannan, Islam, & Tarefder, 2018; Showkat & Singh, 2021). After the conditioning, the specimens were submerged in 10°C water for about an hour and tested for stiffness modulus in wet condition at 10°C.

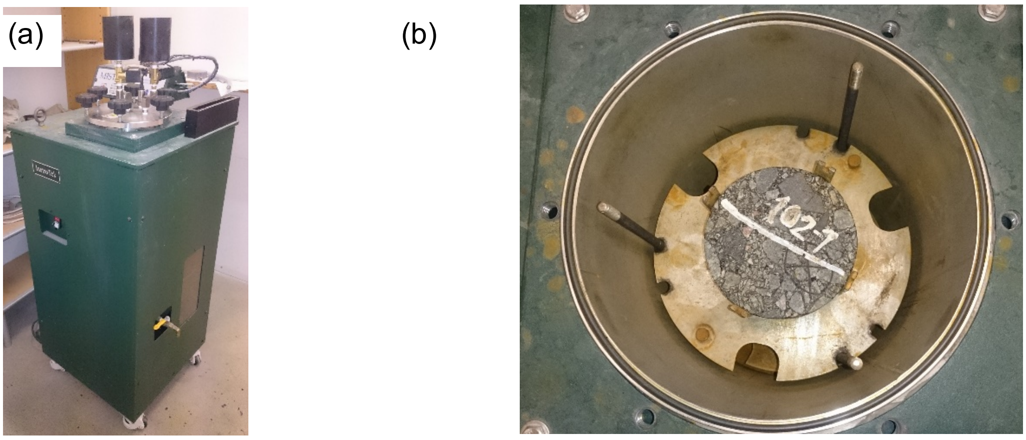

Figure 4-13. (a) MIST equipment, (b) specimen inside the MIST chamber prepared for conditioning (water not poured yet).

4.6.4 Results and discussions

For each mix types, three specimens were tested. Means (of three specimens) of the stiffness modulus values before and after the MIST conditioning for the eight mix types are shown in Figure 4-14. This figure also shows the error bars which represent the maximum and minimum values of the measured stiffness moduli for each mix group.

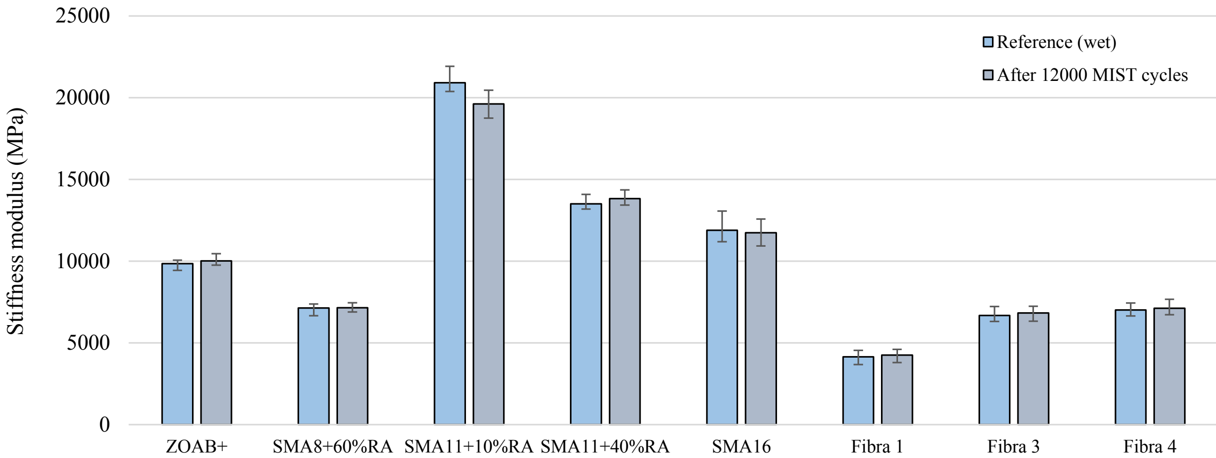

Figure 4-14. Measured stiffness moduli (mean values with error bars) before (reference) and after the MIST conditioning.

In Figure 4-15, the changes in the stiffness modulus values (%) after the MIST conditioning is shown where a positive value indicates an increase in stiffness after the conditioning. From the figures, it can be identified that except for SMA11+10%RA and SMA16, all the specimens showed some increase in their respective stiffness modulus. The maximum change in stiffness was for SMA11+10%RA which is -6.2%. However, for this mix, the difference between the stiffness modulus values within the three specimens are 7.4% and 8.7% with respect to the mean values, respectively for the reference test and after the MIST conditioning. Thus, it may be concluded that the changes in the stiffness moduli are within the natural statistical variation and may be considered insignificant. One possible reason for the increase in stiffness moduli may be that more water was trapped inside the pores of the specimens after the MIST conditioning due to the cyclic application of pore pressure. Again, increase in binder stiffness due to aging in response to moisture conditioning has been reported as well (Ahmad et al., 2018).

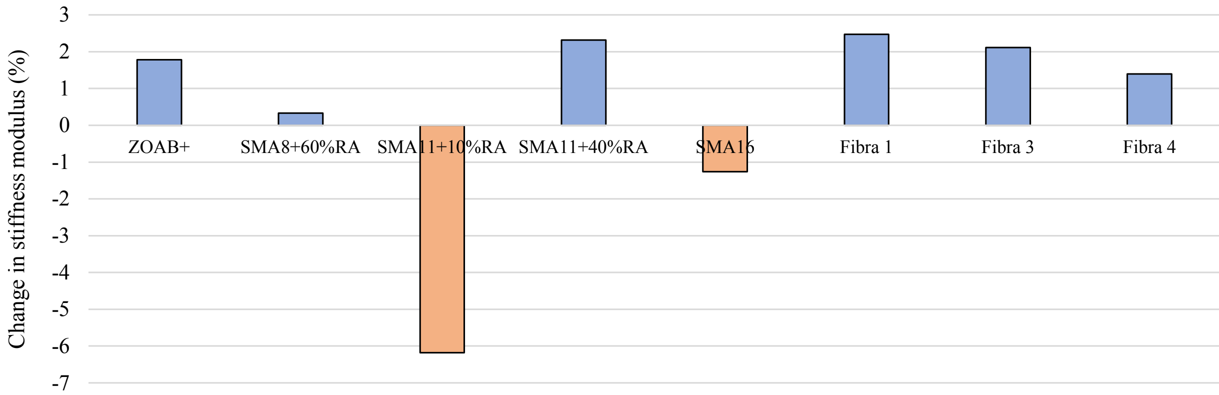

Figure 4-15. Change in stiffness modulus (%) after the MIST conditioning (positive value means increase in stiffness after the conditioning).

4.6.5 Conclusions

In this study, the moisture sensitivity of eight AC mixes were investigated using the MIST conditioning method. Comparing the stiffness modulus values before and after the MIST conditioning, it appears that except for SMA11+10%RA and SMA16, none of the mixes are susceptible to moisture. Although SMA11+10%RA and SMA16 showed some decrease in stiffness after the MIST conditioning, it could simply be due to normal statistical variation in testing. However, it should be noted that the MIST conditioning method primarily simulates the short-term mechanical damage due to moisture. It was found that different kinds of binders may exhibit different behaviours in response to short-term and long-term moisture conditioning (Varveri, Avgerinopoulos, & Scarpas, 2015; Ahmad, Mannan, Islam, & Tarefder, 2018). Thus, for more comprehensive evaluation of moisture susceptibility, other methods such as the EN 12697-12:2018 should be used in conjunction with MIST (Varveri, Avgerinopoulos, & Scarpas, 2015). Similarly, here the impact of moisture only on the stiffness modulus values were evaluated. The moisture impact on other properties such as the indirect tensile strength should be investigated as well (Terrel & Shute, 1989; Chen & Huang, 2008; Varveri, Avgerinopoulos, & Scarpas, 2015).

4.7 Mechanical Properties of Mixtures and Performance Modelling

The report presents laboratory evaluation of the mechanical properties of 8 different types of asphalt concrete surface mixtures, namely, 4 stone mastics asphalt (SMA) and 4 porous asphalt mixtures (PA). The tests consist of cyclic indirect stiffness modulus (IDT) and dynamic shear modulus tests. Additionally, modelling of the permanent deformation using the PEDRO (Said S. F., Hakim, Oscarsson, & Hjort, 2011) and ERAPave PP (Ahmed & Erlingsson, 2021) models have been conducted. The PEDRO model was utilized to evaluate the resistance to rutting of the SMA and PA mixtures whereas ERAPave PP was applied to evaluate the influence of the different SMA and PA mixtures on the rutting and fatigue cracking evolution of three types of pavement structures made of the SMA and PA surface mixtures. The subsequent sections present the results of laboratory tests and modelling.

4.7.1 Frequency sweep stiffness modulus test (IDT)

The cyclic indirect tensile test was conducted to characterize the stiffness of the asphalt mixtures. The test consists of applying a certain number of cyclic (sinusoidal) loading along the vertical diametral plane of a cylindrical specimen to achieve a constant peak tensile strain along the horizontal diametral plane perpendicular to the loading plane. The test was conducted according to the European standard EN 12697-26:2018 – Annex F. Laboratory compacted specimens having a dimeter of 100 mm and thickness of 40 mm were tested at three temperatures (-5, 10 and 20°C) and 8 loading frequencies (16, 10, 5, 2, 1, 0.5, 0.1, 0.05 Hz).

The test results of the IDT tests are presented as master curves of the stiffness modulus and phase angle, respectively. A reference temperature of 10 °C was selected to construct the master curves. A sigmoidal fitting function was used for stiffness modulus master curves, shown in Equation 4-1, and a compound-sigmoidal function shown in Equation 4-2 was used to fit the master curves for phase angle. Arrhenius equation, Equation 4-3, was employed as a shifting function.

$$log(E) = \delta + \frac{\alpha}{1+exp(\beta - \gamma\, log(f_r))}$$

Equation 4-1

$$\varphi = d\left(1 - \frac{e^{\frac{f_r - a}{e}}}{1 + e^{\frac{f_r - a}{e}}}\right) + \frac{c}{1 + \left(\frac{f_r - a}{b}\right)^2}$$

Equation 4-2

$$log(a_T) = R\left(\frac{1}{T+273} - \frac{1}{T_{ref}+273}\right)$$

Equation 4-3

$$f_r = a_T f_T$$

Equation 4-4

where E is the dynamic modulus, f_r is the reduced frequency, f_T is the frequency at temperature T; α, β, γ and δ are sigmoidal fitting function parameters for dynamic modulus master curve; ϕ is phase angle; *a, b, c, d* and *e* are phase angle master curve fitting parameters; a_T is the shift factor, T is the temperature in °C, T_{ref} = 10°C is the reference temperature and R is constant.

The speed, depth and loading frequency relationship, for example, as shown in Equation 4-5can be used to convert traffic speed into loading frequency (Brown, 1973):

$$log\, t = 0.5z - 0.2 - 0.94\, log\, V$$

Equation 4-5

where *t* is the loading time in sec, *z* is the depth in meters and *V* is the speed in km/h. The loading frequency is then calculated as $f_T = \frac{1}{2\pi t}$.

4.7.1.1 SMA IDT test results

Figure 4-16 and Figure 4-17 present the master curves of the stiffness modulus and phase angle, respectively, for SMA mixtures. Equation 4-1, Equation 4-2, Equation 4-3, and Equation 4-4 were used to fit the measured data and the fitting parameters for the master curves are given in Table .

The SMA11 10% RA mixture showed a higher stiffness modulus and lower phase angle values compared to the other SMA mixtures as shown in Figure 4-16. Thus, SMA11 10% RA mixture may provide better resistance to permanent deformation as well as fatigue cracking due to the higher elasticity. SMA11 40% RA demonstrated a slightly higher modulus than SMA16 mixture. However, SMA11 40% RA had a slightly lower phase angle than SMA 16. SMA8 60% RA on the other hand showed the least stiffness modulus among the SMA mixtures.

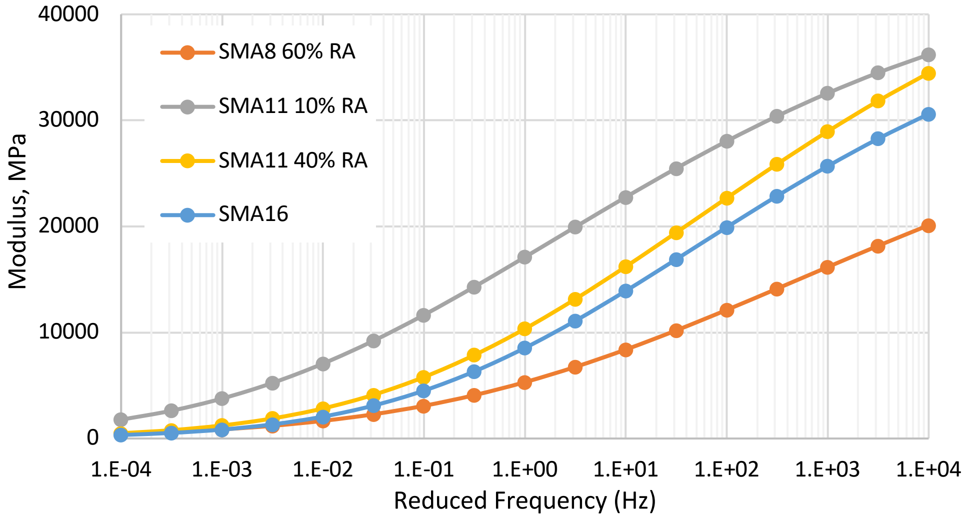

Figure 4-16. Stiffness modulus master curves for SMA mixtures at reference temperature of 10°C.

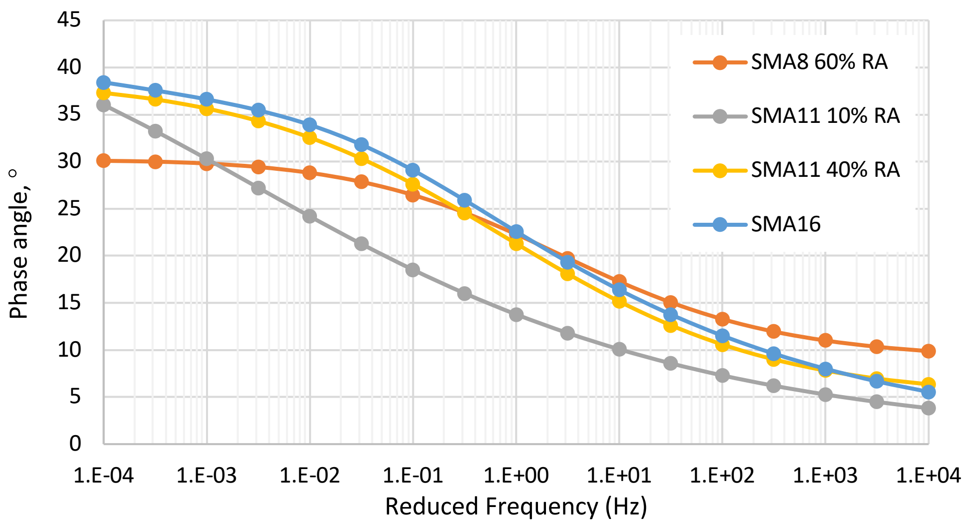

Figure 4-17. Phase angle master curves for SMA mixtures at reference temperature of 10°C.

Table 4-6. Fitting parameters for stiffness modulus and phase angle master curves for SMA mixtures.

Parameter	SMA8 60% RA	SMA11 10% RA	SMA11 40% RA	SMA16
δ	1.21	0.39	0.50	0.72
α	3.35	4.28	4.21	3.92
β	-1.11	-2.19	-1.62	-1.51
γ	0.35	0.37	0.38	0.42
A	0.41	-3.76	-0.10	-1.50
B	19.34	3.82	96.52	2.81
C	9.53	6.43	4.98	9.95
D	21.32	56.62	33.92	43.65
E	1.04	2.55	1.29	2.25
R	12468.57	13842.63	12657.73	11727.30

4.7.1.2 PA IDT test results

The stiffness modulus and phase angle master curves for PA mixtures are presented in Figure 4-18 and Figure 4-19, respectively. Table presents the corresponding fitting parameters for the master curves. As shown in the figures, ZOAB+ mixture exhibited a higher stiffness values at higher loading frequencies and slightly lower modulus at higher temperature or lower frequencies. Also, the phase angle values, ZOAB+ showed a higher phase angle values especially at intermediate to lower frequencies. PA8 panacea and PA8 aramid showed a very similar levels of stiffness modulus and phase angle for all loading frequencies. The PA8 mixture showed the lowest stiffness modulus values among all the PA mixtures.

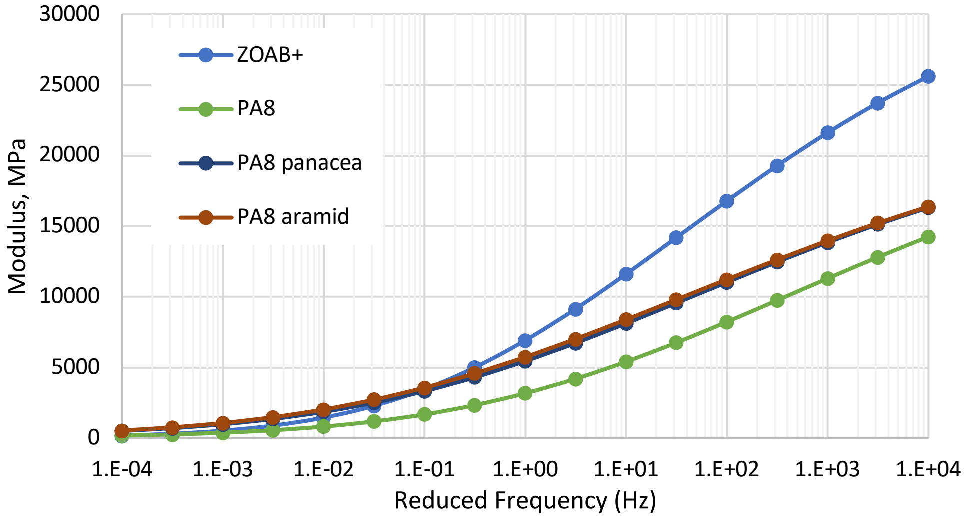

Figure 4-18. Stiffness modulus master curves for PA mixtures at reference temperature of 10°C.

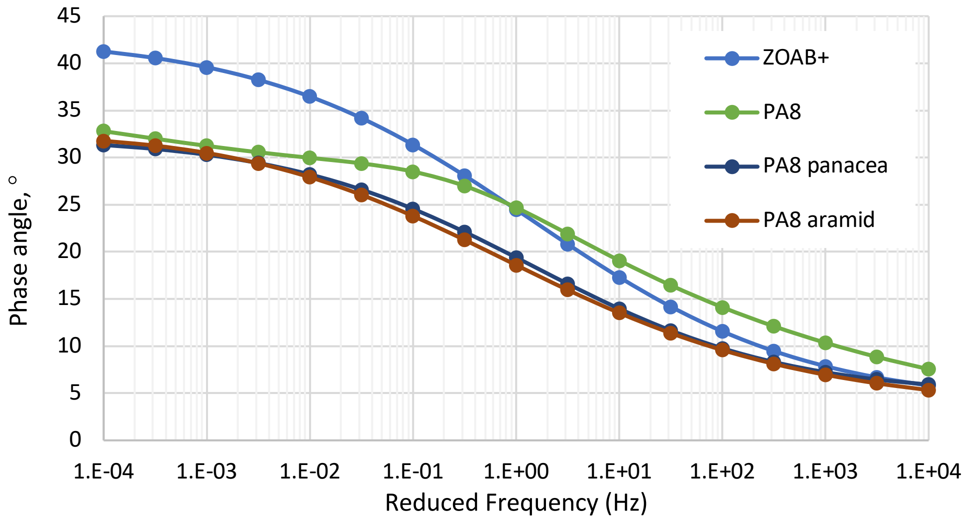

Figure 4-19. Phase angle master curves for PA mixtures at reference temperature of 10°C.

Table 4-7. Fitting parameters for stiffness modulus and phase angle master curves for PA mixtures.

Parameter	ZOAB+	PA8	PA8 Panacea	PA8 Aramid
δ	0.50	1.11	1.49	1.22
α	4.05	3.27	2.89	3.16
β	-1.56	-1.00	-1.26	-1.41
γ	0.45	0.39	0.39	0.37
A	0.16	-0.57	0.16	-0.20
B	357.92	2.14	888.89	8.56
C	3.78	7.56	4.77	5.01
D	39.11	39.40	27.46	29.30
E	1.32	2.72	1.22	1.37
R	11806.01	11208.57	12652.61	12782.99

4.7.2 Frequency sweep shear modulus test

The dynamic shear modulus test was conducted in accordance with the method and the equipment developed at Swedish National Road and Transport Research Institute, VTI. According to this method, the two sides of a cylindrical asphalt specimen having diameter of 150 mm and thickness of ¼ of the sample diameter is glued to two steel plates using epoxy. The glued specimen is then mounted on the shear box device where one of the plates is rigidly fixed and the other is exposed to a vertical sinusoidal cyclic loading over a range of frequencies. Further details on the testing procedure can be found in (Said, Hakim, & Oscarsson, 2013). The dynamic shear testing is usually conducted at four temperatures: -5, 10, 30 and 50°C, and eight loading frequencies: 16, 8, 4, 2, 1, 0.5, 0.1 and 0.05 Hz. Figure 4-20 shows the shear box apparatus and the test setup. The shear test results are presented as master curves of shear modulus and phase angle and Equation 4-1, Equation 4-2, Equation 4-3, and Equation 4-4 were used to construct the master curves from the measured data.

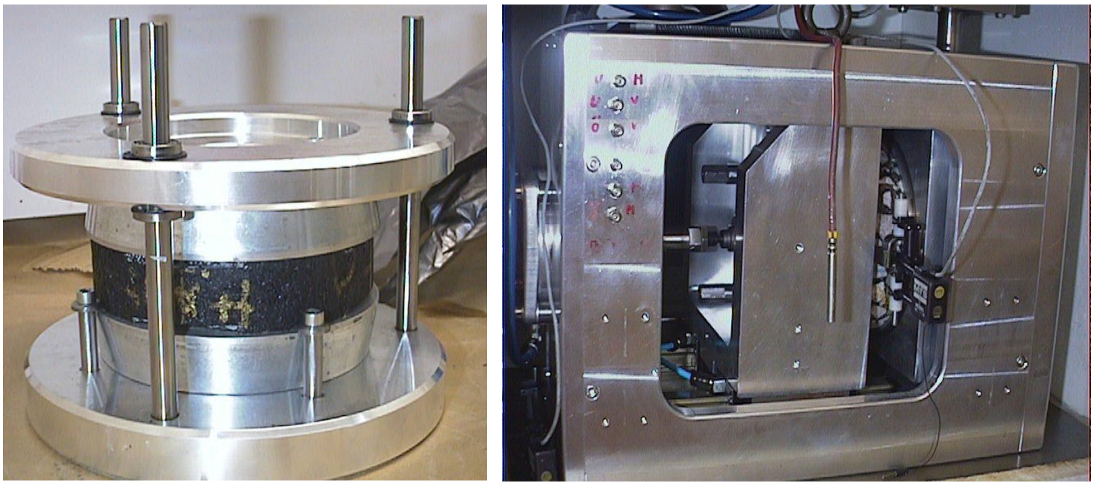

Figure 4-20. Dynamic shear modulus test setup.

4.7.2.1 Shear test results for SMA mixtures

The shear modulus and phase angle master curves for SMA mixtures are shown in Figure 4-21 and Figure 4-22, respectively. The fitting parameters for the master curves are given in Table .

As for the IDT stiffness modulus tests, the SMA11 10% RA mixture showed a higher shear modulus values compared to the other SMA mixtures as shown in Figure 4-21. SMA11 40% RA and SMA16 mixtures demonstrated a very similar shear modulus values for all frequency ranges. The shear modulus of SMA8 60% RA was least among the SMA mixtures particularly for intermediate to higher frequency regions.

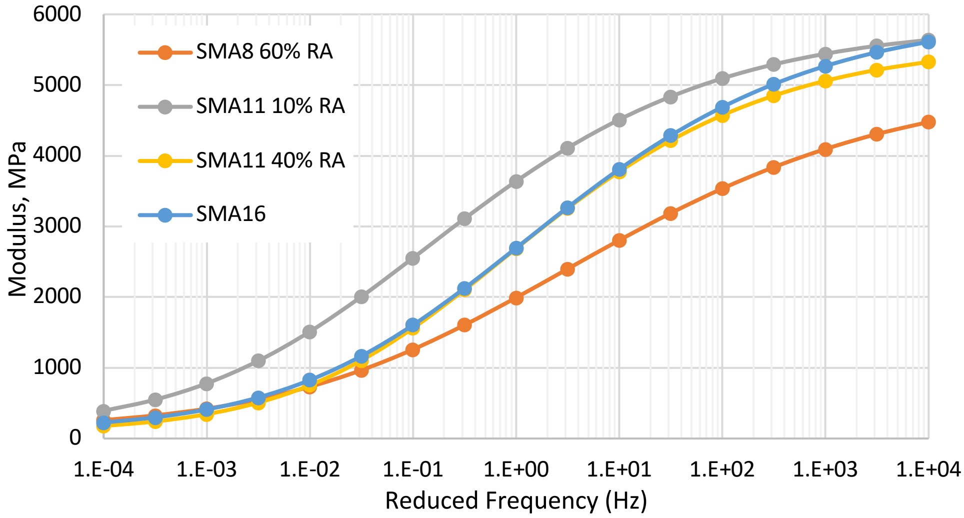

Figure 4-21. Shear modulus curves for SMA mixtures at reference temperature of 10°C.

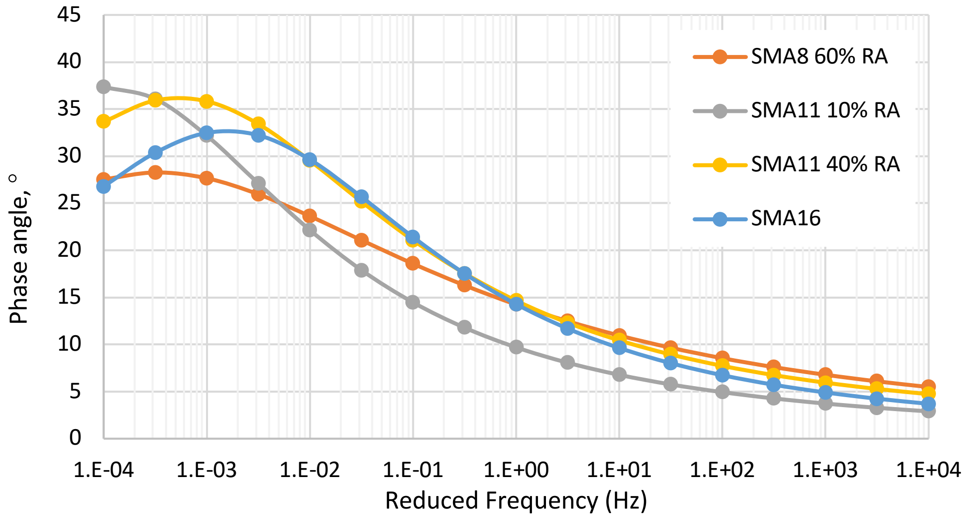

Figure 4-22. Phase angle master curves for SMA mixtures at reference temperature of 10°C.

Table 4-8. Fitting parameters for shear modulus and phase angle master curves for SMA mixtures.

Parameter	SMA8 60% RA	SMA11 10% RA	SMA11 40% RA	SMA16
δ	1.96	1.90	1.79	1.94
α	1.74	1.87	1.95	1.41
β	-1.19	-2.08	-1.63	-0.50
γ	0.56	0.65	0.71	0.86
a	-4.10	-3.92	-3.27	-1.47
b	3.69	2.32	2.64	2.87
c	31.93	35.94	35.61	28.17
d	-9.44	2.86	1.16	2.05
e	0.71	1.98	291.27	20.17
R	11079.25	11912.53	11045.08	10013.58

4.7.2.2 Shear test results for PA mixtures

Figure 4-23 and Figure 4-24 display the shear modulus and phase angle master curves for PA mixtures, respectively. Figure 4-17The fitting parameters for the master curves are given in Table . The ZOAB+ mixture exhibit a higher shear modulus values at higher loading frequencies and slightly lower modulus at higher temperature or lower frequencies. Also, PA8 panacea and PA8 aramid showed a very similar levels of shear modulus and phase angle values for all loading frequencies. The shear modulus of PA8 mixture was the lowest among the PA mixtures.

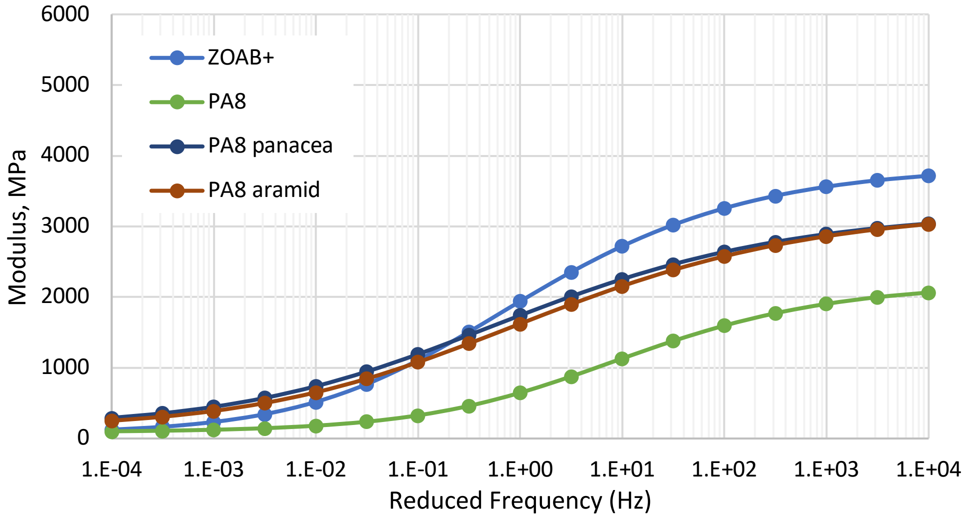

Figure 4-23. Shear modulus master curves for PA mixtures at reference temperature of 10°C.

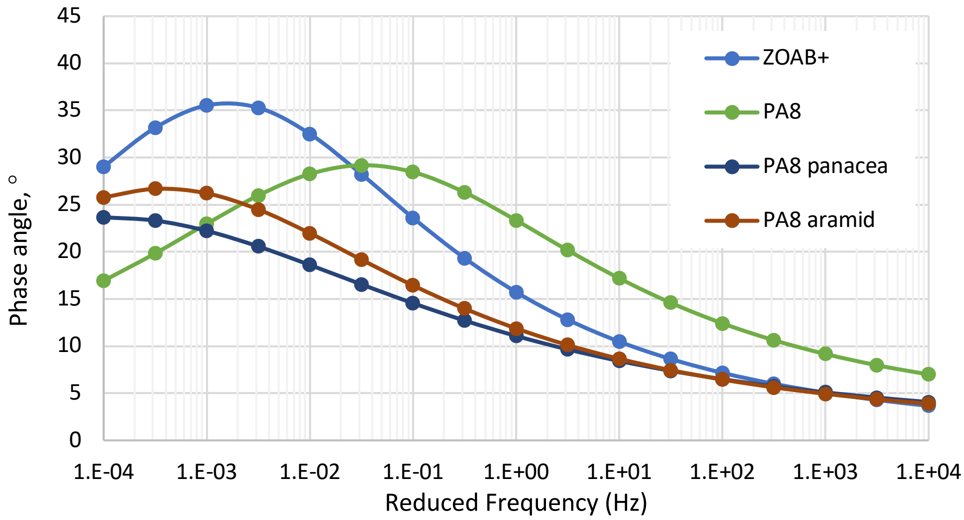

Figure 4-24. Phase angle master curves for PA mixtures at reference temperature of 10°C.

Table 4-9. Fitting parameters for shear modulus and phase angle master curves for PA mixtures.

Parameter	ZOAB+	PA8	PA8 Panacea	PA8 Aramid
δ	1.73	1.94	2.13	2.05
α	1.85	1.41	1.38	1.46
β	-1.65	-0.50	-1.43	-1.35
γ	0.77	0.86	0.64	0.63
a	-2.80	-1.47	-3.40	-3.41
b	2.56	2.87	3.72	3.06
c	37.07	28.17	20.14	26.55
d	-2.59	2.05	6.02	0.30
e	12.24	20.17	0.84	0.96
R	10003.51	10013.58	10001.35	10001.58

4.7.3 Predicted effects of ageing on asphalt mixtures

In order to evaluate the effects of ageing on mechanical properties of asphalt mixtures, this study used prediction models to obtain the master curves after ageing. Test data of recovered binders were input to the prediction models. This section describes the adopted prediction approach and presents the prediction output.

4.7.3.1 Prediction models

The Hirsch model (Christensen, Pellinen, & Bonaquist, 2003) was adopted in this study for predicting the mechanical properties of asphalt mixtures with related test data of recovered binders. It is a physics-based model and considers asphalt mixture as a three-phase composite of aggregates, bitumen, and air voids. By this model, these phases within asphalt mixture are in an arrangement combining parallel and series components. The overall property of asphalt mixture depends on the property and volume fraction of each phase. A parameter called contact volume Pc represents the parallel proportion in the total volume. The full expression of the Hirsch model proposed by Christensen et al. (2003) for asphalt mixture dynamic modulus $|E^*|$ (in psi) is written as:

$$|E_m^*| = Pc_E\left[4200000\left(1-\frac{VMA}{100}\right)+3|G_b^*|\left(\frac{VFA\times VMA}{10000}\right)\right] + (1-Pc_E)\left[\frac{1-\frac{VMA}{100}}{4200000}+\frac{VMA}{VFA\times 3|G_b^*|}\right]^{-1}$$

Equation 4-6

where VMA is the voids content in the mineral aggregate in percent; VFA is the voids content filled with the binder in percent; $|G_b^*|$ is the complex shear modulus of binder in psi; and Pc_E (dimensionless) is the contact volume for dynamic modulus, defined as:

$$Pc_E = \frac{\left(20+\frac{VFA\times 3|G_b^*|}{VMA}\right)^{0.58}}{650+\left(\frac{VFA\times 3|G_b^*|}{VMA}\right)^{0.58}}$$

Equation 4-7

It should be noted that this model assumes incompressibility of the binder. This is to say that the Poisson's ratio is 0,5 and the extensional modulus $|E_b^*|$ of binder is approximately 3 times of the complex shear modulus $|G_b^*|$.

Christensen et al. (2003) also proposed the expression for asphalt mixture shear modulus $|{G_m}^*|$ (in psi). It is written as:

$$|G_m^*| = Pc_G\left[601000\left(1-\frac{VMA}{100}\right)+|G_b^*|\left(\frac{VFA\times VMA}{10000}\right)\right]+(1-Pc_G)\left[\frac{1-\frac{VMA}{100}}{601000}+\frac{VMA}{VFA\times|G_b^*|}\right]^{-1}$$

Equation 4-8

In this case, the contact volume Pc_G (dimensionless) is expressed as:

$$Pc_G = \frac{\left(3+\frac{VFA\times|G_b^*|}{VMA}\right)^{0.678}}{396+\left(\frac{VFA\times|G_b^*|}{VMA}\right)^{0.678}}$$

Equation 4-9

The Hirsch model equations show that the models for dynamic modulus and shear modulus are actually in a uniform form with different constant values. Considering different constant values for different materials, a general form of the Hirsch model for dynamic modulus can be written as:

$$|E_m^*| = Pc_E\left[m_E\left(1-\frac{VMA}{100}\right)+3|G_b^*|\left(\frac{VFA\times VMA}{10000}\right)\right]+(1-Pc_E)\left[\frac{1-\frac{VMA}{100}}{m_E}+\frac{VMA}{VFA\times 3|G_b^*|}\right]^{-1}$$

Equation 4-10

The contact volume Pc_E can be written as:

Conférence Européenne des Directeurs des Routes
Conference of European Directors of Roads

$$Pc_E = \frac{\left(p_{E1} + \frac{VFA \times 3|G_b^*|}{VMA}\right)^{p_{E3}}}{p_{E2} + \left(\frac{VFA \times 3|G_b^*|}{VMA}\right)^{p_{E3}}}$$

Equation 4-11

The m_E, p_{E1}, p_{E2}, and p_{E3} are model constants for dynamic modulus.

Similarly, a general form of the Hirsch model for shear modulus can be written as:

$$|G_m^*| = Pc_G\left[m_G\left(1 - \frac{VMA}{100}\right) + |G_b^*|\left(\frac{VFA \times VMA}{10000}\right)\right] + (1 - Pc_G)\left[\frac{1 - \frac{VMA}{100}}{m_G} + \frac{VMA}{VFA \times |G_b^*|}\right]^{-1}$$

Equation 4-12

The contact volume Pc_G can be written as:

$$Pc_G = \frac{\left(p_{G1} + \frac{VFA \times |G_b^*|}{VMA}\right)^{p_{G3}}}{p_{G2} + \left(\frac{VFA \times |G_b^*|}{VMA}\right)^{p_{G3}}}$$

Equation 4-13

The m_G, p_{G1}, p_{G2}, and p_{G3} are model constants for shear modulus. The constant values proposed by Christensen et al. (2003), both for dynamic modulus and shear modulus, are listed in Table 4-10.

Table 4-10. Hirsch model constant values proposed by Christensen et al. (2003).

Model constants	m_E	p_{E1}	p_{E2}	p_{E3}	m_G	p_{G1}	p_{G2}	p_{G3}
Constant values by Christensen et al. (2003)	4,20E+06	20	650	0,58	6,01E+05	3	396	0,678

4.7.3.2 Fitting of model constants for unaged asphalt mixtures

Considering different model constant values for different materials, this study used the least squares method to obtain the constant values for each unaged asphalt mixture. It was done by fitting the prediction output by the Hirsch model to the mechanical test data of asphalt mixtures presented in the previous sections. The complex shear modulus $|G_b^*|$ of binder was from the DSR testing of recovered binders presented also previously in this report. Towards the reference temperature 10 °C, the same shift factors were applied to the complex shear modulus of binder as to the modulus of asphalt mixture (R values in Table 4-6 through Table 4-9). The VMA and VFA values of the tested asphalt mixture samples were input to the Hirsch model, as listed in Table 4-11. The best fit could then be reached, and model constant values could be obtained. The obtained constant values for unaged asphalt mixtures are listed in Table 4-12, and the reached best fits are presented in Annex I. It should be noted that the obtained constant values were based on limited measurement data of binder and their validity is expectedly within and near the frequency range of the fitting.

Table 4-11. VMA and VFA values of asphalt mixture samples.

Volumetric parameter	VMA (%), IDT sample	VFA (%), IDT sample	VMA (%), shear test sample	VFA (%), shear test sample
SMA8 60% RA VMA	15,0	95,1	15,1	94,4
SMA11 10% RA	16,4	90,3	16,1	92,3
SMA11 40% RA	15,7	93,8	16,1	91,3
SMA16	16,5	90,3	16,5	89,8
ZOAB+	25,0	46,8	26,6	43,0
PA8	34,7	30,6	33,4	32,4
PA8 panacea	33,1	32,6	32,9	32,9
PA8 aramid	33,4	32,3	33,8	31,7

Table 4-12. Model constant values obtained for unaged asphalt mixtures.

Model constants	m_E	p_{E1}	p_{E2}	p_{E3}	m_G	p_{G1}	p_{G2}	p_{G3}
SMA8 60% RA VMA	1,23E+06	24	1258	0,658	8,67E+06	24	1719	0,425
SMA11 10% RA	2,14E+06	3,6	3106	0,839	4,27E+06	17	1042	0,500
SMA11 40% RA	1,19E+06	2,3	1173	0,774	7,92E+05	7,7	166	0,468
SMA16	1,21E+06	4,1	1173	0,727	2,02E+06	5,4	230	0,409
ZOAB+	1,20E+06	1,4	979	0,782	1,54E+07	2,1	1715	0,433
PA8	4,20E+06	0,33	553	0,724	8,49E+05	3,0	62,5	0,303
PA8 panacea	5,86E+06	1,2	467	0,501	7,66E+06	0,99	218	0,287
PA8 aramid	4,50E+06	1,0	467	0,561	3,35E+06	1,1	114	0,302

4.7.3.3 Effects of ageing

In order to evaluate the effects of ageing, the master curves of asphalt mixtures after ageing were predicted with the Hirsch model in this study. The same model constant values were used for aged asphalt mixtures as obtained for the unaged (Table 4-12). This means an assumption that the asphalt mixture does not change its mechanical behaviour after ageing other than the hardening of binder. The complex shear modulus $|G_b^*|$ of recovered binder from the aged asphalt mixture was by the DSR testing presented in the previous sections. The same shift factors were applied to the binders from aged asphalt mixtures as to those from the unaged. The same VMA and VFA values were used for aged samples as for the unaged asphalt mixture samples (Table 4-11). Due to the limited validity of the obtained constant values, the prediction was firstly conducted only within and near the frequency range of the fitting. As examples, the prediction results for asphalt mixture SMA8 60% RA VMA are presented in Figure 4-25 (IDT dynamic modulus) and Figure 4-26 (shear modulus) while results for all asphalt mixtures are shown in Annex II.

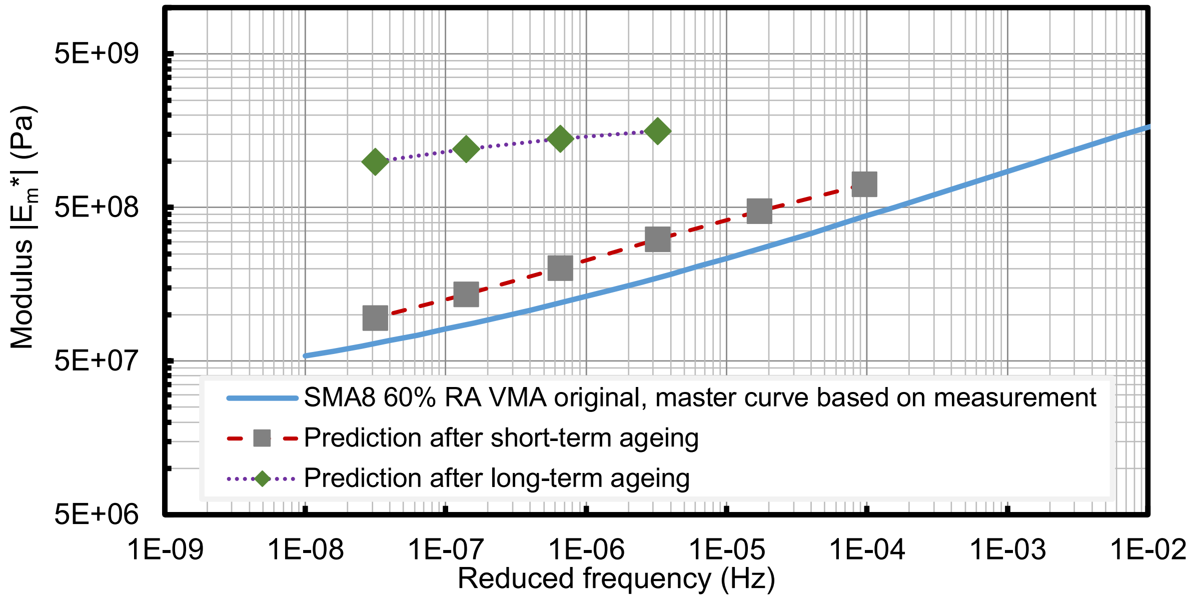

Figure 4-25. Prediction of IDT dynamic modulus after ageing for asphalt mixture SMA8 60% RA VMA, T_{ref}=10 °C.

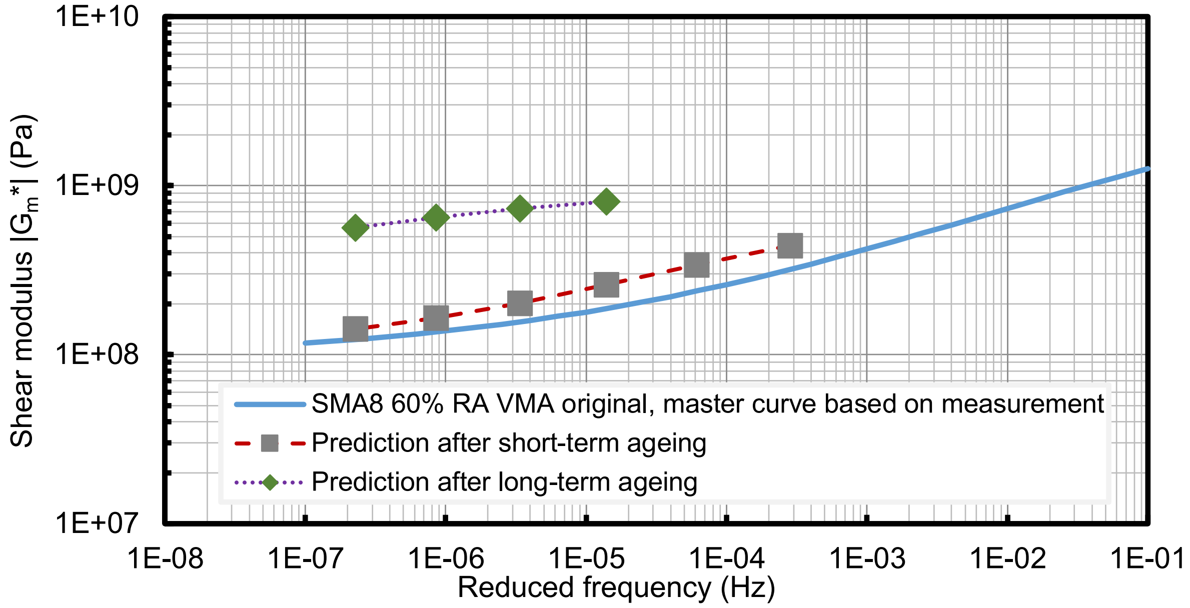

Figure 4-26. Prediction of shear modulus after ageing for asphalt mixture SMA8 60% RA VMA, T_{ref}=10 °C.

In Figure 4-25 and Figure 4-26, as well as in Annex II, the prediction results indicate the effects of ageing on asphalt mixture modulus. For all asphalt mixtures, both the IDT dynamic modulus and the shear modulus increases after ageing. The longer the ageing conditioning lasts, the more modulus increases after the ageing. This means that the ageing makes asphalt mixtures stiffer, most probably due to the hardening of binders. A shifting effect can be observed for both the IDT dynamic modulus and shear modulus results towards lower frequencies after ageing, without significantly changing the shape of curves. However, the sensitivity of different asphalt mixtures to ageing is different. This is to say that, according to the model prediction, the asphalt mixtures behave differently in terms of how much their curves are shifted after the ageing. For example, the curves of PA8 panacea and PA8 aramid are much more towards lower frequencies after the ageing compared to the curves of SMA11 10% RA and SMA11 40% RA.

This shift factor due to ageing of each asphalt mixture was determined based on the measurement and prediction results in Figure 4-25, Figure 4-26 as well as Annex II. Table 4-13 lists the determined $\log(a_T)$ values for both IDT dynamic modulus and shear modulus after short-term and long-term ageing. The results are also presented in a bar chart as Figure 4-27. The $\log(a_T)$ value may indicate the sensitivity of an asphalt mixture to ageing and thus was used to predict master curves of the aged asphalt mixtures.

Table 4-13. Shift factor $\log(a_T)$ from the unaged asphalt mixture due to ageing.

Shift factor $\log(a_T)$ from the unaged asphalt mixture	After short-term ageing, IDT test	After long-term ageing, IDT test	After short-term ageing, shear test	After long-term ageing, shear test
SMA8 60% RA VMA	-0,86	-4,00	-0,76	-3,54
SMA11 10% RA	-0,88	-1,83	-0,74	-1,57
SMA11 40% RA	-0,77	-1,87	-0,65	-1,63
SMA16	-1,23	-3,23	-1,04	-2,74
ZOAB+	-0,90	-2,32	-0,75	-1,93
PA8	-1,72	-2,68	-1,28	-2,20
PA8 panacea	-2,01	-4,35	-1,56	-3,36
PA8 aramid	-1,92	-4,34	-1,45	-3,24

The determined $\log(a_T)$ values due to ageing were applied to the whole master curves of unaged asphalt mixtures for both IDT dynamic modulus and shear modulus. This could lead to the master curves after short-term and long-term ageing. As examples, the predicted master curves for asphalt mixture SMA8 60% RA VMA are presented in Figure 4-28 (IDT dynamic modulus) and Figure 4-29 (shear modulus) while results for all asphalt mixtures are shown in Annex III. With these predicted master curves as the basis, the effects of ageing on the pavement durability and performance will be further analysed and discussed in the following sections.

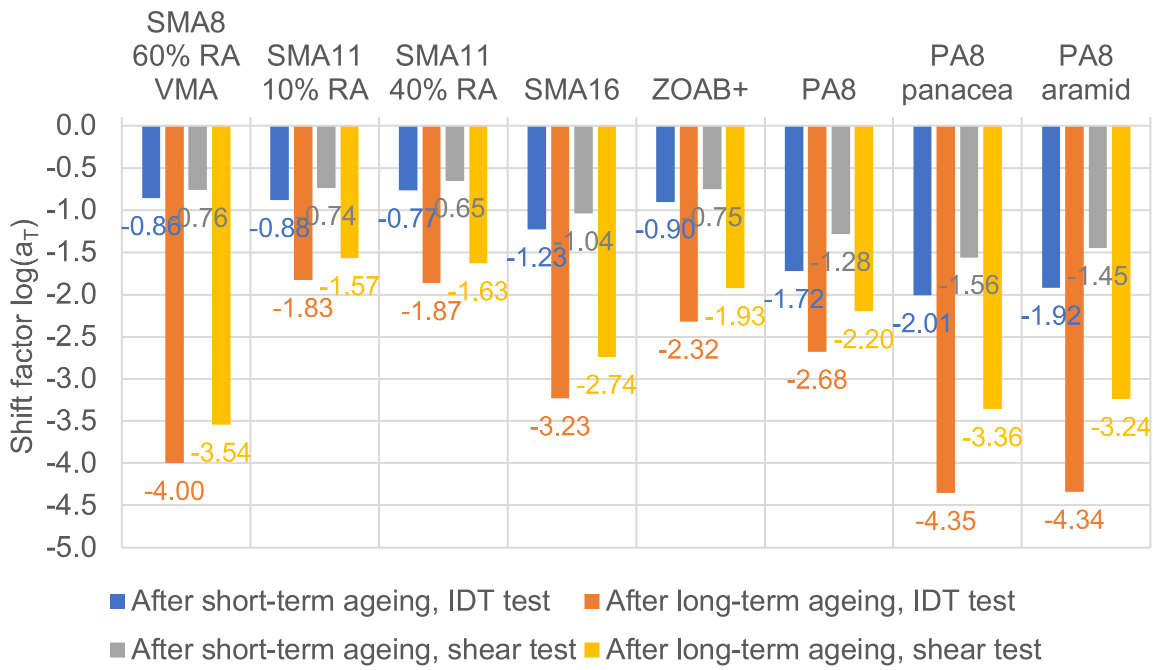

Figure 4-27. Bar chart of shift factor log(a_T) due to ageing of asphalt mixtures.

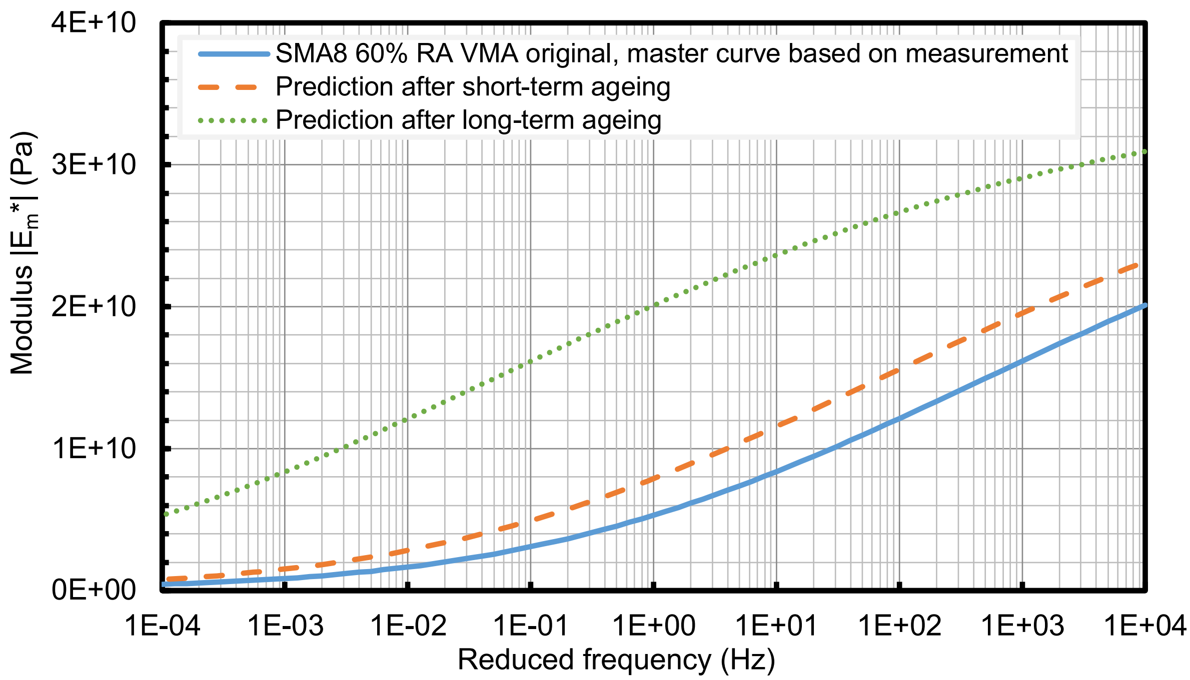

Figure 4-28. IDT dynamic modulus master curves by shift factor due to ageing for asphalt mixture SMA8 60% RA VMA, T_{ref}=10 °C.

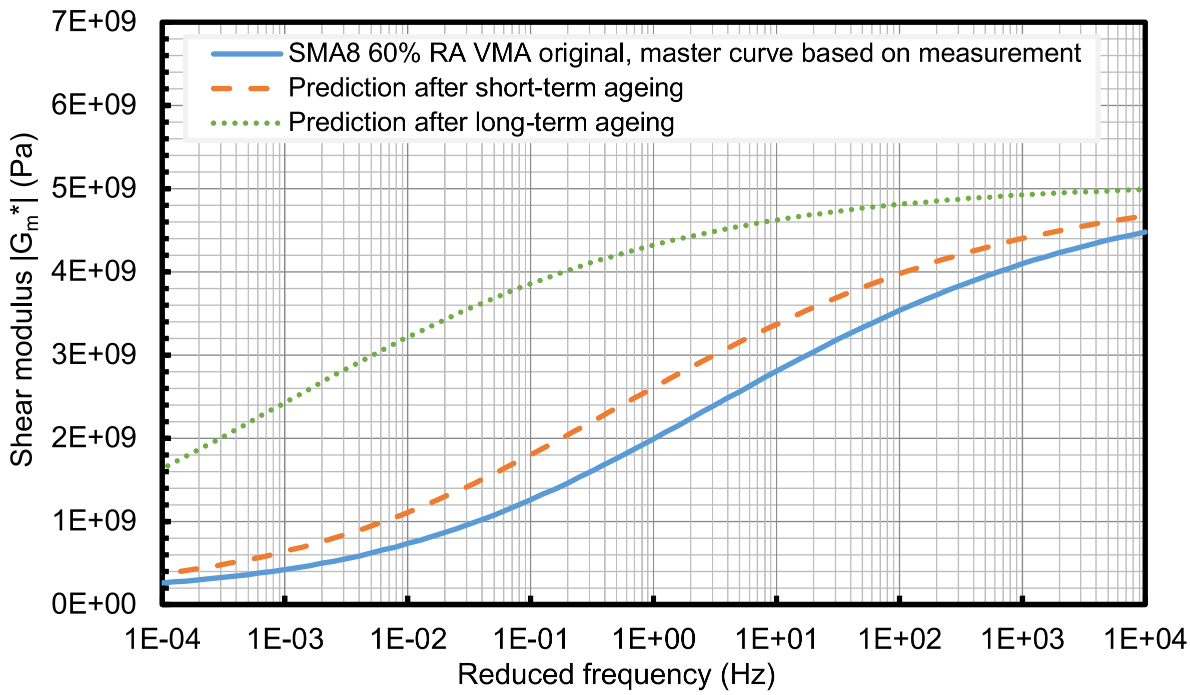

Figure 4-29. Shear modulus master curves by shift factor due to ageing for asphalt mixture SMA8 60% RA VMA, T_{ref}=10 °C.

4.7.4 Mixture performance modelling using PEDRO model

A linear viscoelastic uni-layer permanent strain model PEDRO (Permanent Deformation of asphalt concrete layers for Roads) was used to evaluate the performance of the different SMA and PA mixes. The PEDRO model estimates the permanent deformation due to post compaction or volume decrease and shear flow (Said S. F., Hakim, Oscarsson, & Hjort, 2011). In this section we present the results of permanent deformation calculations using temperature data from Sweden. The input data for the PEDRO model are:

- viscosity of bituminous mixtures at frequency corresponding to the maximum phase angle
- hourly traffic volume, traffic loading and speed
- standard deviation of the lateral traffic wander distribution
- hourly temperature data
- thickness of the bituminous layer

An asphalt thickness of 40 mm was assumed in all PEDRO calculations. Furthermore, traffic data corresponding to the road class (Motorway in Table 4-14) were used for the analysis. The viscosity of the mixes, i.e., the viscosity at peak phase angle, were derived from the dynamic shear modulus and phase angle master curves for unaged and sort-term aged mixtures as shown in Equation 4-14.

$$|\eta^*| = \frac{|G^*|}{\omega}$$

Equation 4-14

where η^* is complex viscosity in Pa s, G^* is complex shear modulus in Pa and ω is angular frequency rad/s corresponding to the maximum value of phase angle. The PEDRO model assumes that the mix has the least resistance to permanent deformation at ω where the phase angle is maximum (Said S. F., Hakim, Oscarsson, & Hjort, 2011). The hourly asphalt temperature at 20 mm depth, Figure 4-30, was used for PEDRO analysis. The temperature was derived from a weather station in Stockholm area.

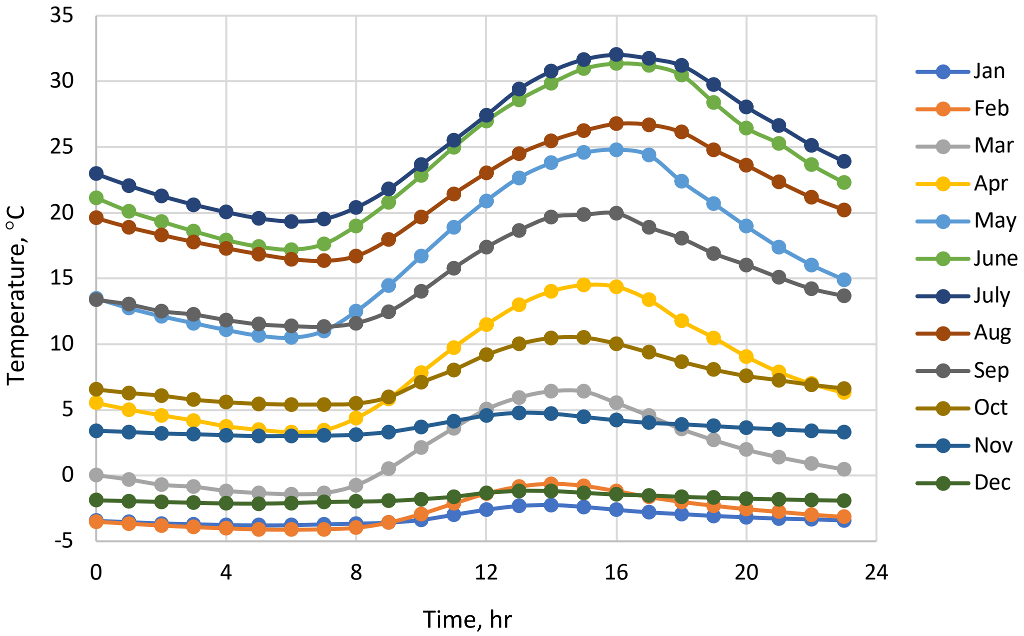

Figure 4-30. Temperature data for PEDRO calculation.

The viscosity of the mixes was adjusted to consider the aging using the power function in Equation 4-15.

$$\eta_2 = \eta_1 * \left(\frac{t_2}{t_1}\right)^n$$

Equation 4-15

where η_1 and η_2 are the viscosities at time t_1 and t_2, respectively, *n* is material constant. *n* = 0.08 was used for the analysis. The default aging constant n = 0.08 was used for PEDRO calculation based on unaged mixture properties.

The PEDRO model is not calibrated for porous asphalt and SMA mixes with a higher proportion of recycled materials. Thus, calibration factor based on previous experiences were employed in the present analysis.

The subsequent section presents the results of PEDRO calculations.

4.7.4.1 PEDRO modelling of SMA and PA mixtures

The predicted permanent deformations, based on unaged mixture properties, for the different SMA and PA mixes are shown in Figure 4-31. The SMA11 10% RA showed the best rutting resistance compared to the other SMA mixes followed by the SMA8 having 60% RA. SMA11 having 40% RA and SMA16 produced similar performance. Note that, even though the stiffness modulus and the shear modulus values of the SMA8 60% RA mixture were lower than the SMA11 40% RA and SMA16, it has produced a better performance in terms of predicted rutting. This is because the input to the PEDRO model is the viscosity of the mix at frequency corresponding to the maximum phase angle. The frequency at which the phase angle is maximum happens at lower frequency for the SMA 8 60% RA mixture which led to lower predicted rutting. In general, all the SMA mixes displayed a good rutting performance according to the PEDRO model.

For the PA mixes, the PA8 panacea and PA8 aramid produced very similar performance. Whereas the ZOAB+ showed a relatively poor rutting performance. The reason could be the slightly lower shear modulus of the ZOAB+ mix at higher temperature and a maximum phase angle located at relatively lower frequency. The PA8 mix was in the PEDRO analysis since the peak phase angle, Figure 4-24, occurs at a very high frequency which resulted in too low viscosity.

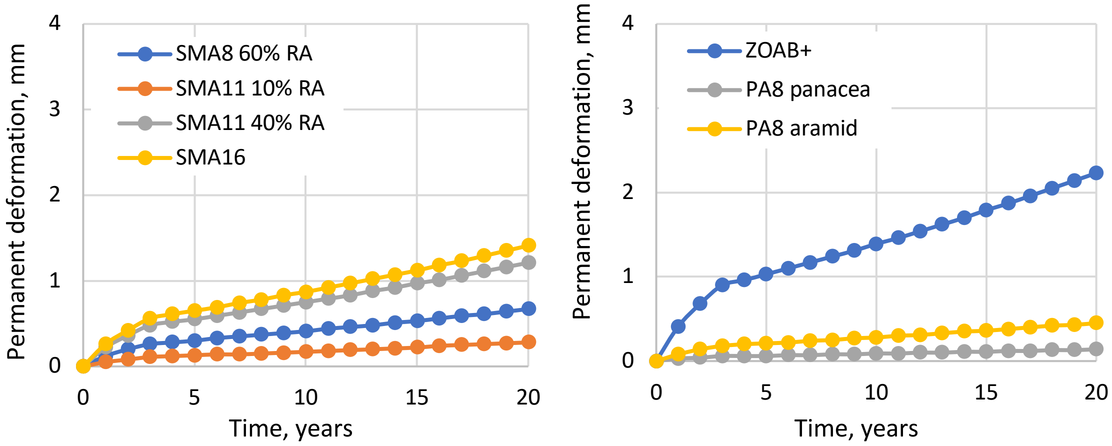

Figure 4-31. Predicted permanent deformation using the PEDRO model for SMA (left) and PA (right) mixtures based on unaged mixture properties.

The PEDRO calculations were repeated using viscosity data based on predicted short-term aged properties and the results are shown in Figure 4-32. All the SMA mixtures showed improved resistance to permanent deformation. Again, the SMA11 10% RA showed the best rutting resistance compared to the other SMA mixes. The SMA8 having 60% RA. SMA11 and SMA 16 similar rutting performance. The short-term ageing had the most impact on SMA16. The SMA11 40% RA was the least affected by short-term aging.

For the PA mixes, PA8 panacea, PA8 aramid and PA were significantly affected by the short-term aging with 93 % decrease in rutting. The ZOAB+ mixture was the least affected.

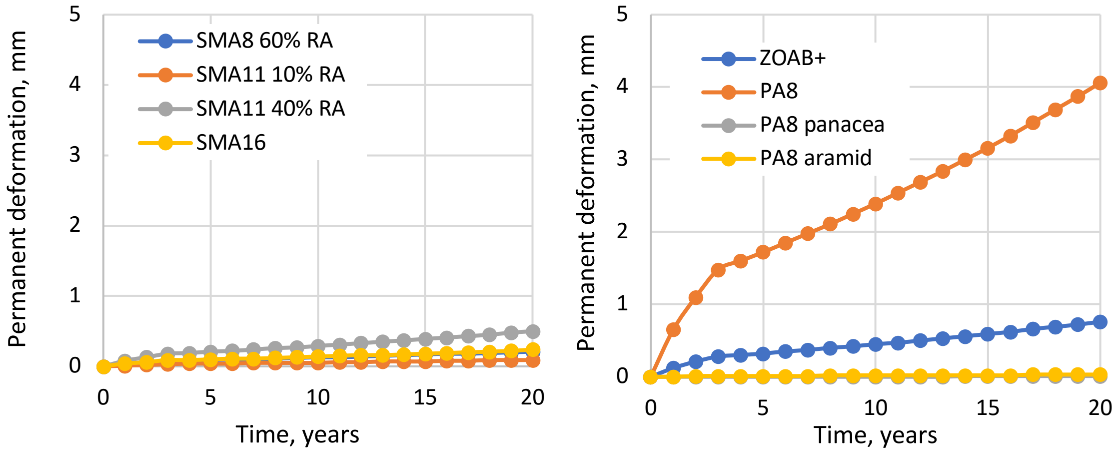

Figure 4-32. Predicted permanent deformation using the PEDRO model for SMA (left) and PA (right) mixtures based on short - term aged properties.

4.7.5 Pavement performance modelling using ERAPave PP

A Mechanistic empirical pavement analysis and design program (ERAPave PP) (beta version) currently under development phase was employed to evaluate the influence of the different surface mixtures on the rutting and fatigue cracking performance of three types of pavement structures commonly used in Sweden for Motorway (Motorväg), national road (Riksväg), and country roads (Länsväg). The main input data required for the ERAPave PP program are:

- pavement layer thickness
- the stiffness modulus master curves of the bituminous bound layers
- the resilient moduli of unbound granular layers and subgrade
- Average daily temperature for asphalt layers
- Degree of saturation for unbound layers
- traffic volume and loading
- standard deviation of the lateral traffic wander distribution
- parameters for permanent deformation and fatigue cracking models

A permanent deformation model for bituminous layers similar in expression to the AASHTOWare (previously MEPDG) model is implemented in the ERAPave PP program. Additionally, a model developed at VTI (Rahman, Erlingsson, & Ahmed, 2021) is implemented to predict the permanent deformation contribution from unbound base, subbase, and subgrade layers. The permanent strain/deformation models are expressed as:

$$\varepsilon_p = f(\varepsilon_r, T, N)$$

Equation 4-16

Where ε_p is permanent strain/deformation, *T* is temperature, *N* is the number of load cycle.

For fatigue cracking, a model shown in Equation 4-17 is used in ERAPave PP. The model relates the tensile strain at the bottom of the asphalt layer to the number of load cycles to failure due to fatigue cracking N_f.

$$N_f = k_1 \varepsilon_t^{-k_2} E^{-k_3}$$

Equation 4-17

where f_1, f_2 and f_3 are material constants and ε_t and E are the tensile strain in μm/m at the bottom of the asphalt layer and the modulus in MPa of the asphalt layer, respectively.

The fatigue damage from each stress level is accumulated according to the Miner's hypothesis (Huang, 2004), Equation 4-18. For *m* different load/stress levels each applied with n_i cycles, and if N_i is the number of cycles to failure corresponding to each load level, then the failure due to fatigue cracking of the combined loading occurs when:

$$D_R = \sum_{i=1}^{m} \frac{n_i}{N_i}$$

Equation 4-18

where D_R is the damage ratio. If D_R > 1 the pavement has reached its ultimate carrying capacity and can no longer deliver its services.

Input parameter for commonly used binder and bituminous base layers were used for the ERAPave PP analysis. The master curves of the binder and bituminous base layers used in the analysis are shown in Figure 4-33. The bituminous layers of the pavement structures were placed over 80 mm of unbound granular base layer and 420 mm of subbase layers. Modulus values of 400 MPa, 250 MPa and 100 MPa were assumed for unbound base, subbase, and subgrade layers, respectively. The pavement structures and traffic data considered for the analysis are shown in Table 4-14. A total of 24 (8 surface mixes * 3 pavement types) ERAPave PP analysis were conducted.

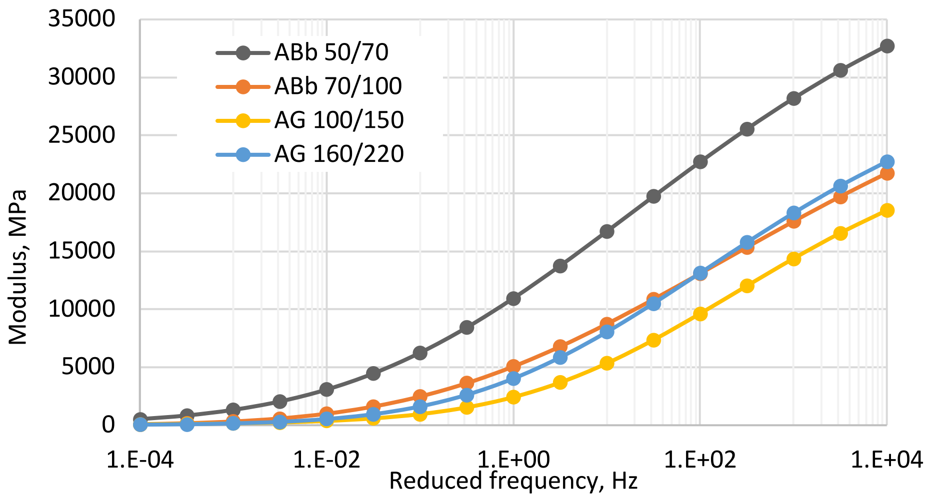

Figure 4-33. Stiffness modulus master curves of for binder and bituminous base layers assumed for the ERAPave analysis.

Table 4-14. Selected Swedish pavement structures for ERAPave PP analysis.

Road type	Layer	Mix	Thickness, mm	ADT	Heavy truck %
Motorway	Surface	SMA/PA	40	13000	18
	Binder	ABb 50/70	60		
	Bit. base	AG 100/150	70		
National Roads	Surface	SMA/PA	40	3000	12
	Binder	ABb 70/100	40		
	Bit. base	AG 160/220	70		
Country Road	Surface	SMA/PA	40	1100	10
	Bit. base	AG 160/220	50		

The average daily temperature in the asphalt layers for the ERAPave PP analysis was derived from one of the weather stations in Stockholm area. Figure 4-34 shows the temperature in the asphalt layer at 20 mm, 65 mm, and 140 mm, representing the temperature at mid depth of the surface layer, binder layer and bituminous base layer, respectively.

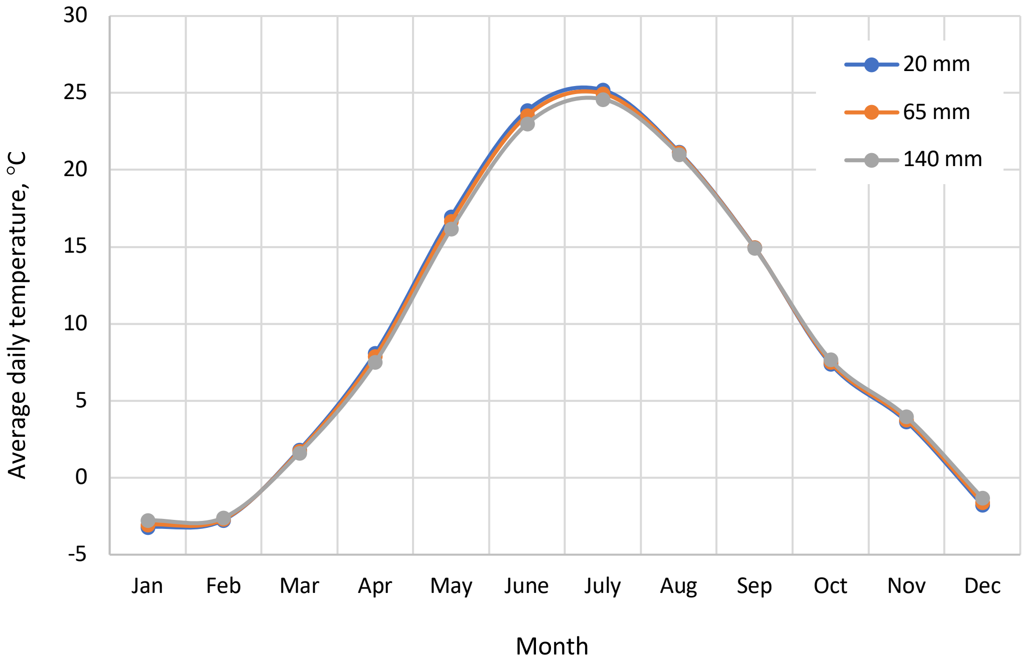

Figure 4-34. Temperature in the asphalt layer at 20 mm, 65 mm, and 140 mm from the surface of the pavement.

The following sections present the evolution of total permanent deformation and damage due to fatigue cracking for the pavement structures having surface layers made of different SMA and PA mixers.

4.7.5.1 ERAPave PP modelling results for SMA mixtures

Figure 4-35, Figure 4-36, and Figure 4-37 presents the predicted permanent deformation and damage due to fatigue cracking for Motorway, National Road, and Country Road, respectively. It is clear from the figures that the influence of the surfacing layer on the development of rutting or fatigue cracking particularly for Motorway with high traffic volume (Figure 4-35) and for Country Road having low traffic volume (Figure 4-37). In general, the SMA11 10% RA mixture produced the best performance in terms of rutting and fatigue cracking. All the SMA mixtures showed nearly similar levels of rutting and fatigue damage for the national road having intermediate traffic volume.

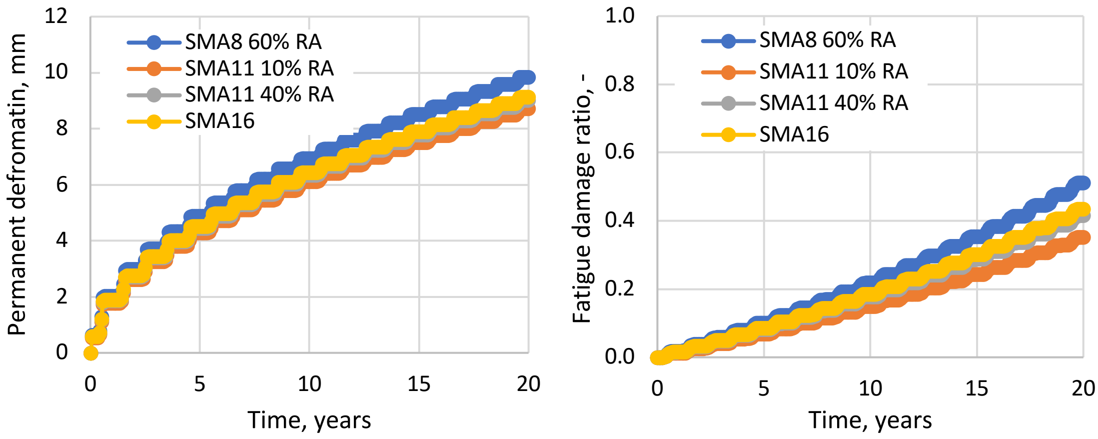

Figure 4-35. Predicted permanent deformation and fatigue damage for a typical motorway in Sweden for the SMA mixtures.

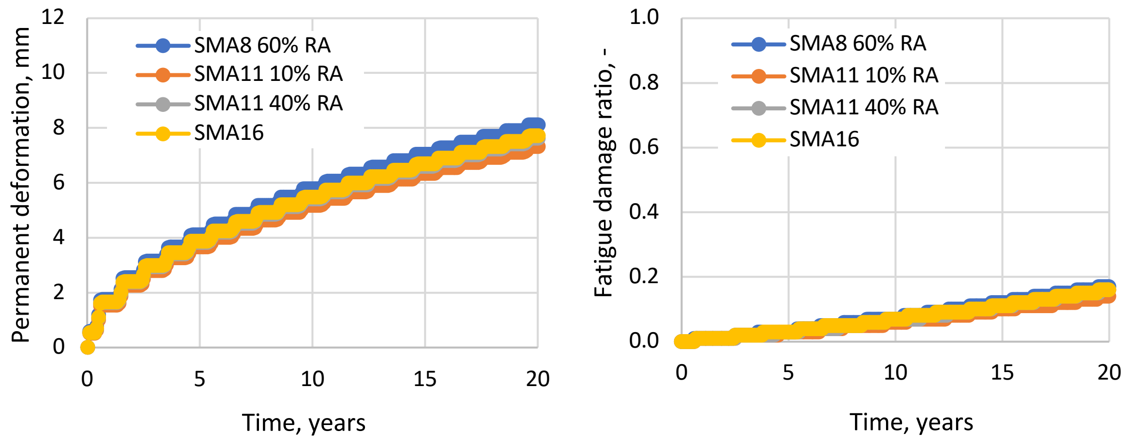

Figure 4-36. Predicted permanent deformation and fatigue damage for a typical national road in Sweden for the SMA mixtures.

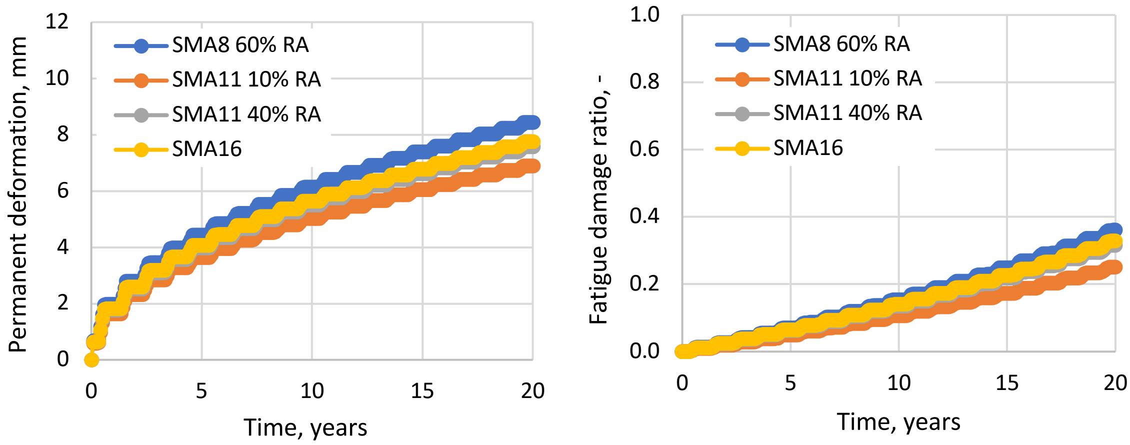

Figure 4-37. Predicted permanent deformation and fatigue damage for a typical country road in Sweden for the SMA mixtures.

The surface layer or SMA deformations for pavement structures for Motorway and National Roads are shown in Figure 4-38. In general, the SMA layers contributed a very small part of the total permanent deformation. The SMA8 60% RA showed a relatively poor performance among the SMA mixes. The SMA surface layer deformations for Country Road are not presented as the SMA layer deformations are negligible.

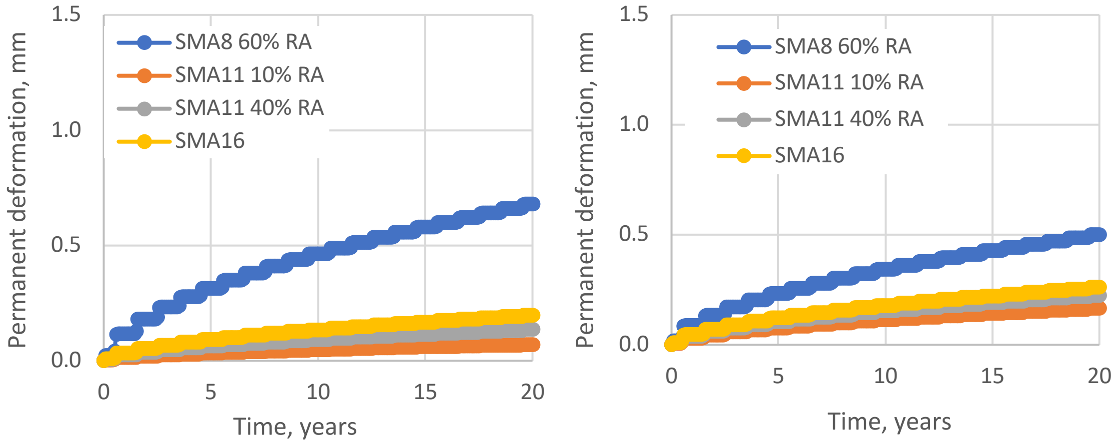

Figure 4-38. Predicted surface layer (SMA) deformation for a typical Motorway (left) and National Road (right) with SMA mixes.

The results presented in Figure 4-35 to Figure 4-38 are based on stiffness modulus master curves of unaged mixtures. The ERAPave PP analysis were also conducted considering the predicted short-term stiffness modulus of the SMA mixtures. Figure 4-39 to Figure 4-41 present the predicted total permanent deformations and fatigue damages for the three types of pavement structures.

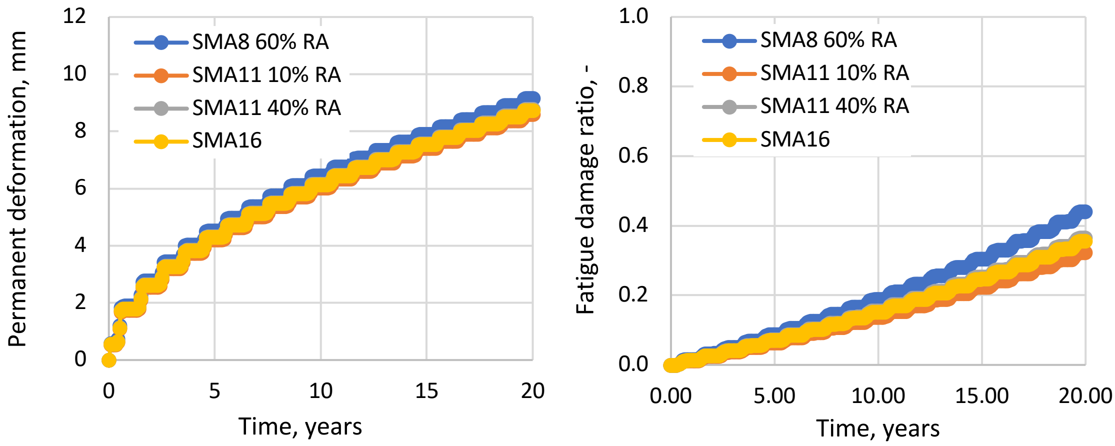

Figure 4-39. Predicted permanent deformation and fatigue damage for a typical motorway in Sweden for the short-term aged SMA mixtures.

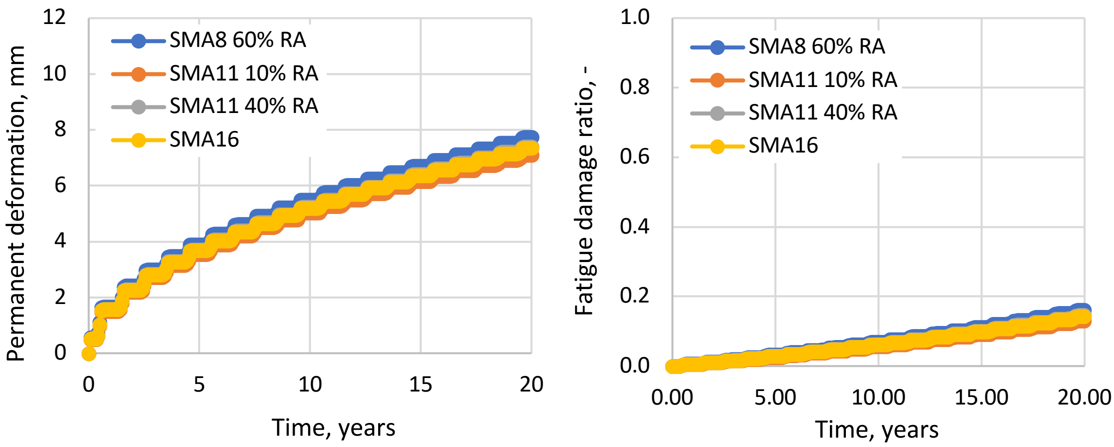

Figure 4-40. Predicted permanent deformation and fatigue damage for a typical National Road in Sweden for the short-term aged SMA mixtures.

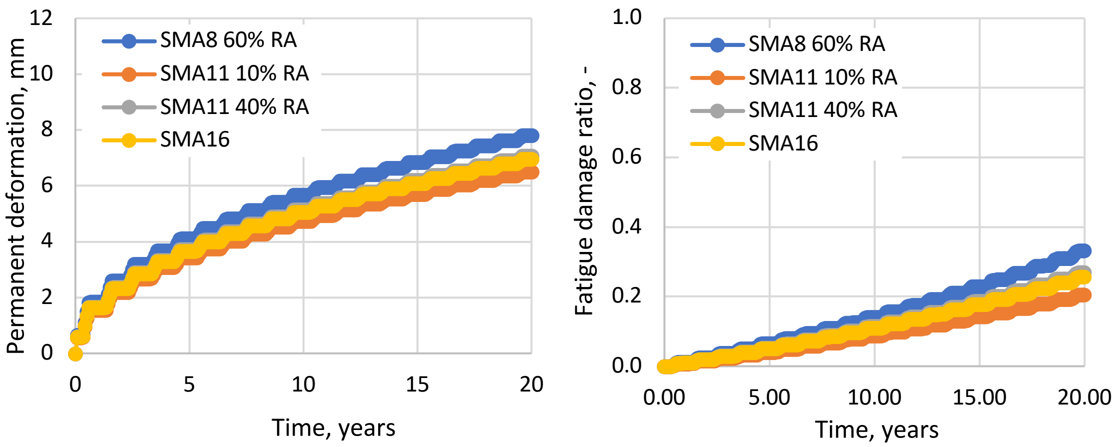

Figure 4-41. Predicted permanent deformation and fatigue damage for a typical Country Road in Sweden for the short-term aged SMA mixtures.

The short-term aged SMA deformations for Motorway and National Road types are shown in Figure 4-42Figure 4-38. In general, the SMA layers contributed a very small part of the total permanent deformation for all types of roads. The SMA surface layer deformations for Country Road are not presented since the SMA layer deformations are negligible.

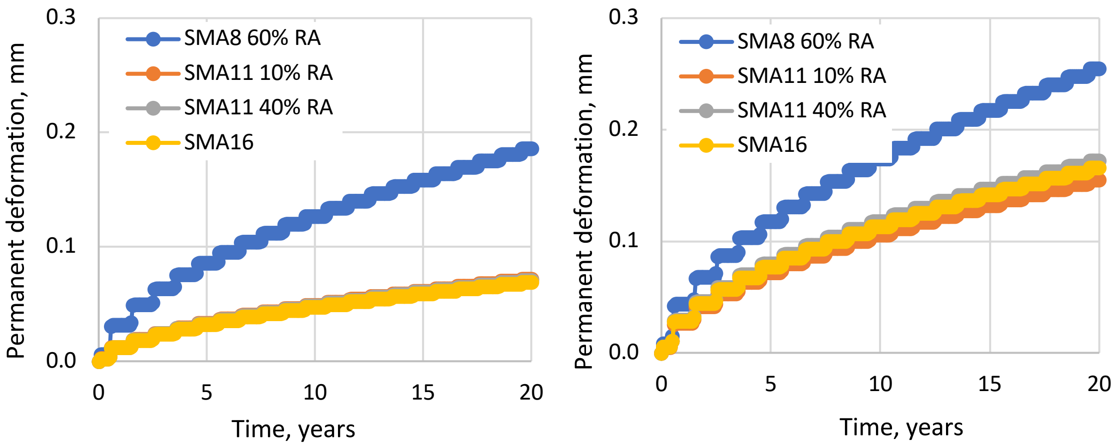

Figure 4-42. Predicted surface layer (SMA) deformations for a typical Motorway (left) and National Road (right) based on short-term aged SMA mixes.

4.7.5.2 ERAPave PP modelling results for PA mixtures

The calculated permanent deformation and damage due to fatigue cracking for Motorway, National Road, and Country Road made of PA surfacing are shown in Figure 4-43, Figure 4-44, and Figure 4-45, respectively. The predicted rutting and fatigue damages are relatively higher for PA mixes compared to the SMA mixes presented in the previous section. The ZOAB+, PA8 panacea and PA8 aramid mixtures produced very similar performance for rutting and fatigue cracking for all the pavement structures and traffic classes considered. The PA8 mixture produced the least rutting resistance compared to the three PA mixtures.

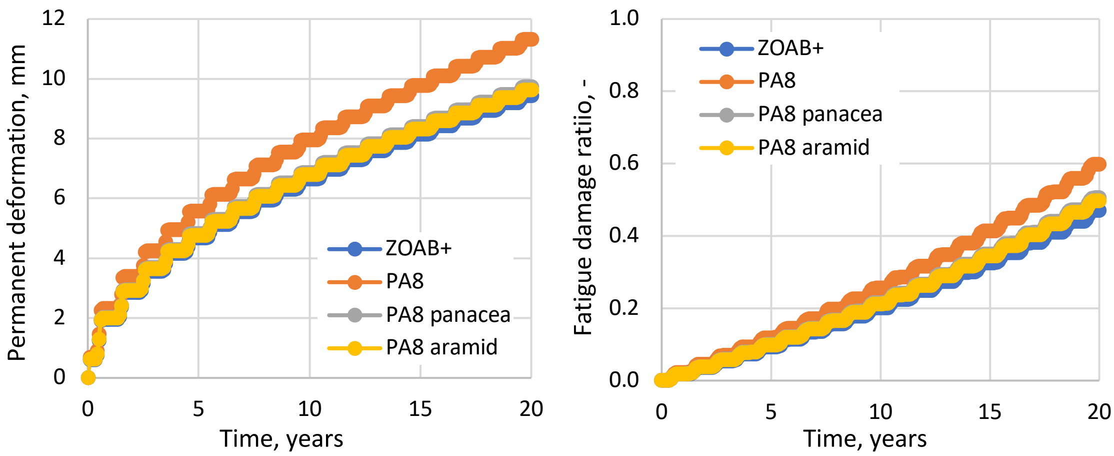

Figure 4-43. Predicted permanent deformation and fatigue damage for a typical motorway in Sweden for the PA mixtures

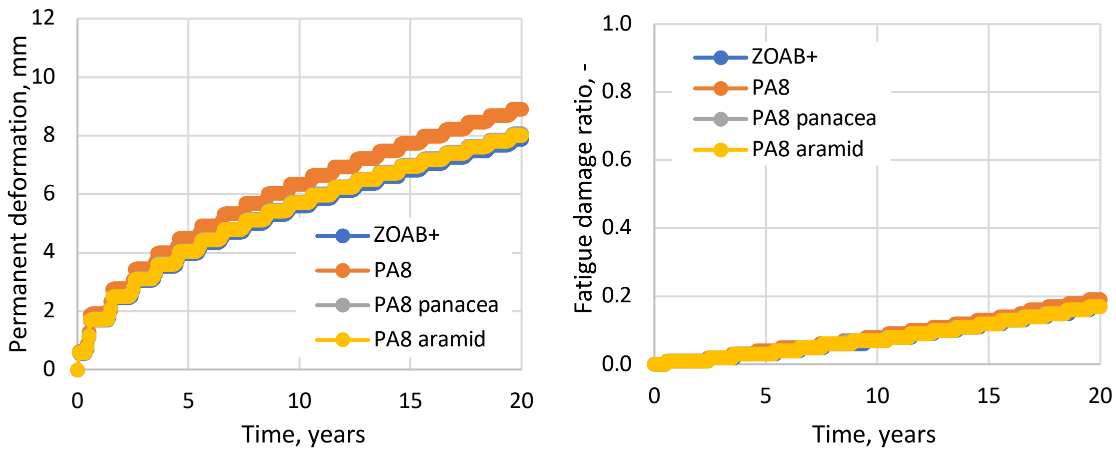

Figure 4-44. Predicted permanent deformation and fatigue damage for a typical national road in Sweden for the PA mixtures.

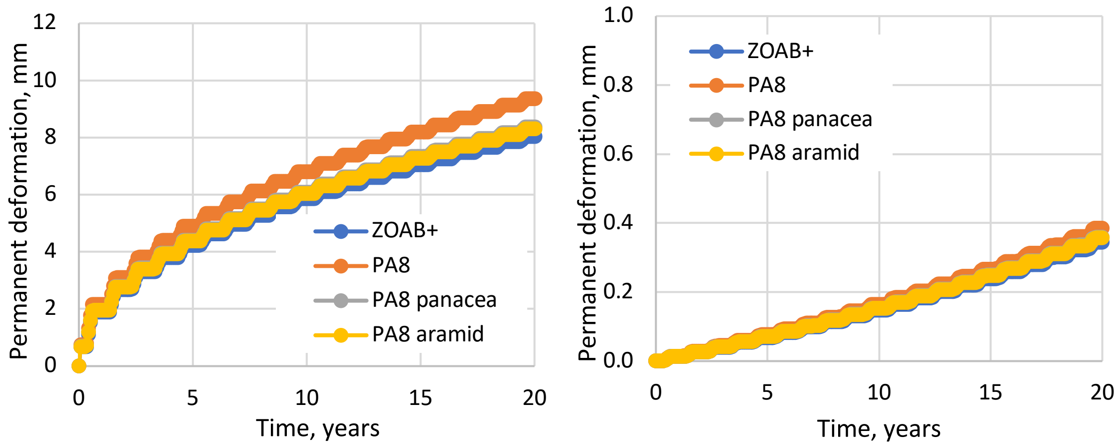

Figure 4-45. Predicted permanent deformation and fatigue damage for a typical country road in Sweden for the PA mixtures.

The deformations of the PA surface layers for Motorway and National Road structures are shown in Figure 4-46Figure 4-38. The PA8 surface layer contributed most of the total rutting. The PA layers deformation for the Country Road is not presented as the PA layer deformations were negligible.

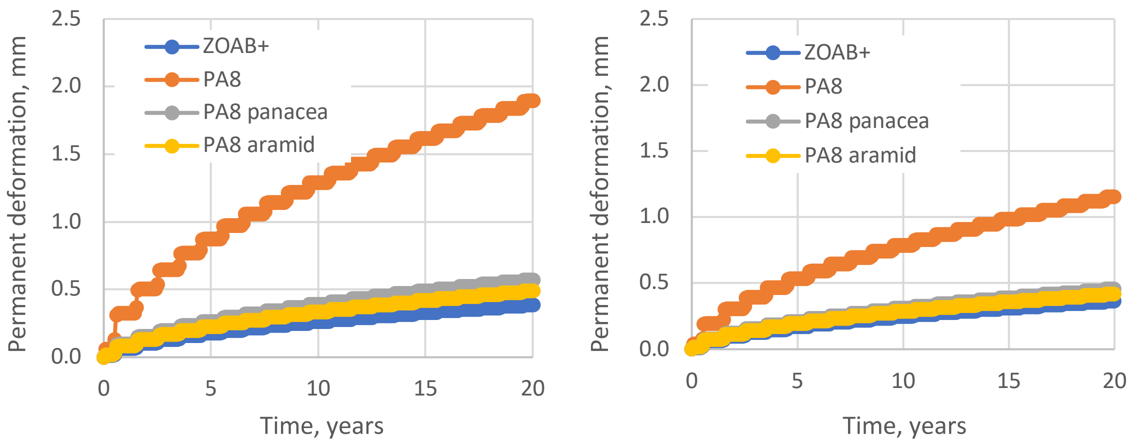

Figure 4-46. Predicted surface layer (PA) deformation for a typical Motorway (left) and National Road (right) with PA mixes.

Figure 4-47 to Figure 4-49 display the predicted total permanent deformations and fatigue damages for the three types of pavement structures using stiffness modulus master curve parameters of the short-term aged PA surface mixtures.

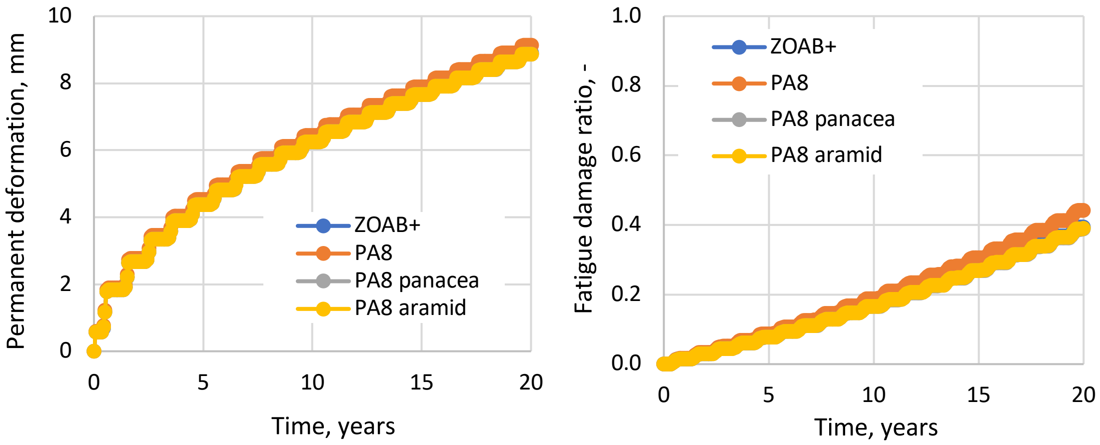

Figure 4-47. Predicted permanent deformation and fatigue damage for a typical motorway in Sweden for the short-term aged PA mixtures.

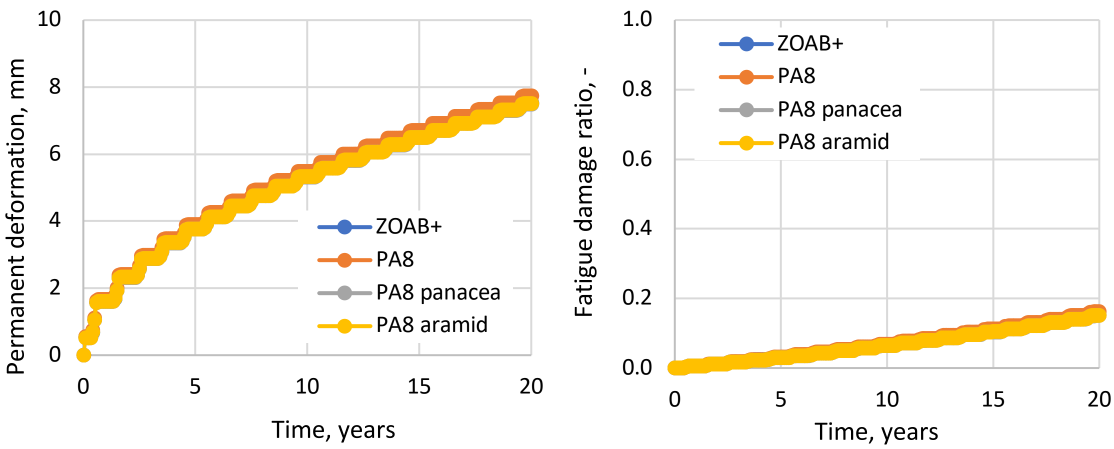

Figure 4-48. Predicted permanent deformation and fatigue damage for a typical national road in Sweden for the short-term aged PA mixtures.

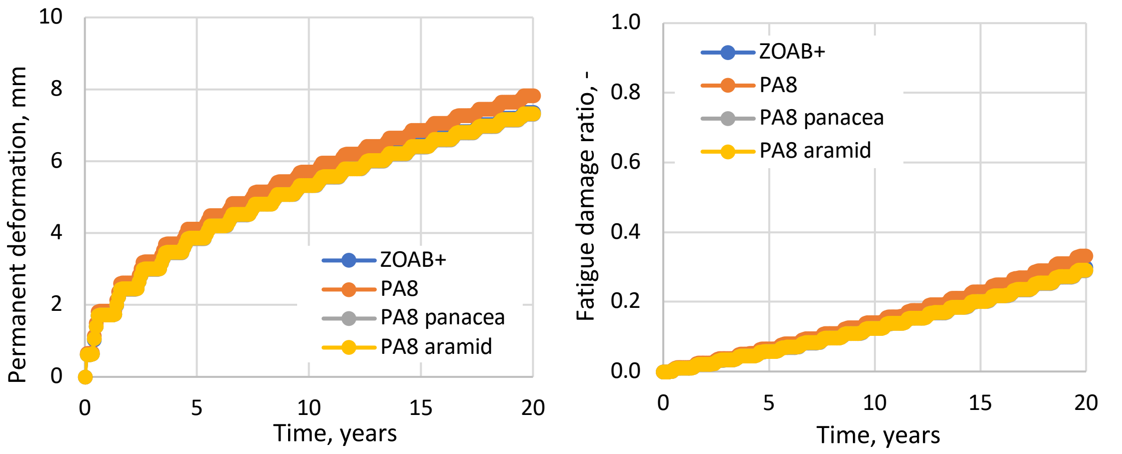

Figure 4-49. Predicted permanent deformation and fatigue damage for a typical country road in Sweden for the short-term aged PA mixtures.

The deformations of the short-term aged PA surface layers for Motorway and National Road structures are shown in Figure 4-50Figure 4-38. The short-term aged PA surface layers contributed insignificant amount of rutting for all types of roads. The PA layers deformation for the Country Road is not presented as the PA layer deformations were negligible.

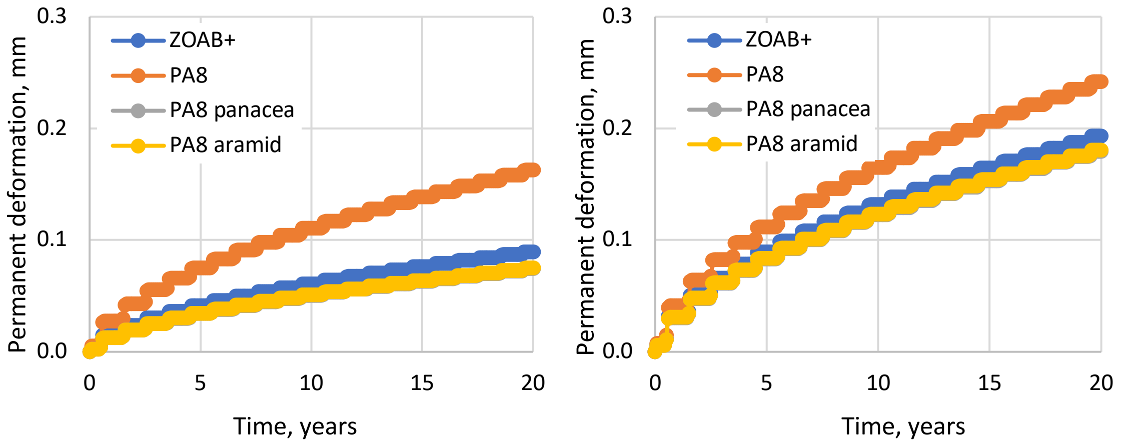

Figure 4-50. Predicted surface layer (PA) deformation for a typical Motorway (left) and National Road (right) for the short-term aged PA mixes.

4.7.6 Pavement performance modelling based on ViaStructura

The following mechanistic empirical pavement analysis was performed using road structures and climate conditions typical for Lithuania.

4.7.6.1 Introduction to mechanistic empirical pavement analysis and design program ViaStructura

Mechanistic empirical pavement analysis and design program ViaStructura is a universal WEB system for pavement structure modelling and decision making developed by the Lithuanian Road Administration under the Ministry of Transport and Communications (hereinafter - LAKD). ViaStructura can be used to determine the pavement damage characteristics based on material mechanistic properties under specific traffic and climate conditions. The flowchart of the pavement performance analysis of ViaStructura is shown in Figure 4-51. The system also generates reports of calculation results and accumulates the archival data.

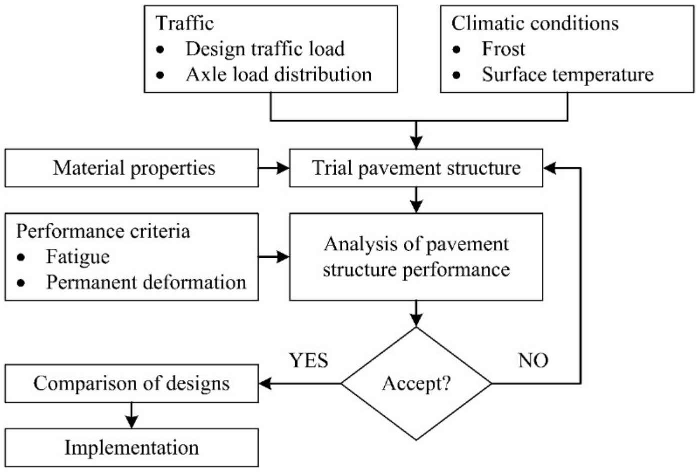

Figure 4-51. The flowchart of the pavement performance analysis of ViaStructura[1]

The main input data required for the ViaStructura:

- traffic volume, loading, and coefficients to determine the design ESAL (such as: standard deviation of the lateral traffic wander distribution
- temperature ranges of pavement surface (the percentage distribution of pavement surface temperature intervals)
- subgrade soil type, frost depth, specific environment situation to determine the minimal (frost heave resistant) thickness of pavement structure
- thickness of the pavement layers
- bonding at each interlayer
- modulus and Poisson' coefficient of each layer (the stiffness modulus master curves of the asphalt layers, the elastic modulus of concrete base layers, and the deformation moduli of unbound granular layers and subgrade)
- parameters for permanent deformation and fatigue boundary limit functions (models)

ViaStructura evaluates the performance of the flexible pavement structure based on permanent deformation and fatigue boundary limit functions. The permanent deformation models for unbound base and subbase layers and subgrade were adapted from RDO Asphalt[2] model. The permanent deformation prediction for asphalt layers is under development and currently unavailable in ViaStructura. The permanent deformation models are expressed as:

[1] Vaitkus, A., Kleizienė, R. & Karbočius, M. (2021) ViaStructura – A New Way of Pavement Structure Design. The 30th International Baltic Road Conference proceedings (submitted)

[2] FGSV 498. (2009). Richtlinien Für Die Rechnerische Dimensionierung Des Oberbaus von Verkehrsflächen Mit Asphaltdeckschicht RDO Asphalt 09 [Guidelines for Mathematical Dimensioning of Foundations of Traffic Surfaces with a Course Asphalt Surface]. Köln, Germany

$$N_{lim.,i-j} = 10^{\frac{1}{0.7}\left(\frac{0.00875 \cdot E_{v2}}{\sigma_{zz,i-j} \cdot \gamma}\right)}$$

Equation 4-19

where E_{v2} – the deformation modulus of unbound layer/subgrade, MPa; $\sigma_{zz,i-j}$ – vertical stress under load i and temperature j, MN/m^2; γ – safety factor.

For fatigue cracking, a model shown in Equation 4-20 is used in ViaStructura. This boundary limit function was adapted from Austrian pavement structure design methodology RVS 03.08.68[3]. The model relates the tensile strain at the bottom of the asphalt layer to the number of load cycles to failure due to fatigue cracking N_f.

$$N_{lim.,i-j} = \frac{k_1(T)}{F_{(\varepsilon 6)}} \cdot \left(\frac{S_{mix}(T)}{\sigma_{v,i-j} \cdot \gamma_{AC}}\right)^{k_2(T)}$$

Equation 4-20

where $S_{mix}(T)$ – temperature-dependent stiffness modulus of asphalt mix, MN/m2; $\sigma_{v,i-j}$ – vertical stress under load i and temperature j, MN/m^2; γ_{AC} – safety factor; $F_{(\varepsilon 6)}$ – fatigue factor depending on type of binder and strain of the asphalt layer at 10^6 load cycles determined by a four-point bending test according to EN 12697-24; $k_1(T)$, $k_2(T)$ – temperature factors.

The stresses, strains and displacements of the design pavement structure are calculated with high-performance analysis algorithm MnLayer. The algorithm was developed by professor Lev Khazanovich and Qiang Wang at the University of Minnesota in 2008[4] and it was implemented to ViaStructura.

The cumulative damage effect is a ratio between design load cycles application and boundary load cycles from each load i at temperature j (also called as Miner's hypothesis, Huang, 2004). The Miner's hypothesis was used to estimate all pavement performance functions. The failure of the combined loading at combine temperatures are determined according:

$$Damage = \sum \frac{N_{design,i-j}}{N_{lim.,i-j}}$$

Equation 4-21

where $N_{design,i-j}$ – design load cycles for the load i and temperature j; $N_{lim.,i-j}$ – limit load cycles for the load i and temperature j. If *Damage* > 1 the pavement has reached its ultimate carrying capacity and can no longer deliver its services.

So, the expected pavement structure performance is based on mechanistic models (characteristics) of the asphalt mixture of base layer and materials of the unbound base, subbase layers, and subgrade. The performance models were calibrated based on empirical data collected in the road network of Lithuania. Therefore, the results of a structure with a new (unknown) material determined with ViaStructura have to be assessed critically. Also, the expected lifetime determined with ViaStructura represents failure modes of the entire structure and does not cover the failure specific to the surface layer (such as aging, ravelling and/or road wear).

---

[3] FSV. (2016). Rechnerische dimensionierung von asphaltstrassen RVS 03.08.68 [Mathematical dimensioning of asphalt roads]. Vienna, Austria

[4] Khazanovich, L., & Wang, Q. (2007). MnLayer: High-performance layered elastic analysis program. Transportation Research Record, 2037, 63–75. https://doi.org/10.3141/2037-06

4.7.6.2 Pavement structure and other input parameters

This chapter presents the input data used for pavement relative performance analysis for a northeast part of Europe. The materials and thickness of layers (shown in Table 4-15) were selected from Lithuania guidelines (marked as LTU). The pavement performance analysis was carried out for pavement structures with different surface layer asphalt mixtures ZOAB+, SMA16, SMA11 40% RA and SMA11 10% RA, which showed the best results in the CRS. During this analysis, the aging of the materials was not evaluated.

The equivalent standard axle load (of a single wheel 10t weight) was determined for 20 years with a yearly increase of 0.03%. The average daily traffic flow with heavy vehicle percentages according to road types presented following:

- Motorway case study – 13000 ADT with 18% trucks; (3,5m width four lanes, two directions traffic).
- National road case study – 3000 ADT with 12% trucks (3,5m width two lanes, two directions traffic).
- Country road case study – 1100 ADT with 10% trucks. (3,5m width two lanes, two directions traffic).

Table 4-15. Pavement structures analyzed with ViaStructura.

Road type (Case study)	Layer	Mix	LTU typical structures	
			Thickness, mm	Modulus at 20°C
1	*2*	*3*	*6*	*7*
Motorway (MW)	AC Surface	PLCM mixes	40	Depends on mix
	AC Binder	AC 16 AS (50/70)	80	6000
	AC base	AC 32 PS (50/70)	140	5400
	Unbound base	Crushed aggregate	200	350
	Unbound subbase	Gravel	340	100
	Subgrade	SB soil	-	45
National Roads (NR)	AC Surface	PLCM mixes	40	Depends on mix
	AC Binder	AC 16 AS (50/70)	40	6000
	AC base	AC 32 PS (50/70)	100	5400
	Unbound base	Crushed aggregate	200	350
	Unbound subbase	Gravel	300	100
	Subgrade	SB soil	-	45
Country Road (CR)	AC Surface	PLCM mixes	40	Depends on mix
	AC base	AC 22 PN (70/100)	100	5300
	Unbound base	Crushed aggregate	200	350
	Unbound subbase	Gravel	300	100
	Subgrade	SB soil	-	45

The pavement structure window provides a table with the thickness, type, material name, stiffness modulus, and adhesion coefficient of the pavement structure layers. The analysis points are set up automatically according to structure and performance functions: at the bottom of asphalt layers and top of each unbound base layer and subgrade. The stress and strains estimation are based on multilayer elastic theory in the analysis points.

Figure 4-52 shows the surface temperature ranges according to the zones of Lithuania.

The temperature profile (gradient) of asphalt layers is determined according to Speth's (1985) and Hess's (1996) model. The relative performance of pavement structures with different surface courses were evaluated according to Zone II.

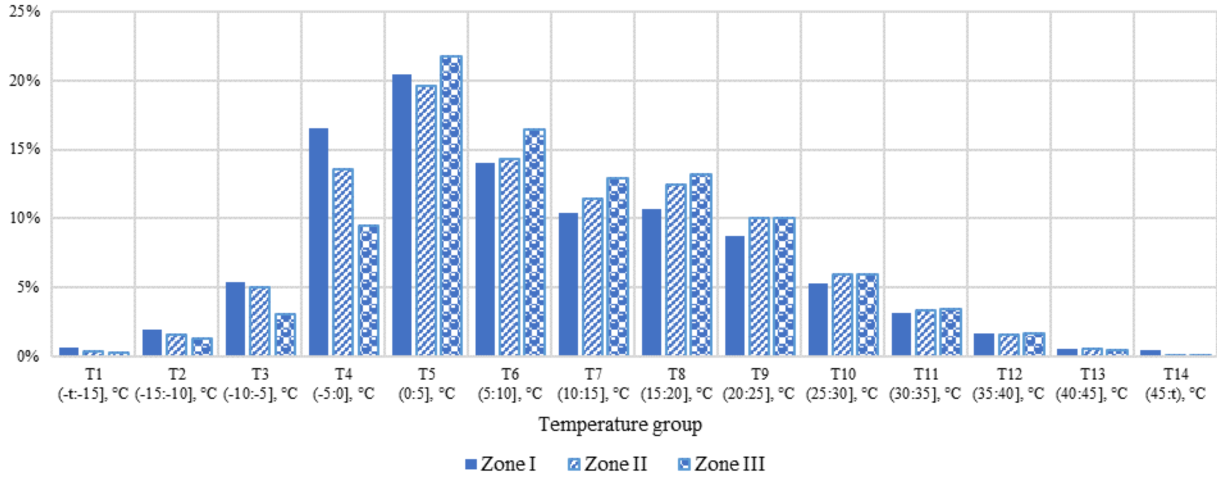

Figure 4-52. Asphalt surface temperature ranges according zones of Lithuania.

4.7.6.3 ViaStructura modelling results for analysis of asphalt surface layer mixtures

This chapter presents the estimated results of the expected performance of the traditional Lithuanian (LTU) structures for a northeast part of Europe, taking into account the local climate, building practice, and traffic conditions. The pavement structures modeled with ViaStructura are detailed in Table 4-15. A total of 12 (4 asphalt mixtures of surface layer x 3 road types) analysis cases were conducted with ViaStructura.

Figure 4-53, Figure 4-54, and Figure 4-55 present the predicted permanent deformation and damage due to fatigue cracking for a Motorway. After traffic analysis, the equivalent standard exile load (ESAL) equal to 17.96 mln per design life (20 years).

According to ViaStructura results for the LTU pavement structures set up for Motorway, the damage can be expected at 25 years in service with ZOAB+ surface layer, 27 years in service with SMA16, 29 years in service with SMA11 40% RA surface layer, and 33 years in service with SMA11 10% RA. Though similar tendencies can be seen, the best relative performance and longest lifetime were determined for pavement structure with SMA11 10% RA.

However, the results determined for the LTU pavement structures can be different comparing with other countries. This is due to traditional structures on the Motorways in Lithuania are designed and constructed applying stricter safety factors. The safety factors were determined based on empirical data collected in the road network of Lithuania and incorporated into the performance functions. Therefore, the expected performance of the pavement structures (shown in Figure 4-53) may not represent the actual performance since the safety factors strains (distort) the damage curves closer to empirical data.

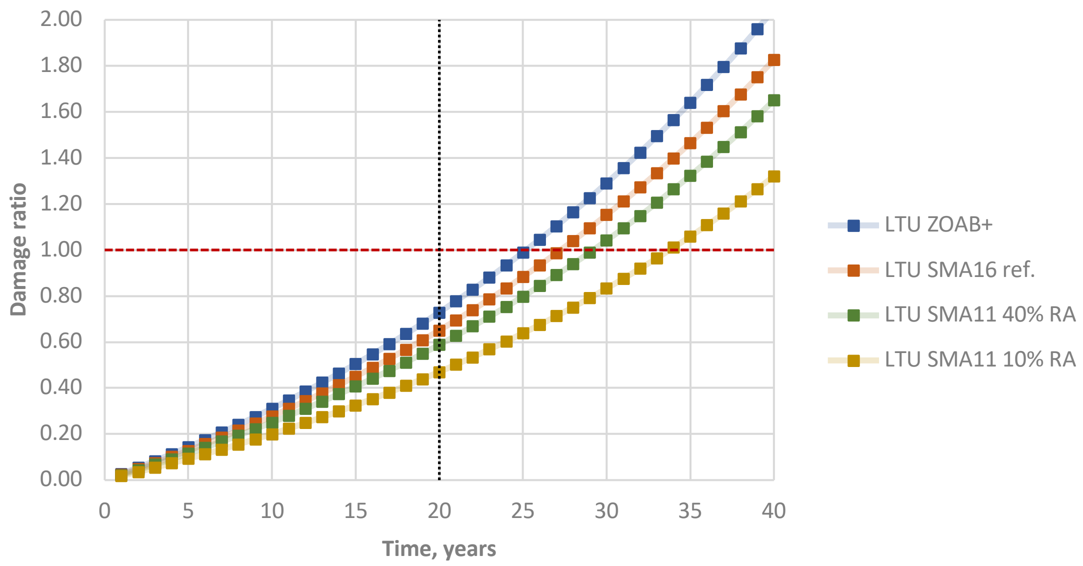

Figure 4-53. Predicted fatigue cracking damage of asphalt layers for a Motorway case study.

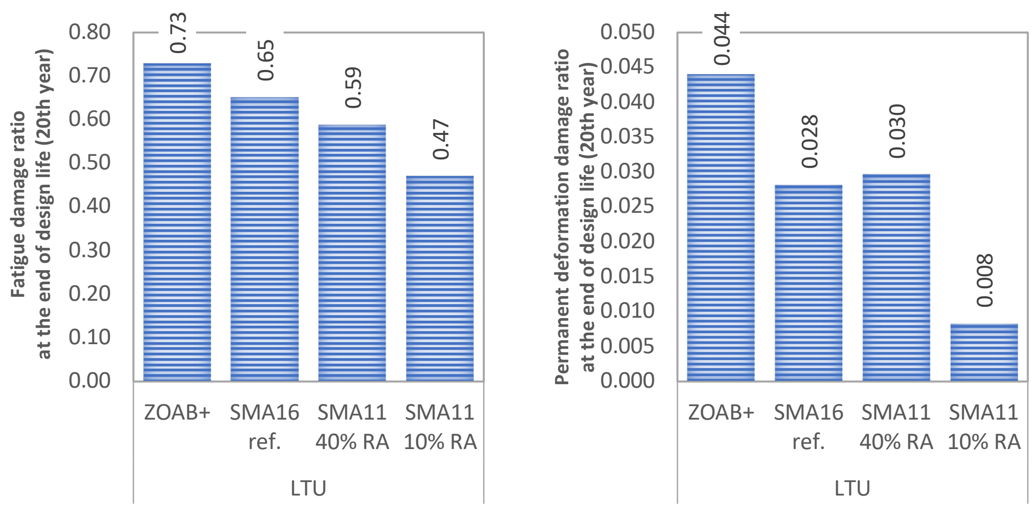

Figure 4-54. Predicted damage ratio of the asphalt fatigue-cracking (left) and unbound base permanent deformation (right) at the end of design life for a Motorway case study.

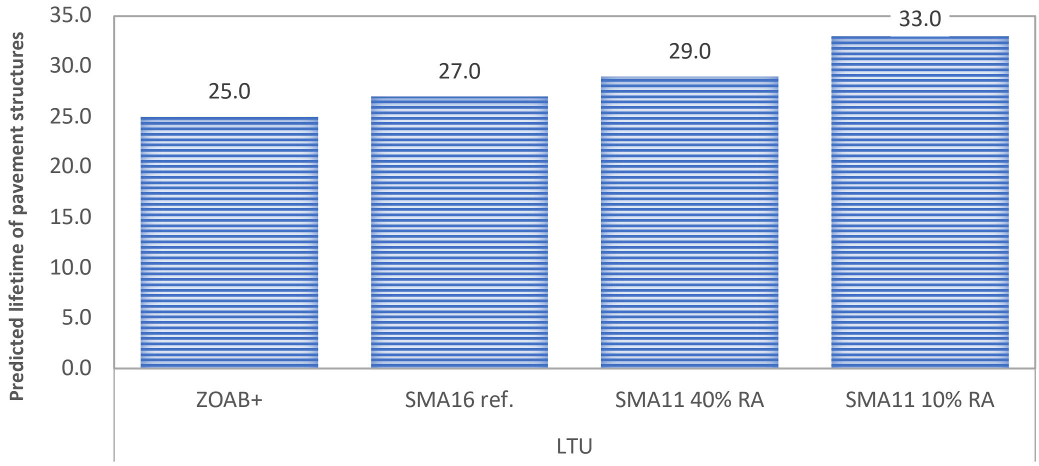

Figure 4-55. Predicted lifetime of pavement structures for a Motorway case study.

Figure 4-56 and Figure 4-57 presents the predicted permanent deformation and damage due to fatigue cracking for a National road case study. After traffic analysis the ESAL equal to 2.03 mln per design life. According to ViaStructura results, the damage in the LTU pavement structures set up for National road can be expected at 23 years in service of a structure with ZOAB+ surface layer, 25-26 years in service structures with SMA16 and SMA11 40% RA surface layers, and 31 years in service a structure with SMA11 10% RA. The asphalt fatigue cracking was the critical damage, so permanent deformations of the unbound layers were insignificant for all pavement structures. The best expected performance was determined for pavement structure with SMA11 10% RA.

Figure 4-59 and Figure 4-60 presents the predicted permanent deformation and damage due to fatigue cracking for a Country road case study. After traffic analysis the ESAL equal to 0.47 mln per design life. According to ViaStructura results, the critical damage in the LTU pavement structure set up for Country road can be expected at 29 years in service of a structure with ZOAB+ surface layer, 31-32 years in service structures with SMA16 and SMA11 40% RA surface layers, and 36 years in service a structure with SMA11 10% RA. Again, the critical damage was fatigue cracking of the asphalt; the permanent deformations of the unbound layers were insignificant for all pavement structures. Better performance was determined for pavement structure with SMA11 10% RA.

To summarize the analysis results of chapter 4.7.6 can be noted that mechanical properties (master curve of stiffness modulus) of wearing layer mixtures (ZOAB+, SMA16, SMA11 40% RA or SMA11 10% RA) can cause the deviation of an expected lifetime for the entire pavement structure by 7-8 years determined with ViaStructura.

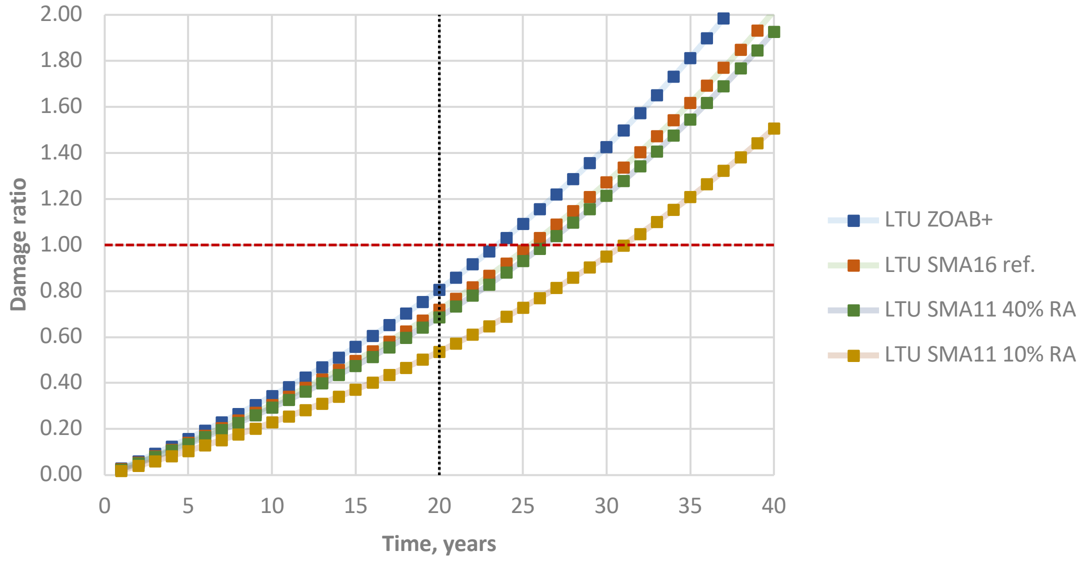

Figure 4-56. Predicted fatigue cracking damage of asphalt layers for a National road case study.

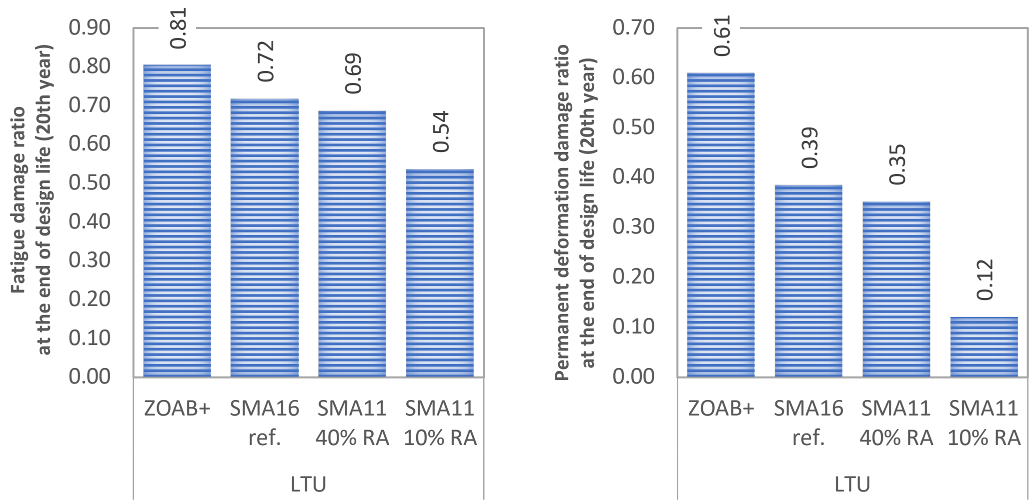

Figure 4-57. Predicted damage ratio of the asphalt fatigue-cracking (left) and unbound base permanent deformation (right) at the end of design life for a National road case study

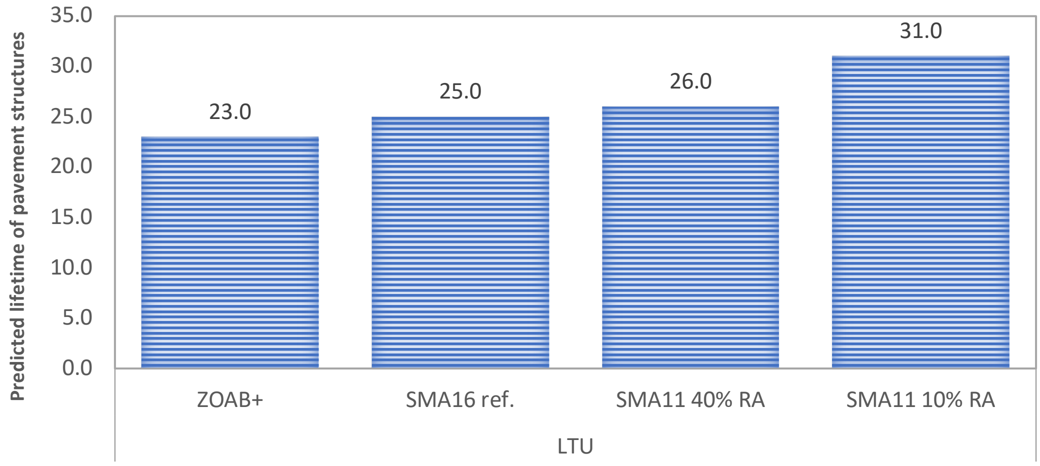

Figure 4-58. Predicted lifetime of pavement structures for a National road case study.

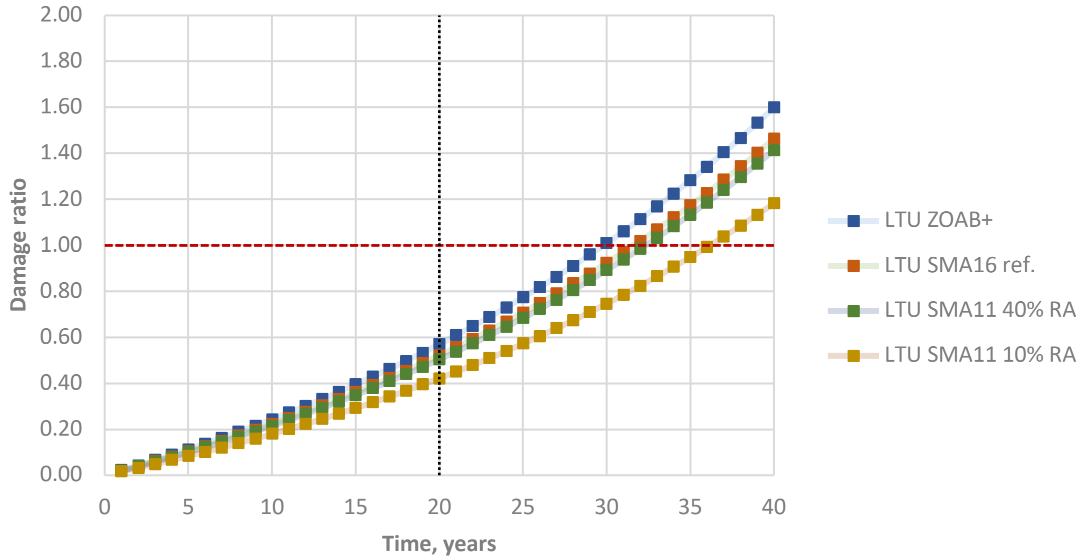

Figure 4-59. Predicted fatigue cracking damage of asphalt layers for a Country road.

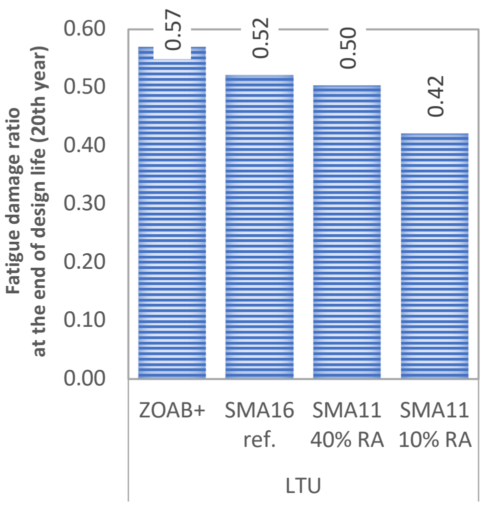

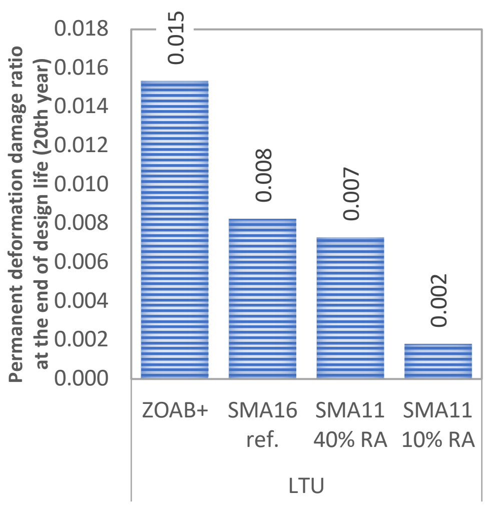

Figure 4-60. Predicted asphalt fatigue-cracking damage ratio (left) and unbound base permanent deformation (right) at the end of design life for a Country road case study

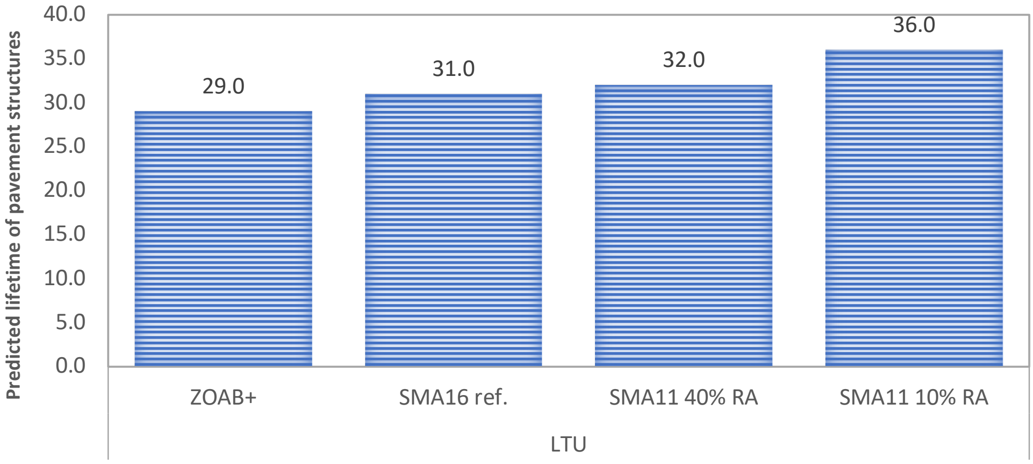

Figure 4-61. Predicted lifetime of pavement structures for a Country road case study.

4.7.7 Summary

The stiffness modulus and shear modulus of eight asphalt mixtures, four stone mastic asphalt (SMA) and four porous asphalt (PA) mixtures, were evaluated in this chapter. The unaged asphalt mixtures were experimentally characterised in laboratory, while the Hirsch model was used to obtain the modulus master curves of asphalt mixtures after ageing based on the test data of recovered binders. The PEDRO and ERAPave PP models were used model and predict the performance of asphalt mixtures in different pavement structures.

The tests indicated that the SMA11 10%RA mixtures showed the highest stiffness and shear modulus. Whereas the SMA11 40%RA and SMA16 produced similar level stiffness and shear modulus values. The SMA8 60%RA showed the least stiffness modulus and shear modulus values.

For the PA, ZOAB+ mixture exhibited a higher stiffness values at higher loading frequencies (lower temperature) and slightly lower modulus at lower frequencies (higher temperature). Also, the phase angle values, ZOAB+ showed a higher phase angle values especially at intermediate to lower frequencies. PA8 panacea and PA8 aramid showed a very similar stiffness modulus and phase angle values over all loading frequencies. The PA8 mixture showed the lowest stiffness modulus values among all the PA mixtures. The shear modulus tests confirmed the result of stiffness modulus tests and produced the same ranking of the PA mixtures.

The SMA11 10% RA showed the best rutting resistance compared to the other SMA mixes followed by the SMA 8 having 60% RA. SMA11 having 40% RA and SMA16 produced similar performance.

For the PA mixes, the PA8 panacea and PA 8 aramid resulted very similar performance. Whereas the ZOAB+ showed a relatively poor rutting performance. The reason could be the slightly lower shear modulus of the ZOAB+ mix at higher temperatures and a maximum phase angle located at relatively lower frequency.

The ERAPave PP analysis revealed that, in general, the SMA11 10% RA mixture produced the best performance in terms of rutting and fatigue cracking. All the SMA mixtures produced nearly similar levels of rutting and fatigue damage for the national road having intermediate traffic volume.

The predicted rutting and fatigue damages were relatively higher for PA mixes compared to the SMA mixes. The ZOAB+, PA8 panacea and PA8 aramid mixtures produced very similar performance for rutting and fatigue cracking for all the pavement structures and traffic classes considered. The PA8 mixture produced the least rutting resistance compared to the other PA mixtures.

5 Accelerated load test

5.1 Objectives and methodology

The objective of the ALT study was to investigate the evolutions of the eight mixtures in a simulated traffic environment in different climatic situations and in different state of ageing.

The test should investigate the mixes propensity to rutting and deformation, ravelling, friction loss, and in the final phase also their sensitivity to cracking in case there are deficiencies in the bearing capacity of the road structure.

5.2 Sample preparation

Asphalt plates were produced from fresh and aged mixes with a roller compactor and a steel frame with the dimensions 50 x 70 x 4 cm. The frame was charged with the amount of mix so that the target density, see Table 4-2, would be reached in the central parts of the plate. Each plate was trimmed, i.e., two short ends of the plate were cut to create a trapezoidal shape, to make them fit into the track of the circular road simulator.

After trimming the plates and fitting them into the track, joints were filled with mortar and the machine run for a few minutes at elevated temperature to push each plate firmly to the base.

There are 28 positions in the machine. Similar materials were placed after each other. The laying order is shown in Table 5-1. Two materials unaged SMA 16 and SMA 11 40% RA were placed in three positions.

Table 5-1. Positioning of plates in CRS

	SMA 16	SMA 11 10 % RA	SMA 11 40 % RA	SMA 8 60 % RA	PA 16	Fibra 1	Fibra 3	Fibra 4
Unaged	22, 25, 26	16	19, 27, 28	13	10	1	4	7
Short term aged, 1 week	23	17	20	14	11	2	5	8
Long term aged, 2 weeks	24	18	21	15	12	3	6	9

Figure 5-1. Laying of asphalt plates in the CRS.

5.3 Test conditions

The test in the CRS was divided in three phases:

1. 35 °C in dry conditions. 60 000 laps
2. ~ 0 °C. Seven freeze-thaw cycles in wet conditions. Each cycle started at -2 °C and gradually increased to 2 °C. 120 000 laps.
3. 30 °C in dry conditions with a soft base. Running until pavement failure. 2 000 laps.

In the final phase 3 the plates were released, and a 19 mm cellular rubber sheet were glued to the bottom of the plate and to the base and then fixed to the track. Joints were filled with mortar.

Four tires, Cooper Discoverer S/T MAXX, LT 235/85 R16, was used in the for the test in the CRS. This tire type is typically used for SUV. The inflation pressure was 3,5 Bar. Each tyre was loaded with 450 kg.

5.4 Evaluation of condition of tests plates in the CRS

The evolution of the condition of the sample plates was followed by

- visual inspections every day
- photography at 0; 60 000; 120 000; 180 000 laps and for documentation of damages observed during visual inspections.
- Texture measurement with a laser instrument mounted on one of the arms of CRS at 20 000, 60 000; 120 000; 180 000 laps
- Friction at 0, 60 000; 120 000; 180 000 laps.
- Transversal profile measurements at 0, 12 000 20 000, 60 000; 120 000; 180 000 laps.

5.5 Visual inspections, ravelling and cracking.

After 12 000 laps there were some stone losses from the long term aged porous asphalt mixes with 8 mm chipping size. See Figure 5-2 to Figure 5-4. These plates were repaired with hard oxidized bitumen.

Figure 5-2. Stone losses after 12 000 laps at 30 °C for long term aged Fibra 1 mix.

Figure 5-3. Stone losses after 12 000 laps at 30 °C for long term aged Fibra 3 mix.

Figure 5-4. Stone losses after 12 000 laps at 30 °C for long term aged Fibra 4 mix.

Figure 5-5 Cracks after 120 000 laps in SMA 8 60 % RA, long term aged.

Table 5-2. Conditions of test plates in the CRS study. Green indicates no failure; Orange indicates beginning of failure – either cracks or ravelling (Rav.). Black indicates that the material has been replaced or repaired.

Laps		SMA 16	SMA 11 10 % RA	SMA 11 40 % RA	SMA 8 60 % RA	PA 16	Fibra 1	Fibra 3	Fibra 4
12 000									
	1 W								
	2 W.						Rav.	Rav	Rav
20 000									
	1 W								
	2 W								
60 000									
	1 W								
	2 W.								
120 000									
	1 W								
	2 W.				Cracks				
180 000									
	1 W								
	2 W.								
180k + 200		Cracks			Cracks	Cracks		Cracks	Cracks
	1 W	Cracks			Cracks	Cracks	Rav	Cracks	Cracks
	2 W.	Cracks				Cracks			
180k + 2000			Cracks	Cracks			Rav		
	1 W		Cracks	Cracks			Rav		
	2 W.		Cracks	Cracks					

The long term aged Fibra mixes failed early in the first phase (high temperature test phase) of the test. Despite large differences in the binder properties after long term ageing, cf. Table 4-5 and Figure B-6 - Figure B-8, ravelling occurred for the three mixes at approximately the same time.

Both the fresh and short term aged Fibra mixes lasted through the second phase (wet freeze thaw test phase) of the test, but cracks appeared in the beginning of the third phase (flexibility test cycle) both for the fresh and short term aged Fibra 3 and Fibra 4 mixes.

Ravelling did not occur on the unaged Fibra 1 mix until the final laps of the third phase. The short term aged Fibra 1 mix started to have noticeable material loss in the beginning of the third phase.

The reference porous asphalt mix, the PA16 or ZOAB+ mix, in all states, fresh, short term aged, and long term aged, got cracks in the plates after the first part of the final 3rd phase. Thus, in this flexibility test the Fibra 1 mix performed better than the ZOAB+ mix which perhaps was to be expected since the Fibra 1 mix contains a polymer modified binder while the ZOAB+ does not.

For the SMA mixes the first mix to show serious flaws was the SMA8 with 60% rejuvenated RA. The long term aged state of this mix got cracks in the plate after the first part of the second phase (wet freeze thaw test phase) of the test. The binder in the long termed aged mix had become quite stiff after the ageing procedure cf. Figure 4-6 and Figure B-1.

Cracks appeared on the unaged and short term aged SMA8 60% RA mixes after the first part of the final 3rd phase.

The reference SMA mix, the SMA16 mix showed no serious ravelling or cracks in the plates until the final 3rd phase, when the plates with mixes in all states, fresh, short term aged, and long term aged, showed some cracks.

Both the SMA11 mixes with 10 and 40 % RA in the mixes, respectively, lasted longer than the reference SMA16 mix. These mixes showed some cracks in the plates first in the final part of the 3rd phase.

5.6 Texture measurements

The texture of the surface was measured with a point laser in the wheel track at during the test. From the texture profile, the MPD (Mean Profile Depth) (the average maximum peak height above the mean surface height, in two consecutive 50 mm sections) and the MPH (Mean Profile Height) was calculated. The MPH is calculated in an analogous way as MPD only that the average maximum valley depth is used instead of the peak height. A change in MPD and MPH values during a test is a good indication of wear, fretting, ravelling or clogging.

Plates of the unaged reference SMA16 mix were placed in positions 22, 25 and 26 in the CRS. Short term aged and long term aged material of the SMA16 mix were placed in position 23 and 24. The MPD and MPH values for these plates are shown in Table 5-3 and in Figure 5-6 and Figure 5-7. The plate to plate variation is what to be expected and there is are only small changes in the texture during the two first phases of the CRS study.

Table 5-3. MPD and MPH for plates of the reference SMA16 mix during CRS study.

	MPD (mm)					MPH (mm)				
SMA16	**Unaged plate 22**	**Unaged plate 25**	**Unaged plate 26**	**Short term aged plate 23**	**Long term aged, plate 24**	**Unaged plate 22**	**Unaged plate 25**	**Unaged plate 26**	**Short term aged plate 23**	**Long term aged, plate 24**
20k rev.	1,19	1,23	0,90	0,94	0,97	2,44	2,12	1,69	2,24	2,15
60k rev.	1,22	1,29	0,92	0,96	0,94	2,38	2,22	1,58	2,11	2,10
120k rev.	1,23	1,33	0,93	0,99	0,96	2,34	2,21	1,59	2,15	2,16
180k rev.	1,24	1,29	0,93	0,99	0,96	2,42	2,25	1,65	2,18	2,18

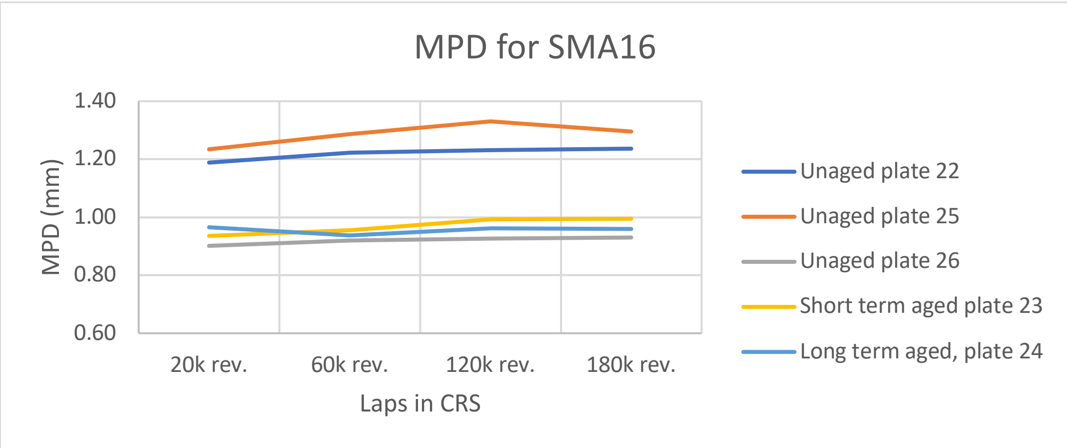

Figure 5-6. Mean profile depth for the reference SMA16 during the CRS test

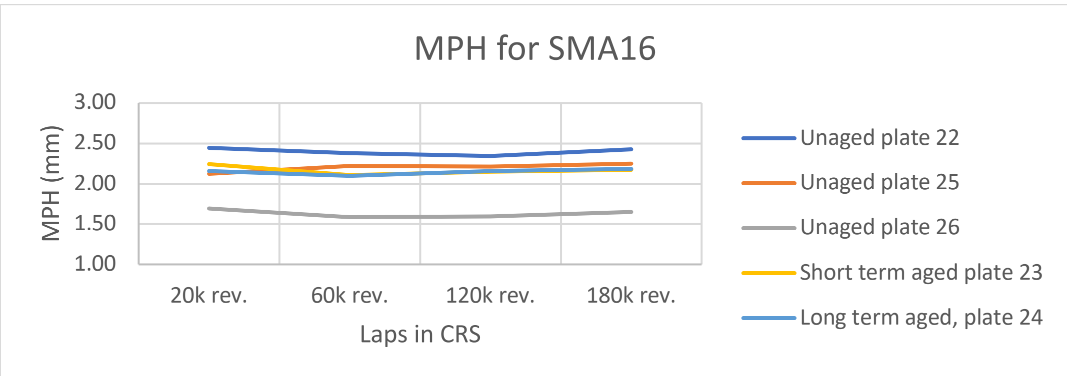

Figure 5-7. Mean profile height for the reference SMA16 during the CRS test

Plates of the SMA11 40% RA was also placed in five positions in the CRS. The texture of the SMA11 40% RA varied only slightly during the test. The data is presented in Table

5-4, Figure 5-8 and Figure 5-9. The plate to plate variations is what to be expected. The MPD was generally lower for this mix compared to the reference mix. The MPH values for the plates with the aged mixes were higher than the plates with unaged mixes indicating that the compaction was affected somewhat by the stiffness of the aged binder.

Table 5-4. MPD and MPH for plates of SMA11 40% RA mix during CRS study.

	MPD (mm)					MPH (mm)				
SMA11 40% RA	Unaged plate 19	Unaged plate 27	Unaged plate 28	Short term aged plate 20	Long term aged, plate 21	Unaged plate 19	Unaged plate 27	Unaged plate 28	Short term aged plate 20	Long term aged, plate 21
20k rev.	0,74	0,65	0,67	0,77	0,82	1,12	1,24	1,07	1,78	2,22
60k rev.	0,73	0,60	0,66	0,78	0,83	0,99	0,94	0,90	1,71	2,16
120k rev.	0,75	0,61	0,67	0,79	0,82	1,04	0,98	0,96	1,69	2,17
180k rev.	0,75	0,60	0,66	0,79	0,84	1,05	1,02	0,96	1,75	2,17

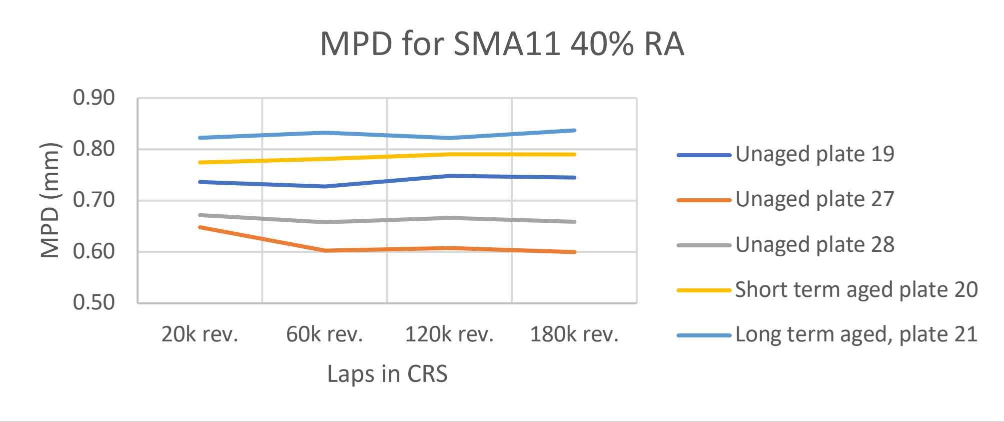

Figure 5-8. Mean profile depth for the SMA11 40% RA during the CRS test

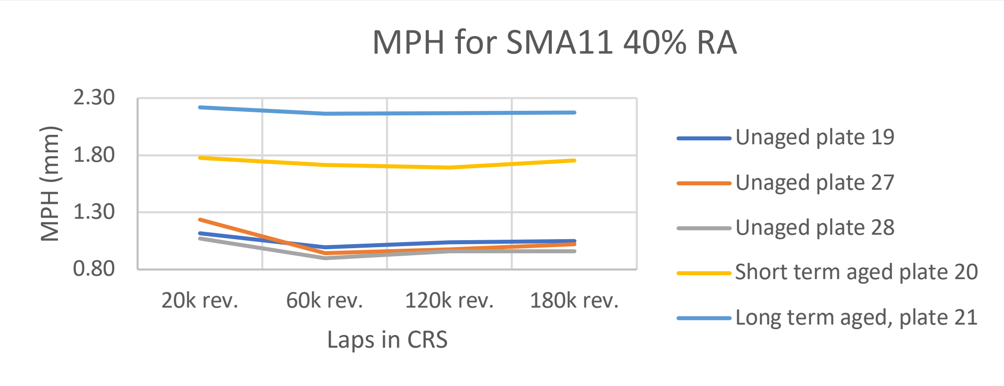

Figure 5-9. Mean profile height for the SMA11 40% RA during the CRS test

The rest of the mixes were placed in three positions in the CRS.

The data for the SMA11 10 % RA and SMA8 60% RA are presented in Table 5-5 and Table 5-6.

Table 5-5. MPD and MPH for plates of SMA11 10% RA mix during CRS study.

	MPD			MPH		
SMA11 10% RA	**Unaged plate 16**	**Short term aged plate 17**	**Long term aged, plate 18**	**Unaged plate 16**	**Short term aged plate 17**	**Long term aged, plate 18**
20k rev.	0,91	0,88	0,93	2,27	2,32	2,36
60k rev.	0,93	0,88	0,92	2,16	2,30	2,31
120k rev.	0,96	0,93	0,92	2,16	2,28	2,32
180k rev.	0,95	0,92	0,92	2,17	2,31	2,35

Table 5-6. MPD and MPH for plates of SMA8 60% RA mix during CRS study.

	MPD			MPH		
SMA8 60% RA	**Unaged plate 13**	**Short term aged plate 14**	**Long term aged, plate 15**	**Unaged plate 13**	**Short term aged plate 14**	**Long term aged, plate 15**
20k rev.	0,66	0,75	0,62	1,30	1,99	1,58
60k rev.	0,68	0,73	0,60	1,24	1,81	1,53
120k rev.	0,68	0,73	0,69	1,28	1,81	1,78
180k rev.	0,69	0,74	0,76	1,28	1,87	1,88

The results for SMA8 60% RA is also presented in Figure 5-10 and Figure 5-11. At 120k laps in the plate with the long term aged mix had begun to crack. The texture increases rapidly when this occurred.

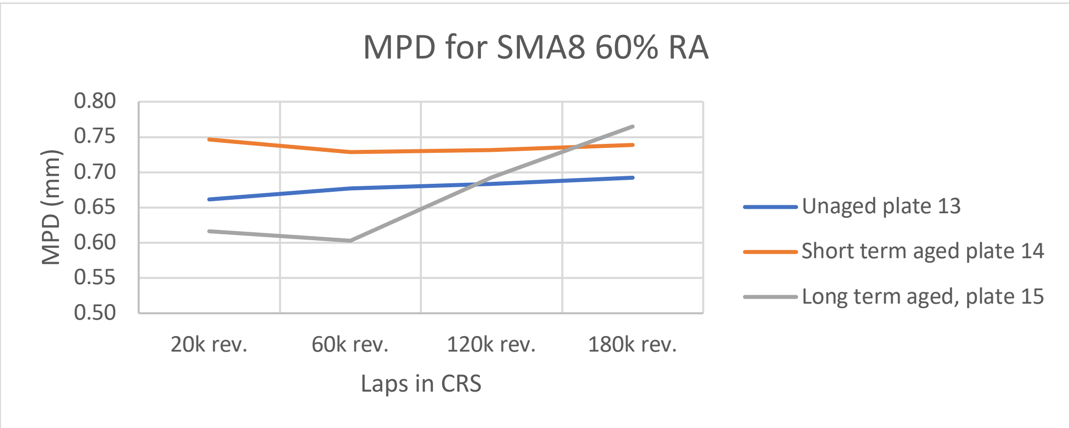

Figure 5-10. Mean profile depth for the SMA8 60% RA during the CRS test.

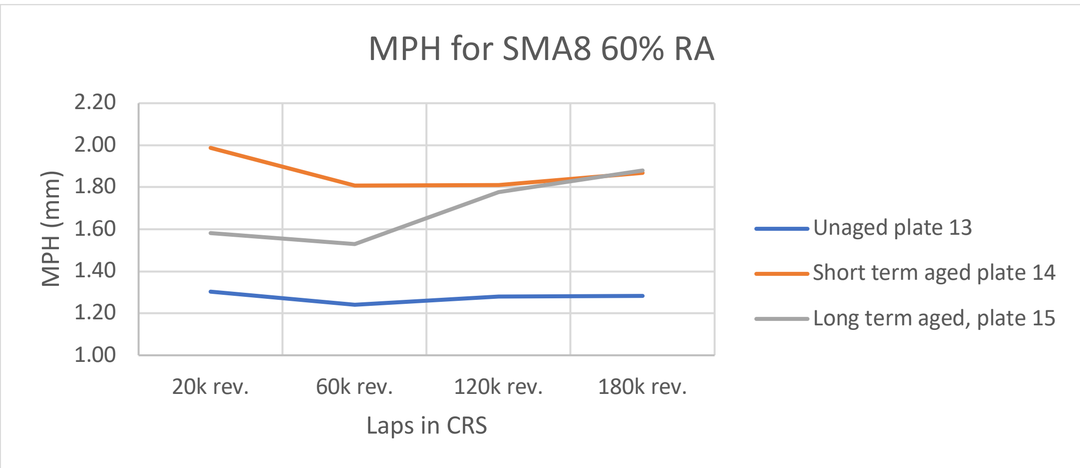

Figure 5-11. Mean profile height for the SMA8 60% RA during the CRS test

For the porous pavements the MPH values is higher compared to the SMA mixes with the same nominal chipping size as can be seen by comparing Figure 5-13 with Figure 5-7.

Table 5-7. MPD and MPH for plates of PA16 mix (ZOAB+) during CRS study.

	MPD			MPH		
PA16	Unaged plate 10	Short term aged plate 11	Long term aged, plate 12	Unaged plate 10	Short term aged plate 11	Long term aged, plate 12
20k rev.	1,18	1,13	1,57	2,56	2,76	3,21
60k rev.	1,29	1,27	1,45	2,64	2,61	3,09
120k rev.	1,34	1,38	1,43	2,70	2,77	3,09
180k rev.	1,37	1,37	1,42	2,77	2,81	3,10

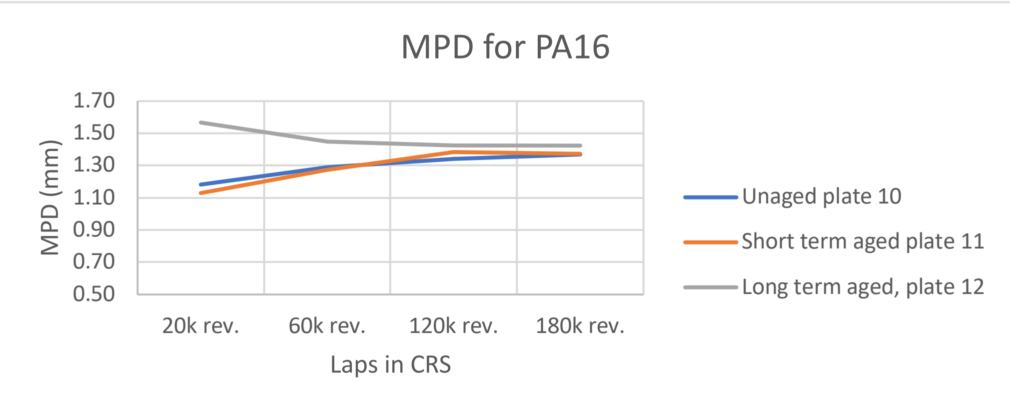

Figure 5-12. Mean profile depth for the reference PA16 (ZOAB+) during the CRS test.

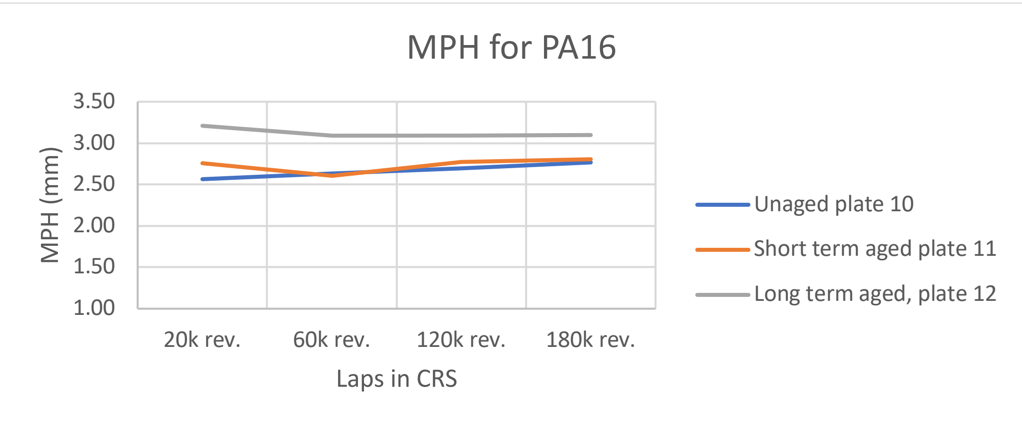

Figure 5-13. Mean profile height for the reference PA16 (ZOAB+) during the CRS test.

The texture results for Fibra 1, 3 and 4 mixes are presented together in Table 5-8, Figure

5-14 and Figure 5-15.

Only the measurements for the plates with unaged mixes and the short term aged mixes are presented in the tables and figures as the plates with the long term aged mixes were repaired early on in the test. The data show that there was no ravelling from the plates in the two first phases of the test.

Table 5-8. MPD and MPH for plates of Fibra mixes during CRS study.

	MPD						MPH					
Fibra mixes	**Fibra 1 Unaged plate 1**	**Fibra 1 Short term aged plate 2**	**Fibra 3 Unaged plate 4**	**Fibra 3 Short term aged plate 5**	**Fibra 4 Unaged plate 7**	**Fibra 4 Short term aged plate 8**	**Fibra 1 Unaged plate 1**	**Fibra 1 Short term aged plate 2**	**Fibra 3 Unaged plate 4**	**Fibra 3 Short term aged plate 5**	**Fibra 4 Unaged plate 7**	**Fibra 4 Short term aged plate 8**
20k rev.	1,62	1,20	1,27	1,15	1,16	1,18	2,82	2,87	2,56	2,66	2,54	2,64
60k rev.	1,82	1,33	1,39	1,30	1,25	1,31	3,22	2,47	2,56	2,61	2,43	2,65
120k rev.	1,64	1,26	1,29	1,26	1,33	1,22	3,20	2,65	2,57	2,70	2,56	2,69
180k rev.	1,64	1,25	1,35	1,30	1,33	1,27	3,34	2,74	2,71	2,70	2,57	2,80

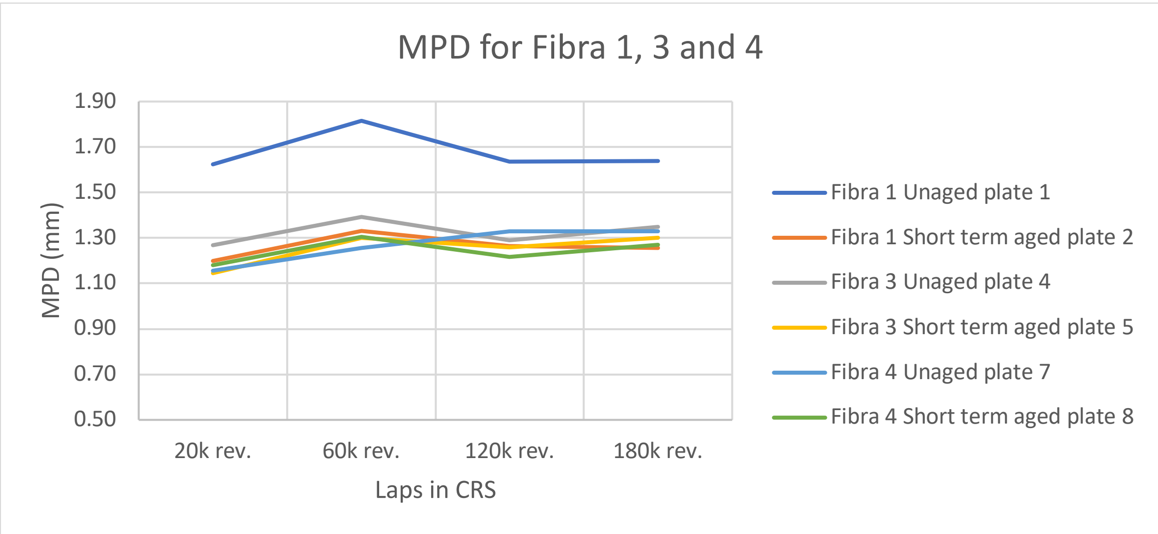

Figure 5-14. Mean profile depth for the Fibra mixes during the CRS test.

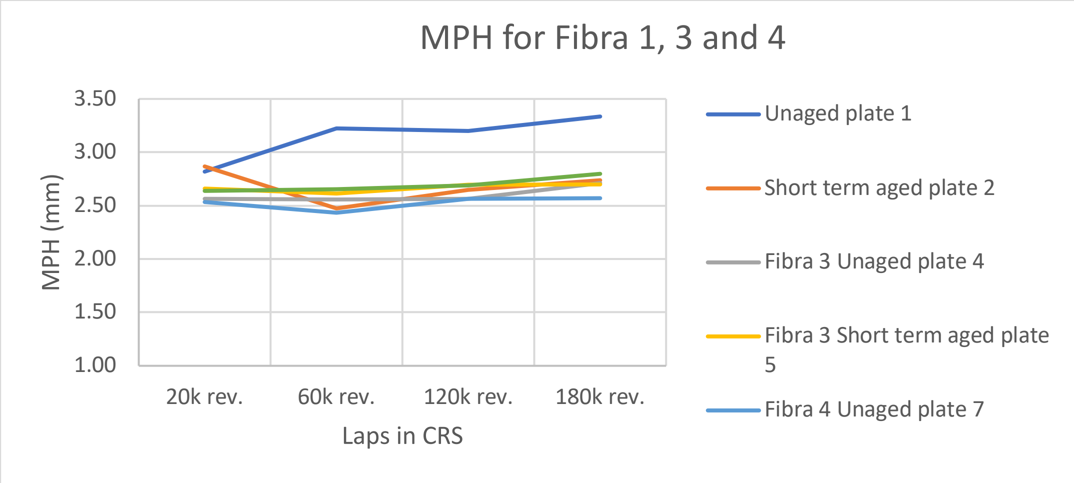

Figure 5-15. Mean profile height for the Fibra mixes during the CRS test.

5.6.1 Conclusions

The texture was generally higher for mixes with larger chipping sizes and larger for porous pavements compared mixes with smaller chippings and dense pavements. The texture measurements was in good agreement with the visual inspections and showed that in most cases the texture of the plates maintained at approximately the same level during phase 1 and 2 of the CRS test. A notable exception was the plate with long term aged SMA8 60% RA where the MPD and the MPH values increased after 60 k laps. This plate showed some cracks in the surface at the same time. Texture measurements was not done on plates with severe revelling or surface that had been repaired.

5.7 Friction measurements

Friction was measured with a portable and dynamic friction tester using the skiddometer principle where the measuring wheel travels at lower speed (75%) compared to the carrying wheels and thus has a constant slip towards the surface (Sjögren, 2019). The friction was measured in the wheel track and in wet conditions. The measuring distance was approximately 0,6 meter on each plate and three repeated measurements was done in at approximately 15 °C. Measurements were done in the beginning and after 60 000; 120 000; 180 000 laps.

The results from the measurements on plates with unaged materials is shown in Table 5-9 and Figure 5-16.

Table 5-9. Mean friction values for all plates with unaged mix during the CRS study.

	0 k	60 k	120 k	180 k
Fibra 1 (PA8)	1,00	0,97	0,95	1,04
Fibra 3 (PA8 panacea)	0,96	1,04	1,01	1,02
Fibra 4 (PA8 aramid)	0,98	1,02	0,99	0,95
ZOAB+ (PA16)	0,91	0,96	0,91	0,79
SMA 8 60% RA	0,96	0,99	0,88	0,79
SMA 11 10% RA	0,91	1,05	0,86	0,80
SMA 11 40% RA	0,93	1,16	0,88	0,80
SMA 16	0,90	1,06	0,82	0,73

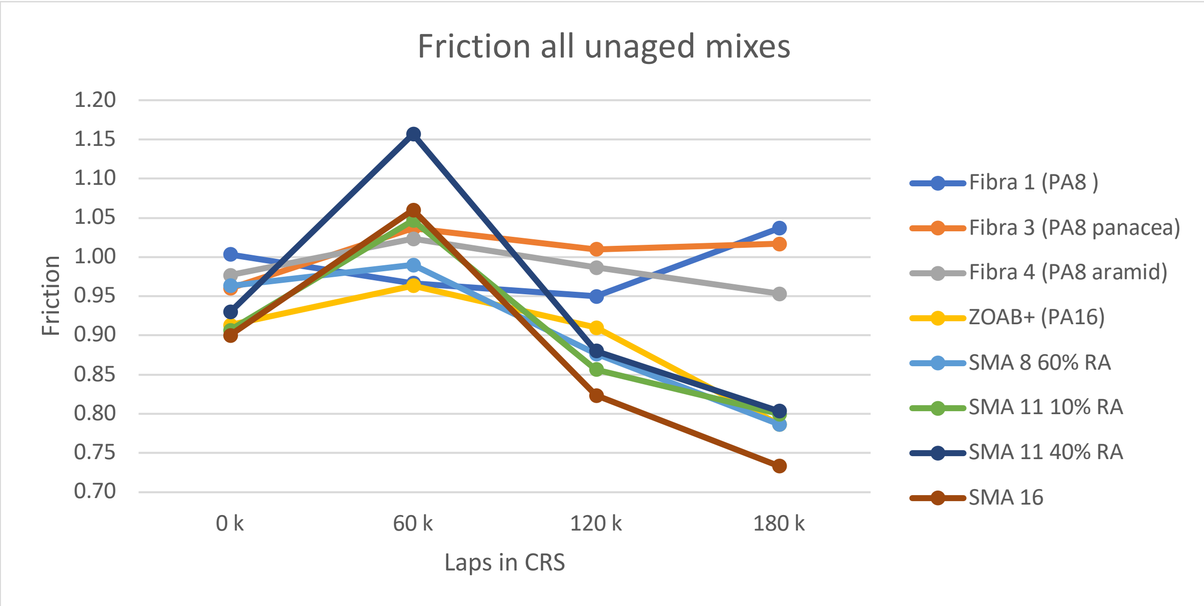

Figure 5-16. Mean friction values for all plates with unaged mix during the CRS study.

The friction remained at reassuring level for the three Fibra mixes thru out the test. All the other mixes the PA16 included, had an initial increase of the friction during the first dry and warm phase of the CRS study and then a continuous drop of the friction during the wet and cold phase. The lowest value recorded was still above 0,7 which is above the usual regulatory limit of 0,5.

There was not much variation between plates with the same type of mix regardless if the mixes was unaged or aged as illustrated with the SMA11 40% RA in Figure 5-17.

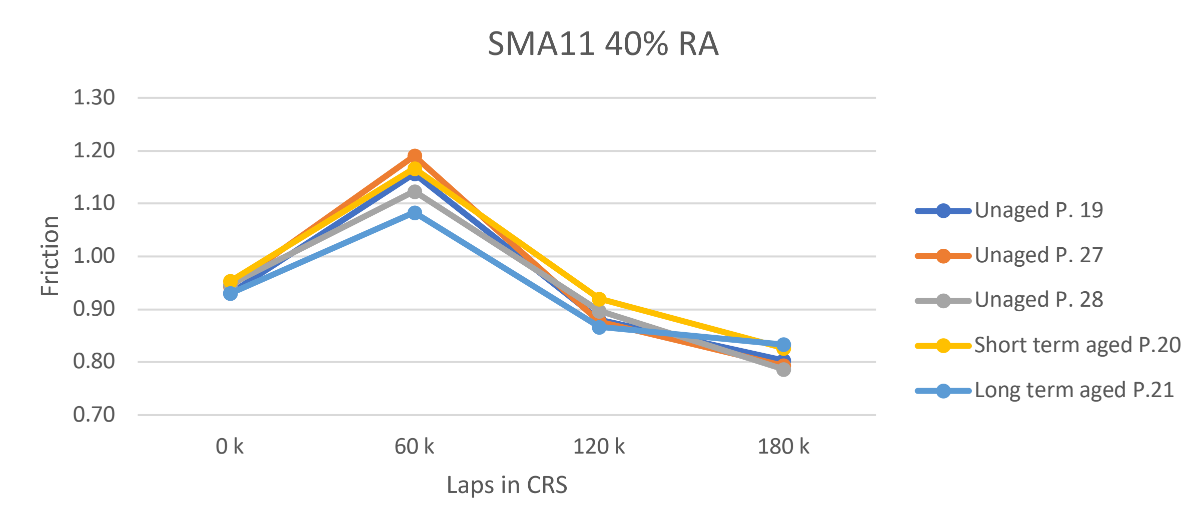

Figure 5-17. Mean friction values for all plates with SMA11 40% RA.

5.8 Profile measurements

Three transversal profiles for each plate were recorded with a laser profilometer before the CRS started and after 12 000 20 000, 60 000; 120 000; 180 000 laps.

Two of the 84 profiles are shown in Figure 5-18 and Figure 5-19. The first figure shows an example when rutting is obvious in the first phase of the test up to 60 000 laps. The second figure is an example where there is some rutting present but not at the same level as in the first example. Table 5-9 summarize the transverse profile measurements and indicates the level of rutting.

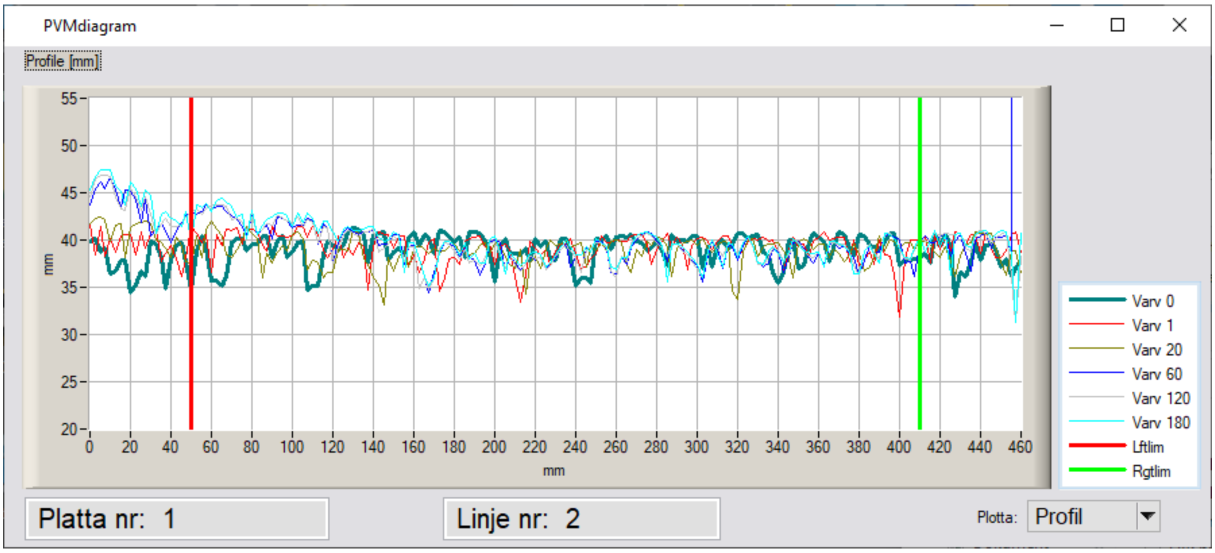

Figure 5-18. Transverse profile of Fibra 1 after 0 (Varv 0); 12 000 (Varv 1) 20 000 (Varv 20); 60 000 (Varv 60); 120 000 (Varv 120); and 180 000 (Varv 180) laps in the CRS.

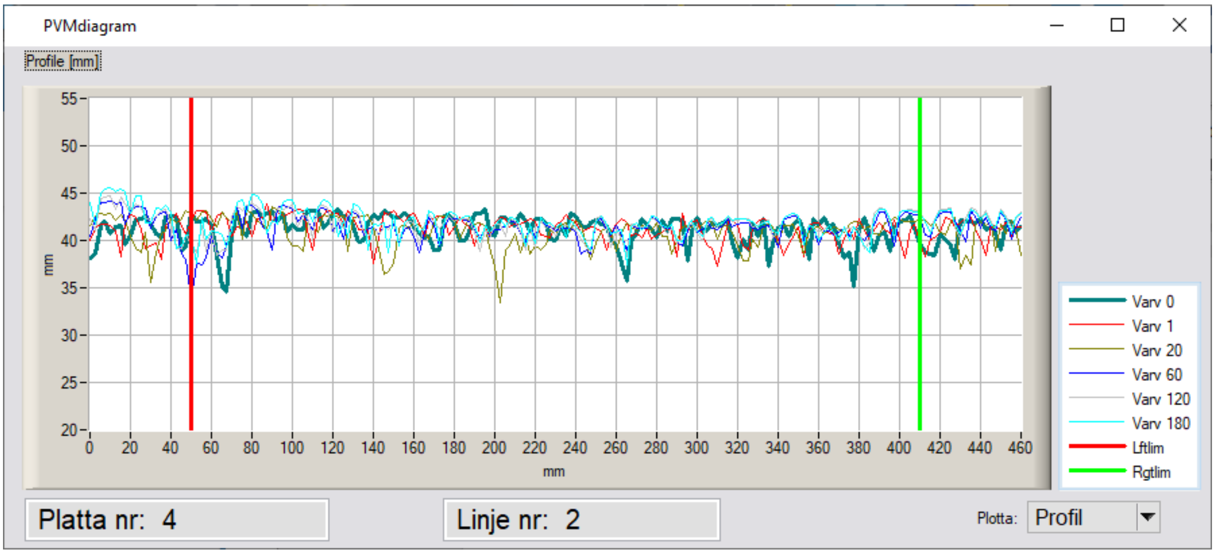

Figure 5-19. Transverse profile of Fibra 3 after 0 (Varv 0); 12 000 (Varv 1) 20 000 (Varv 20); 60 000 (Varv 60); 120 000 (Varv 120); and 180 000 (Varv 180) laps in the CRS.

Table 5-10. Rutting in the CRS study. An uppercase X indicates that profile measurements showed clear signs of rutting. A lowercase x indicates that there are minor rutting in the test.

	SMA16	SMA11 10 % RA	SMA11 40 % RA	SMA8 60 % RA	PA16	Fibra 1	Fibra 3	Fibra 4
Unaged	x	x	X	X	X	X	x	X
Short term aged, 1 week	-	-	-	-	X	_	x	-
Long term aged, 2 weeks	-	-	-	-	-	_		

All plates with unaged material show some extent of rutting. The SMA mixes SMA11 40% RA and SMA8 60% RA demonstrated slightly more rutting than the reference SMA16. Of the porous mixes, Fibra 3 mix had a slightly lower tendency for rutting compared to the other mixes. Most aged materials had little or no tendency for rutting in this test. The PA16 and the Fibra 3 mixes showed some rutting in the short termed aged materials.

6 Factors affecting durability of surface courses. Experts' judgment.

A questionnaire was issued to collect information from local experts regarding the durability of the reference mixes SMA16 and PA16. For the countries where there is little information regarding mixes with nominal mean aggregate size of 16, respondents were asked to answer the questions with regards to NMAS of 11. The questionnaire has been described in Deliverable 2.1 (Jiménez del Barco Carrión, Buttitta, Neves, & Lo Presti, 2021).

In the questionnaire, high-volume roads were defined as having AADT above 4000. roads Low volume roads, medium volume roads in the questionnaire were defined as having AADT between 100 to 400, 401 to 4000, respectively.

6.1 *Distresses triggering pavement resurfacing.*

Experts from Germany, Denmark, Lithuania, Sweden, Norway, and the Netherlands gave answers to questions which types of surface distress that are typical to causing resurfacing for low, medium, and high-volume roads. All experts except one answered that there are procedures or databases in their countries where the distresses, and possible other reasons for pavement maintenance operations, are detailed. The respondents were asked to classify each type of distress in terms of how likely it is that its presence triggered the decision to resurface a pavement with SMA or PA. The distress the respondents could choose among were:

- Fretting (minor material loss)
- Ravelling (severe material loss)

- Rutting
- Road wear
- Low friction
- Cracking (not specified)
- Transverse cracking
- Longitudinal cracking
- Edge cracking
- Block cracking
- Alligator cracking
- Other

The result for the high-volume roads is presented in Table 6-1 for SMA16 or SMA11 and in Table 6-2 for PA16. Not all experts answered the questions for both types of reference mixes.

Table 6-1. Distress likely to trigger resurfacing of high-volume roads with for SMA16 (or SMA11, or SMA11 10%RA). ++ indicates that the distress is likely cause for resurfacing operations. + indicates that the distress is somewhat likely cause for resurfacing operations.

	Denmark	Sweden 1	Sweden 2	Germany	Norway	Lithuania
Answers valid for NMAS	11	16	16	11	16	11
Fretting	++	++			+	++
Ravelling	+	++			+	++
Rutting	+	++	++		++	
Road wear		++			+	
Low friction	+			++		++
Cracking (not specified)		+		++		++
Transverse cracking						
Longitudinal cracking		+			+	++
Edge cracking					+	+
Block cracking						+
Alligator cracking		+				+
Other						+

Table 6-2. Distress likely to trigger resurfacing of high-volume roads with PA16 (or PA11). ++ indicates that the distress is likely cause for resurfacing operations. + indicates that the distress is somewhat likely cause for resurfacing operations.

	Sweden 1	Sweden 2	Netherlands	Germany
Answers valid for NMAS	16	16	16	11
Fretting	++			
Ravelling	++		++	++
Rutting		++		
Road wear	++	++		
Low friction				
Cracking (not specified)				
Transverse cracking				
Longitudinal cracking				
Edge cracking				
Block cracking				
Alligator cracking				
Other			+	

6.2 *Effect of change in traffic volume on durability*

In the questionnaire mentioned above respondents were also asked to estimate the how a change in traffic volume or other factors would eventually change the durability (lifetime). A common assumption in structural road engineering is that the Palmgren-Miner linear damage hypothesis applies, which means that each single loading will contribute to the final failure of the road according to the damage each loading generates. The collected answers from the experts about how service life is expected to change upon changing loadings and environmental conditions is presented in Table 6-3.

Table 6-3. The estimated effect in service life if conditions change.

	Denmark	Sweden 1	Sweden 2	Germany	Norway
AADF 8000 -> 6000	5-15%	5-15%	5-15%	5-15%	5-15%
AADF 16000 -> 12000	0-5%	5-15%	15-25%	5-15%	5-15%
AADF 400-> 300	5-15%	5-15%	0-5%	0-5%	0-5%
AADF 8000 -> half # of freeze-thaw cycle	15-25%	0-5%	5-15%	15-25%	0-5%
AADF 400 -> half # of freeze-thaw cycle	5-15%	0-5%	0-5%	15-25%	0-5%
AADF 8000 -> half # of wet days	5-15%	0-5%	15-25%	5-15%	5-15%
AADF 400 -> half # of wet days	5-15%	0-5%	0-5%	0-5%	0-5%

All experts agree that the service life will only change approximately by 10% (5-15 %) if the traffic volume deceases by 25% for a high-volume road with AADF of 8000. If the Palmgren-Miner linear damage hypothesis would apply, the service life would be inversely proportional to the traffic volume. A decrease in traffic volume by 25 % would lead to an increase of the service life by 33% if traffic would be the only factor responsible for the service life.

For roads with even higher traffic volume, ADDF of 16000, the experts have some disagreements in their estimates, but on the average the estimate on how a decease in traffic volume by 25 % would increase the service life is the same: approximately 10 %.

For low volume roads with an AADF of 400, there is a shift in the estimates of how that would the increase the service life. In this case more experts estimate only a marginal effect (0-5 %) on the service life.

From these answers it can be concluded that there are more factors influencing the service than the traffic volume. Factors that usually is mentioned as influencing service life are aging, wet conditions and wet freeze that cycles. Ageing could be caused by exposure to oxygen and UV radiation. The oxidation rate increases with temperature. It is sometimes postulated that pavements will be able to withstand the loadings of the traffic until the binder have reached a state where it is no longer flexible enough to endure the strains caused by the traffic.

Freeze thaw cycles in wet conditions could have an effect on the properties of asphalt concrete pavements. The experts differed among their estimates about the effect of decreasing the number of freeze thaw cycles in wet conditions. The experts from Norway and Sweden in most cases agree that the service life only increases marginally if number of freeze-thaw cycles decreases. The experts from Denmark and Germany agrees that the effect of freeze-thaw cycles on service life is higher. They estimate that the service life would increase more substantially (approximately 20 %) if the number of freeze-thaw cycles decreases by half.

The estimated effect of decreasing the number of wet days by half is on average approximately 10% for high-volume roads although with some variations among the experts.

The number of wet days and the number of freeze-thaw a pavement is exposed to will increase with service life. Oxidative ageing will also increase with service life.

Since experts agrees that a decrease in traffic volume by 25 % would only increase the expected service life for high volume roads by approximately 10% (5-15 %), instead of 33% which would be expected if service life was only dependent on traffic, it can be concluded that other factors that influences the service life, such as ageing and exposure to wet conditions and freeze-thaw cycles have a substantial influence on the service life.

If the estimates are correct, the calculated 33 % increase in service life when traffic volume decrease by 25%, based on Miners' hypothesis would at the same time increase the number of exposures to wet conditions and freeze-thaw cycles by the same amount and ageing would also be increased. If the service life increases only by 10 % when traffic volume decreases by 25%, the number of wet days and number of freeze-thaw cycles would only increase by 10 % which roughly could only explain less than 5% of the difference between the 33 % estimated by Miners' rule and 10% based on experience. From these considerations it is concluded that ageing probably is of major importance for limiting the service life.

7 Conclusion: Estimates of service life of new mixes

To estimate the relative service life of the new asphalt mixtures compared to the reference mixes based on the results from the laboratory studies we must understand the context in which the new mixes is going to be used in, i.e. in which country and which type of road. We also need to have a picture of which type of distresses are common in that context. The latter information was collected in the questionnaire and presented in Table 6-1 and Table 6-2.

There are many different mechanisms which potentially and eventually put a limit on the service life of a surface course. Three main components for the degradation of the surface courses are ageing, climate and traffic. Ageing is usually a consequence of oxidation or UV light. Climate puts stress on the road surface through freeze-thaw cycles; presence of water; extreme temperatures and temperature cycles. Traffic induces stresses and strain on the surface course. The surface course is also a part of the road structure and thus protects to higher or lesser extent the other parts of the structure. If other layers in the structure fails, this will eventually have consequences for the surface course.

The results from the questionnaire clearly demonstrated that all three mechanisms, traffic, climate and ageing are important for the service lives. Thus, any attempt to predict the service life of new mixes needs to address all three factors. To further complicate the situation there are probably positive and negative synergies between the different factors affecting the service life. E.g. ageing usually leads to a stiffening of the binder which in turn could be beneficial for preventing rutting (deformation) but could also be worsening the layer's resistance to withstand fatigue cracking or resist extreme low temperatures.

In the laboratory studies we have used tests to address traffic, climate and ageing separately and in combinations. The different test used can be summarized in Table 7-1.

Table 7-1. factors and tests used to characterize the durability of materials.

	Test	Effect
Climate	Water sensitivity/MIST	Weakening of material
Ageing	Short and long term oven ageing	Binder stiffness and softening point
Traffic	ALT / CRS	Rutting, ravelling, cracking
Traffic/aging	ALT / CRS aged material	
Traffic/climate	ALT / CRS Water sensitivity and freeze-thaw cycles	
Traffic	Stiffness modulus	Effect on road structure
Traffic	Shear modulus	Rutting

To summarize the outcome of the experimental studies the new mixes were classified as performing better or worse than the reference mix in each study using a scale with five levels from - - to ++ where - - and - indicates much worse and worse performance compared to the reference mix respectively. = indicates equal performance to the reference mix and + and ++ indicates better or much better performance. The compilations are presented in Table 7-2 and Table 7-3.

Table 7-2. Relative performance of new SMA mixes compared to the reference SMA16 mix. The relative performance is indicated with - -, -, =, +, ++ where - - and - indicates much worse and worse, = indicates equal performance and + and ++ indicates better or much better performance.

	Test	SMA11 10%RA	SMA11 40%RA	SMA8 60% RA
Climate	Water sensitivity/MIST	=	=	=
Ageing	Short and long term oven ageing	+ +	+ +	- -
Traffic	ALT / CRS	= ravelling = rutting = cracking = friction	= ravelling - rutting = cracking = friction	= ravelling - rutting = cracking = friction
Traffic/aging	ALT / CRS aged material	= ravelling = rutting + cracking = friction	= ravelling = rutting + cracking = friction	= ravelling = rutting - cracking = friction
Traffic/climate	ALT / CRS Water sensitivity and freeze-thaw cycles	=	=	- aged material
Traffic	Stiffness modulus / road structure performance	+	=	-
Traffic	Shear modulus / rutting	+ +	=	+

Table 7-3. Relative performance of new PA mixes compared to the reference PA16 mix (ZOAB+). The relative performance is indicated with - -, -, =, +, ++ where - - and - indicates much worse and worse, = indicates equal performance and + and ++ indicates better or much better performance.

	Test	Fibra 1 / PA8	Fibra 3 / PA8 panacea	Fibra 4 / PA8 aramid
Climate	Water sensitivity/MIST	=	=	=
Ageing	Short and long term oven ageing	=	- -	- -
Traffic	ALT / CRS	+ ravelling + rutting + cracking + friction	= ravelling = rutting = cracking + friction	= ravelling = rutting = cracking + friction
Traffic/aging	ALT / CRS aged material	- - ravelling + rutting = cracking + friction	- - ravelling + rutting = cracking + friction	- - ravelling + rutting = cracking + friction
Traffic/climate	ALT / CRS Water sensitivity and freeze-thaw cycles	=	=	=
Traffic	Stiffness modulus / road structure performance	-	=	=
Traffic	Shear modulus / rutting	/	+	+

To make the estimations the service lives for the new mixes one needs to compare the relative performance of the new mixes considering the context. In the questionnaire presented in chapter 6, Table 6-1and Table 6-2, there were large differences between different countries regarding the typical distresses that triggers resurfacing. The following examples illustrate the procedure:

Denmark, SMA

Typically, high-volume roads with SMA are resurfaced because of fretting/ravelling and to some extent due to rutting and low friction in Denmark. Since the test result regarding friction and ravelling were the same for the new SMA mixes compared to reference SMA, the only important difference between the mixes is their relative performance regarding rutting where the SMA11 10% RA performed better to much better, and the SMA8 60% RA performed worse (in the CRS study) or better (in the shear modulus test) than the reference SMA. The SMA8

60% RA did age considerably faster than the reference SMA. This could have an effect on the long-term durability of the mix.

Hence it is anticipated that SMA11 10% RA have a slightly longer (+5 %) service life, that the SMA11 40% RA have the same service life, and that SMA8 60% have slightly lower service life (-10 %), compared to the reference SMA. Since the average service life of SMAs on high-volume roads in Denmark is 14 years (Table 3-1) the estimated service lives of the SMA11 10% RA, SMA11 40% RA and SMA8 60% RA, are 15 years, 14 years and 12 years, respectively for high-volume roads.

Sweden and Norway, SMA

These countries have similar road construction practises and studded tires are frequently used in both countries in the wintertime. It is reasonable to assume that the performance of the different mixes is the same in both countries. Since road wear caused by studded tires is not considered in this project, we will ignore this distress although we know that NMAS have a large influence on the anticipated road wear by studded tires. E.g., if the NMAS is decreased from 16 to 11 for a typical SMA the road wear by studded tires will increase by 40 %.

In Sweden and Norway low friction is not often a distress that triggers resurfacing. Ignoring road wear, rutting, cracking and to some extent also ravelling are distresses that is common on high-volume roads that will be resurfaced (Table 6-1).

Again, ignoring the fact that NMAS will be a critical parameter to control the road wear the following test results are of importance for Sweden and Norway: Ravelling were the same for the new SMA mixes compared to reference SMA. With regard to rutting the SMA11 10% RA performed better than the reference SMA16 and the SMA11 40% RA performed equal (shear modulus testing) or slightly worse (in the CRS study) compared to the reference. The SMA8 60% RA performed worse (in the CRS study) or better (in the shear modulus test) than the reference SMA.

Road cracks are important triggers for resurfacing in the Nordic high-volume roads. the SMA11 10% RA have higher stiffness than the reference mix and SMA8 60% RA have lower stiffness while the SMA11 40% RA have similar stiffness as the reference mix. The appearance of structural cracks is projected to appear accordingly. In the CRS study the two SMA11 mixes performed better and the SMA8 performed worse with regards to appearance of cracks.

Taken together the SMA11 10% RA is estimated to have higher durability (+10%) compared to the reference due to its higher resistance to rutting and cracking. The SMA11 60% RA is estimated to have same lifetime or slightly longer lifetime (0 to +5%) compared to the reference SMA since it seems to be more resistant to cracking. The SMA8 60% RA is estimated to have shorter lifetime (-10%) as it is ageing faster, and cracks appeared earlier on in the tests for this mix. Using 9 years as the average lifetime for SMA16 in Sweden and Norway (Table 3-1 Sweden, and 7-10 years in the questionnaire) the estimated lifetimes (again, ignoring the road wear by studded tires) for SMA11 10% RA, SMA11 40% RA and SMA8 60% RA is 10 years, 9 years and 8 years respectively.

Germany, SMA

For high-volume roads in Germany low friction and cracks are the main type of distresses, triggering resurfacing operations. In the test all SMA had approximately the same evolution of friction in the CRS study. The SMA11 10% RA and the SMA11 60% RA performed better regarding cracking in the CRS study compared to the reference SMA. The SMA8 60% RA performed worse. In the structural studies based on the stiffness modulus measurements the SMA11 10% RA had a strong positive effect with regard to structural cracks. The SMA11 60%

had the same structural performance as the reference mix while the SMA8 60% RA had a negative effect on the structural performance. In the questionnaire the average life time for a SMA in Germany was estimated to be 15 years for a high-volume road. Based on the performance regarding cracking and structural performance it is estimated that the SMA11 10% RA have longer (+5%) lifetime, the SMA11 40% RA have the same lifetime, and that SMA8 60% RA have shorter (-10%) lifetime, compared to the reference SMA on high-volume roads. The estimated lifetimes are 16 years, 15 years and 13 years for SMA11 10% RA, SMA11 40% RA and SMA8 60% RA, respectively.

Lithuania, SMA

The situation with regard to distress triggering resurfacing in Lithuania is rather similar to the situation in Germany with the exception that ravelling is also a type of distress triggering resurfacing operations. The SMA performed the same with regard to ravelling in the CRS study. Using 15 years as the estimated lifetime for SMA in Lithuania (Table 3-3) the same estimated lifetimes for the SMA in Germany applies for Lithuania. The estimated lifetimes are 16 years, 15 years and 13 years for SMA11 10% RA, SMA11 40% RA and SMA8 60% RA, respectively.

Sweden, Netherlands and Germany, PA

Ravelling is the main reasons for maintenance operations on porous asphalt pavements in Europe, see Table 6-2. In Sweden road wear and rutting (studded tires?) is also of importance. The ravelling resistance for unaged mixes with fibres were the same as for the reference mix. The ravelling resistance for the unaged PA8 mix was slightly better compared to the reference mix. The ageing was different though for the different mixes. The PA8 mixes with fibres (Fibra 3 and Fibra 4) hardened much more that the reference mix (PA16, ZOAB+) and the PA8 without fibres. The ravelling resistance in the CRS were worse for the PA8 mixes compared to the reference. Since the ravelling resistance is lower for the aged PA8 mixes it is estimated that the service life is slightly lower (-5%) for the Fibra 1 mix and lower (-15%) for the Fibra 3 and Fibra 4 mixes compared to the reference PA16 mix. Since there is a considerable difference in the experience of the average lifetime for a PA16 in the questionnaire, 12 years was used as a reasonable estimate for the lifetime for the reference. Based on this reference value the estimated lifetime for the Fibra 1 mix is 11 years and 10 years for the Fibra 3 and Fibra 4 mixes.

In Table 7-4 and Table 7-5 the estimated service life for the new mixes and the service life for the reference mixes are summarized.

Table 7-4. Estimated lifetimes for SMA mixes on high-volume roads in years.

Country\Mix	SMA16	SMA11 10% RA	SMA11 40% RA	SMA8 60% RA
Denmark	14	15	14	12
Sweden & Norway	9	10	9	8
Germany & Lithuania	15	16	15	13

Table 7-5. Estimated lifetimes for PA mixes on high-volume roads in years.

Country\Mix	PA16 (ZOAB+)	PA8 (Fibra 1)	PA8 panacea (Fibra 3)	PA8 aramid (Fibra 4)
Sweden, Netherlands and Germany	12	11	10	10

8 References

Ahmad, M., Mannan, U. A., Islam, M. R., & Tarefder, R. A. (2018). Chemical and mechanical changes in asphalt binder due to moisture conditioning. *Road Materials and Pavement Design, 19*(5), 1216-1229. doi:10.1080/14680629.2017.1299631

Ahmed, A. W., & Erlingsson, S. (2021). *Description of an ME Program ERAPave PP.* Linköping: VTI, The Swedish National Road and transport Research Institute.

Alisov, A., Riccardi, C., Schrader, J., Cannone Falchetto, A., & Wistuba, M. (2020). A novel method to characterise asphalt binder at high temperature. *Road Materials and Pavement Design*, pp. 143-155.

Briessinck, M., Moffatt, M., Perveneckas, Z., & Seiler, L. (2016). Expected Service Life of Wearing Courses. Paris: PIARC.

Brown, S. F. (1973). Determination of young's modulus for bituminous materials in pavement design. *Highway Research Record, 431*, 38-49.

Buchanan, M. S., & Vernon, M. M. (2005). *Laboratory Accelerated Stripping Simulator for Hot Mix Asphalt (Report No. FHWA/MS-DOTRD- 04-167).* Mississippi: Mississippi State University.

Chen, X., & Huang, B. (2008). Evaluation of moisture damage in hot mix asphalt using simple performance and superpave indirect tensile tests. *Construction and Building Materials, 22*, 1950-1962.

Christensen, D., Pellinen, T., & Bonaquist, R. (2003). Hirsch model for estimating the modulus of asphalt concrete. *Journal of the Association of Asphalt Paving Technologists, 72*, pp. 97-121.

Christensen, J., & et al. (2005). *Economic Evaluation of Long-Life Pavements PHASE 1.* Paris, France: OECD PUBLICATIONS.

De la Roche C. et al., V. d. (2009). Development of a laboratory bituminous mixtures aging protocol. *Procs. Int. Conf. on Advanced Testing and Characterisation of BituminousMaterials.*

EAPA. (2007). *Long-Life Asphalt Pavements – Technical version.* Brussels: European Asphalt Pavement Association.

Fan, L., Lin, J., Wei, J., Zhang, Y., & Wang, L. (2014). Viscoelastic characteristics of asphalt binders at softening point temperature. *China Petroleum Processing and Petrochemical Technology, 16*(3), pp. 19-25.

Htet, Y. M. (2007). An assessment of moisture induced damage in asphalt pavements. *Master's thesis*. Worcester, United States: Worcester Polytechnic Institute.

Mallick, R. B., Pelland, R., & Hugo, F. (2005). Use of accelerated loading equipment for determination of long term moisture susceptibility of hot mix asphalt. *International Journal of Pavement Engineering, 6*(2), 125-136. doi:10.1080/10298430500158984

Mollenhauer, K., Mouillet, V., Pierard, N., Tusar, M., & Gabet, T. (2012). Laboratory aging of asphalt mixtures : simulation of reclaimed asphalt and application as test method for durability. *5th Eurasphalt & Eurobitume Congress.* Turkey: EAPA. Retrieved from https://hal.archives-ouvertes.fr/hal-00850875

Petersen, J., Robertson, R., Branthaver, J., Harnsberger, P., Duvall, J., Kim, S., . . . Bahia, H.

(1994). *Binder Characterization and Evaluation: Volume 1. Report No. SHRP-A-367.* Washington, D.C.: SHRP.

Rahman, M. S., Erlingsson, S., & Ahmed, A. W. (2021). Modelling the Permanent Deformation of Unbound Granular Materials in Pavements. *Road Materials and Pavement Design (Submitted)*.

Said, S. F., Hakim, H., Oscarsson, E., & Hjort, M. (2011). Prediction of flow rutting in asphalt concrete layers. *International Journal of Pavement Engineering, 12*(6), 519-532.

Said, S., Hakim, H., & Oscarsson, E. (2013). Rheological characterization of asphalt concrete using a shear box. *Journal of Testing and Evaluation, 41*(4), 602-610. doi:10.1520/JTE20120177

Schrader, J., & Wistuba, M. (2019). On the use of a novel Binder-Fast-Characterization-Test. *RILEM 252-CMB-Symposium on Chemo-Mechanical Characterization of Bituminous Materials* (pp. 123-128). Cham: Springer.

Schrader, J., Wistuba, M., Cannone Falchetto, A., Riccardi, C., & Alisov, A. (2020). A new Binder-Fast-Characterization-Test using a Dynamic Shear Rheometer and its application for rejuvenating reclaimed asphalt binder. *Journal of Testing and Evaluation, 48*(1). doi:10.1520/JTE20180893

Showkat, B., & Singh, D. (2021). Effect of MIST conditioning on the air voids and permeability of hot asphalt mixes containing reclaimed asphalt pavement. *Road Materials and Pavement Design*. doi:10.1080/14680629.2021.1910549

Subhy, A. (2017). Advanced analytical techniques in fatigue and rutting related characterisations of modified bitumen: Literature review. *Construction and Building Materials, 156*, pp. 28-45.

Terrel, R. L., & Shute, J. W. (1989). *Summary report on water sensitivity.* SHRP-A/IR-89-003.

Varveri, A., Avgerinopoulos, S., & Scarpas, A. (2015). Experimental evaluation of long- and short-term moisture damage characteristics of asphalt mixtures. *Road Materials and Pavement Design*. doi:10.1080/14680629.2015.1066705

Walther, A., Büchler, S., Cannone Falchetto, A., Wang, D., Riccardi, C., & Wistuba, M. (2019). Experimental investigation on asphalt mixtures prepared with reclaimed asphalt pavement and rejuvenators based on the BTSV method. *Road Materials and Pavement Design, 20*(7), pp. 1695-1708.

Wellner et al., F. (2015). *ALLBACK2PAVE; Deliverable No D2.1; High-content RA warm asphalt mixture design.*

Zhang, H., Anupam, K., Scarpas, A., & Kasbergen, C. (2018). Comparison of Different Micromechanical Models for Predicting the Effective Properties of Open Graded Mixes. *Transportation Research Record*. doi:10.1177/0361198118794713

Zhu, J., Lu, X., Langfjell, M., & Gudmarsson, A. (2021). Quantitative relationship of fundamental rheological properties of bitumen with the empirical Ring and Ball softening point. *Road Materials and Pavement Design, 22*(S1), pp. S345-S364.

Appendix A. Hirsch model constant fitting for unaged asphalt mixtures

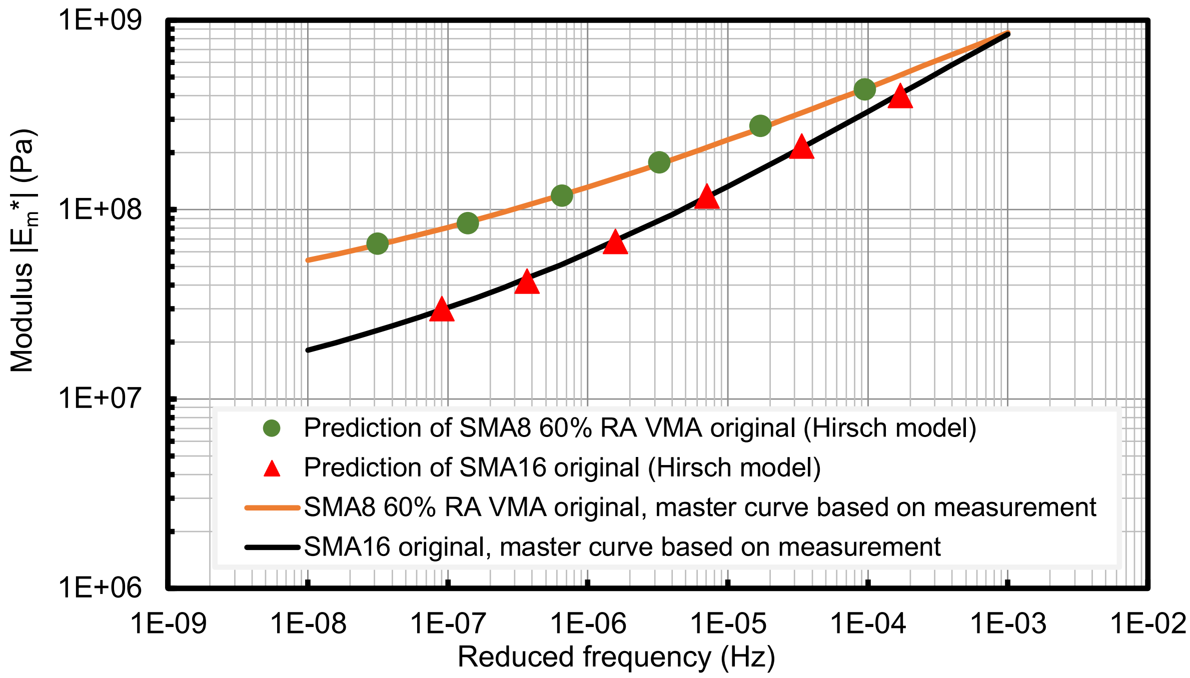

Figure A-1. Fitting results of IDT dynamic modulus for unaged asphalt mixtures SMA8 60% RA VMA and SMA16, T_{ref}=10 °C.

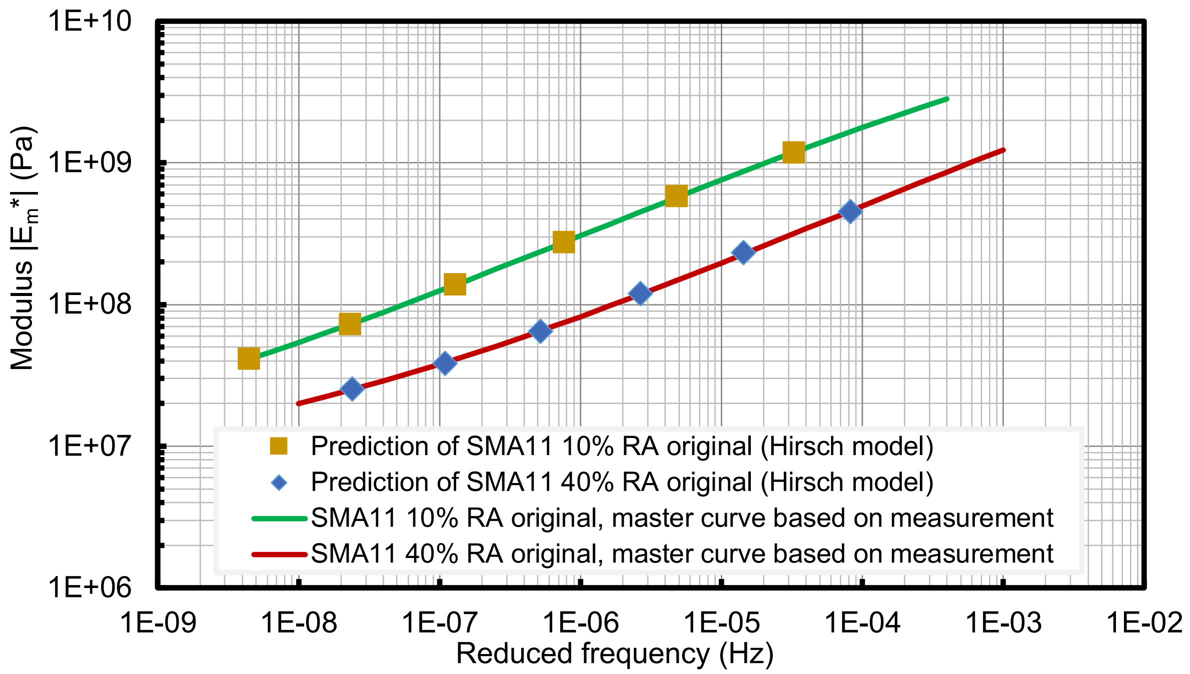

Figure A-2. Fitting results of IDT dynamic modulus for unaged asphalt mixtures SMA11 10% RA and SMA11 40% RA, T_{ref}=10 °C.

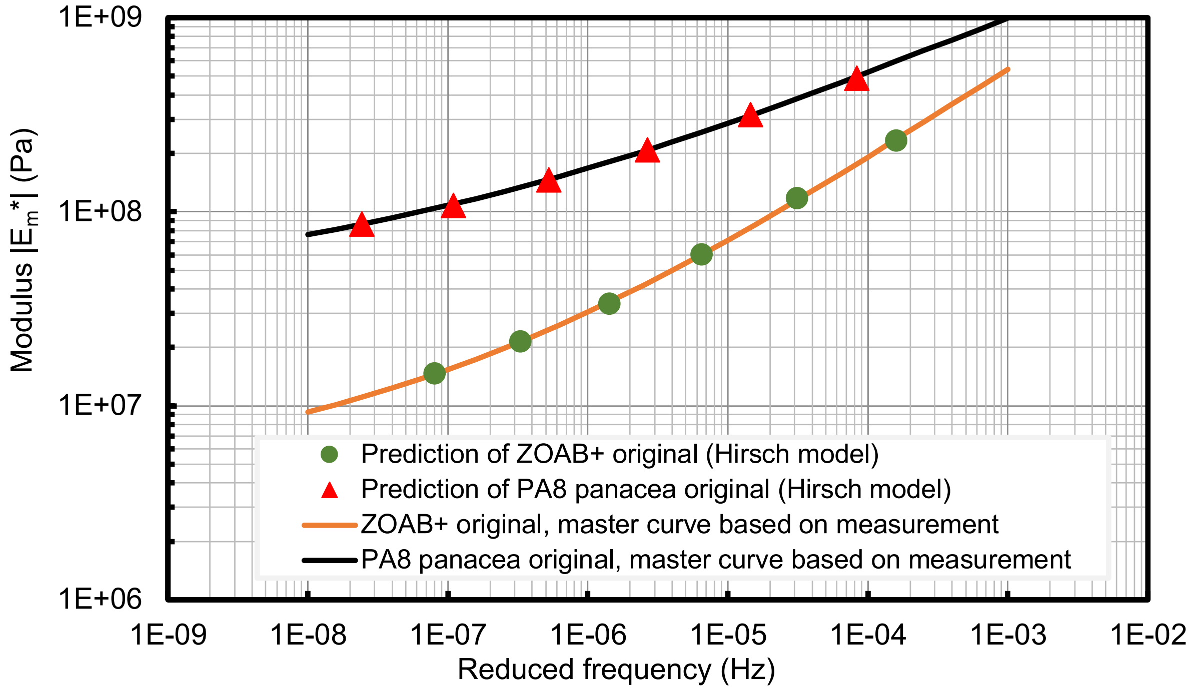

Figure A-3. Fitting results of IDT dynamic modulus for unaged asphalt mixtures ZOAB+ and PA8 panacea, T_{ref}=10 °C.

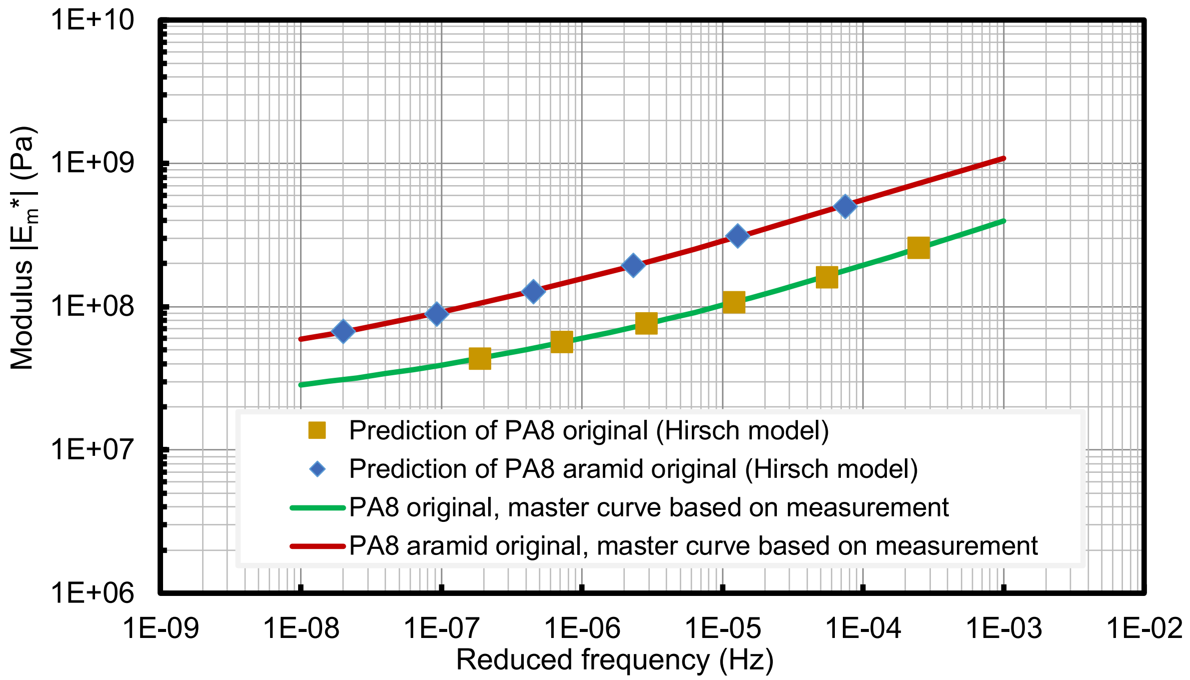

Figure A-4. Fitting results of IDT dynamic modulus for unaged asphalt mixtures PA8 and PA8 aramid, T_{ref}=10 °C.

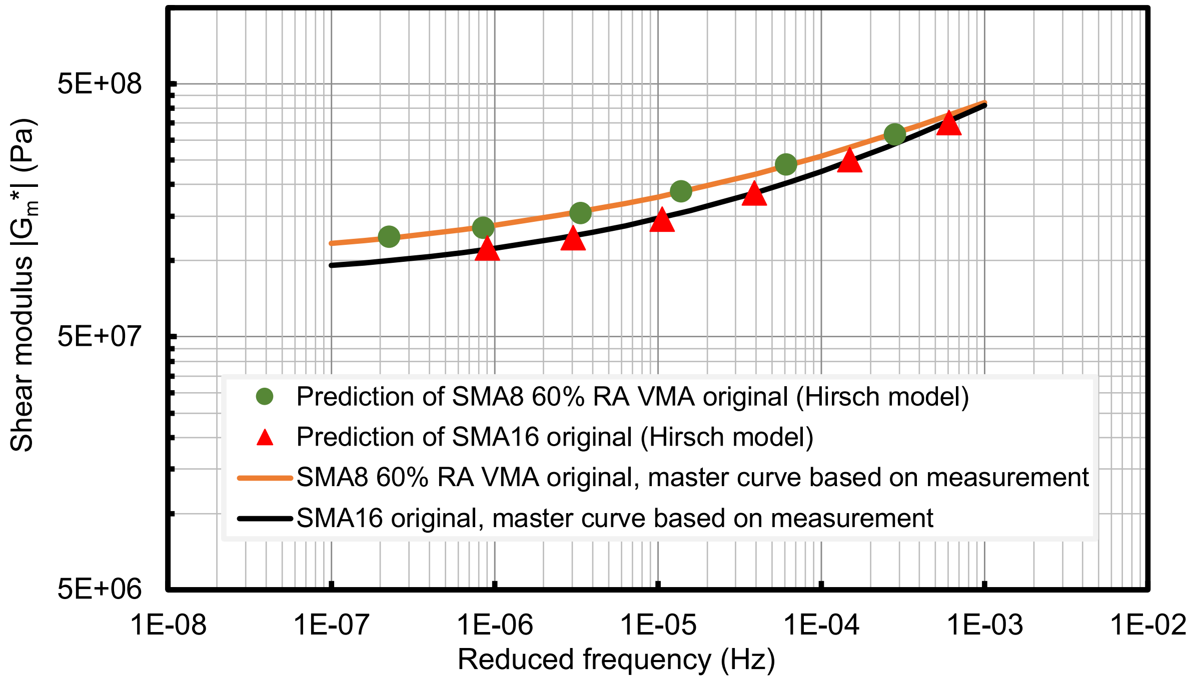

Figure A-5. Fitting results of shear modulus for unaged asphalt mixtures SMA8 60% RA VMA and SMA16, T_{ref}=10 °C.

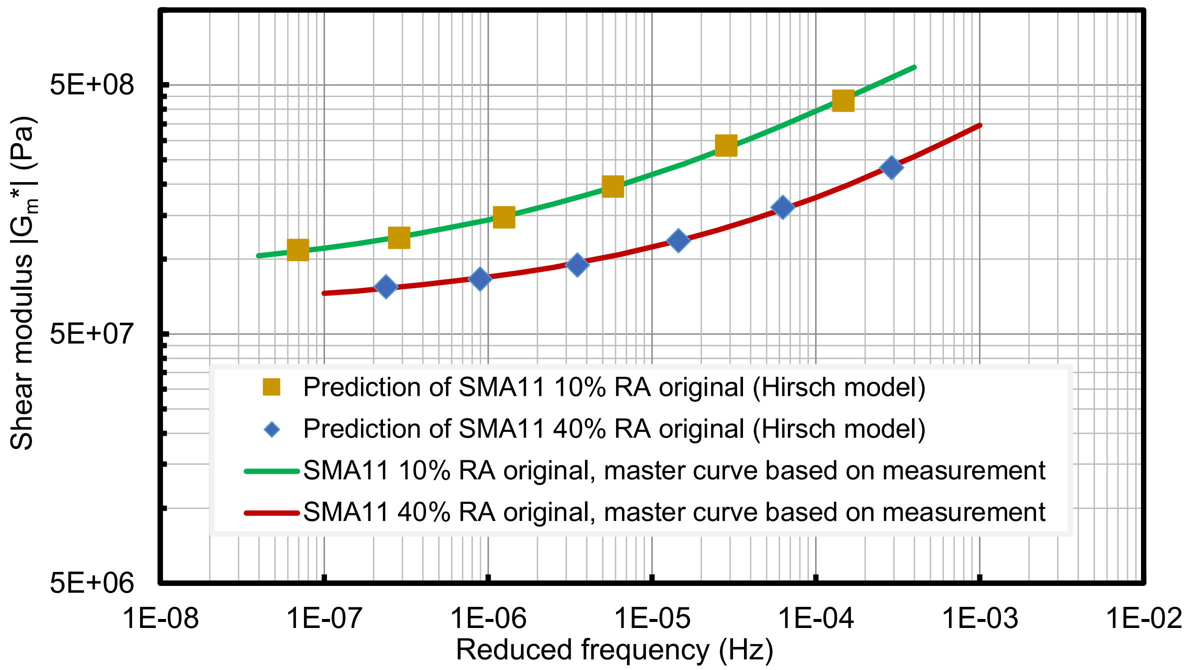

Figure A-6. Fitting results of shear modulus for unaged asphalt mixtures SMA11 10% RA and SMA11 40% RA, T_{ref}=10 °C.

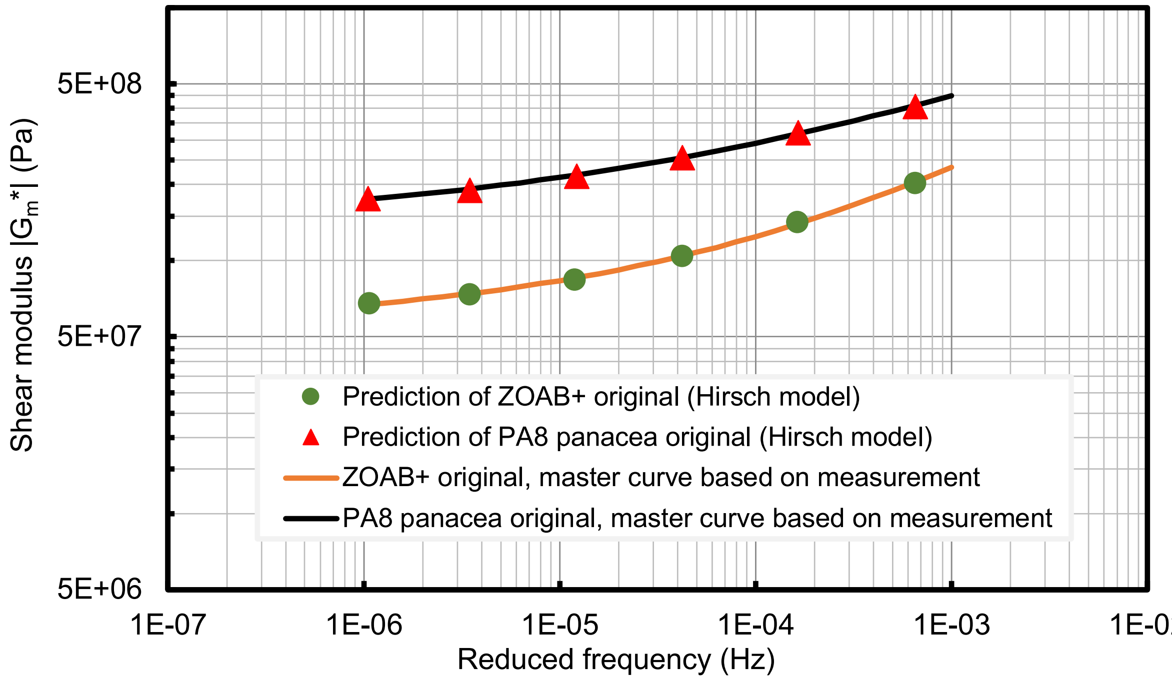

Figure A-7. Fitting results of shear modulus for unaged asphalt mixtures ZOAB+ and PA8 panacea, T_{ref}=10 °C.

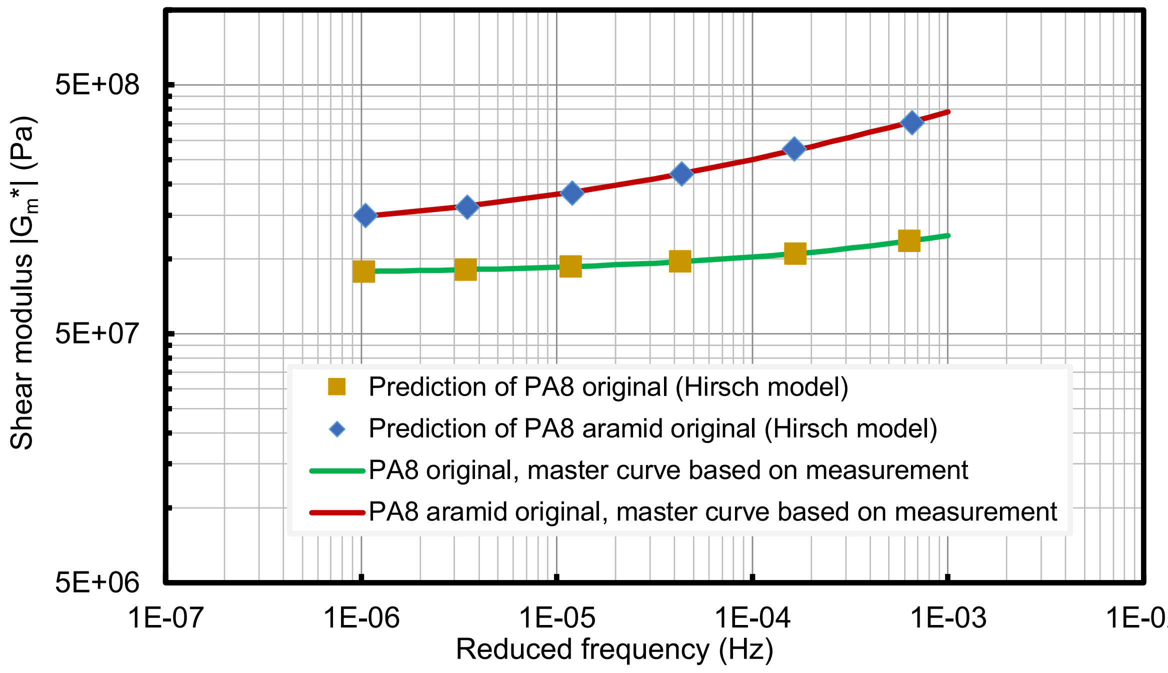

Figure A-8. Fitting results shear modulus for unaged asphalt mixtures PA8 and PA8 aramid, T_{ref}=10 °C.

Appendix B. Prediction of asphalt mixture modulus after ageing

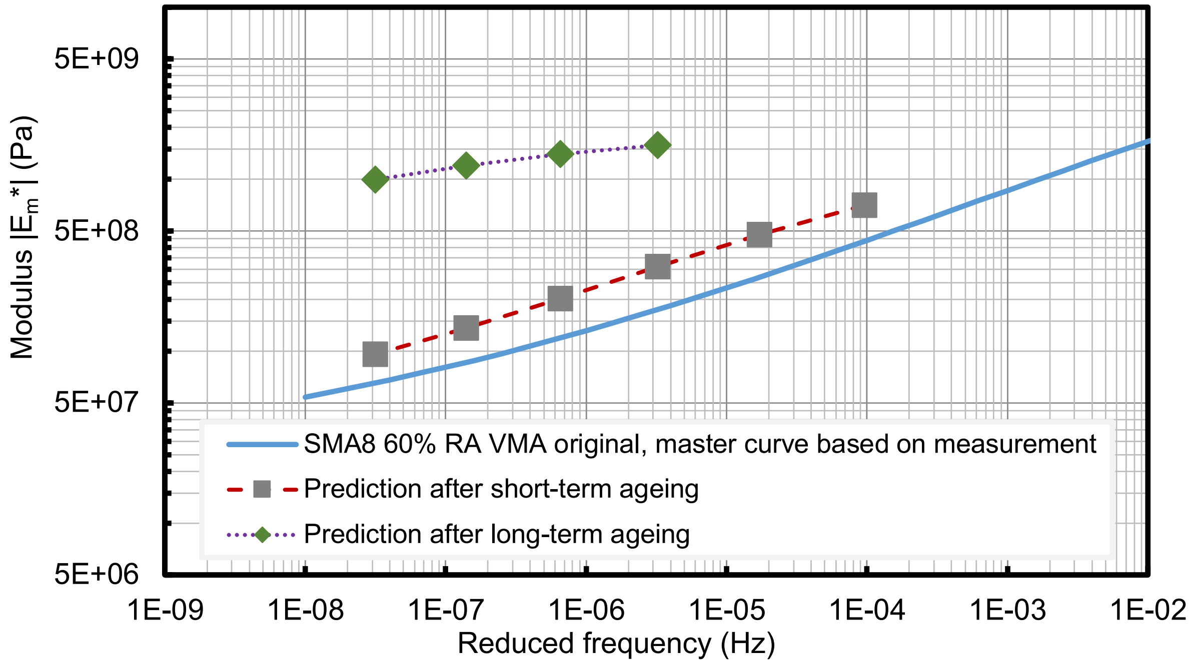

Figure B-1. Prediction of IDT dynamic modulus after ageing for asphalt mixture SMA8 60% RA VMA, T_{ref}=10 °C.

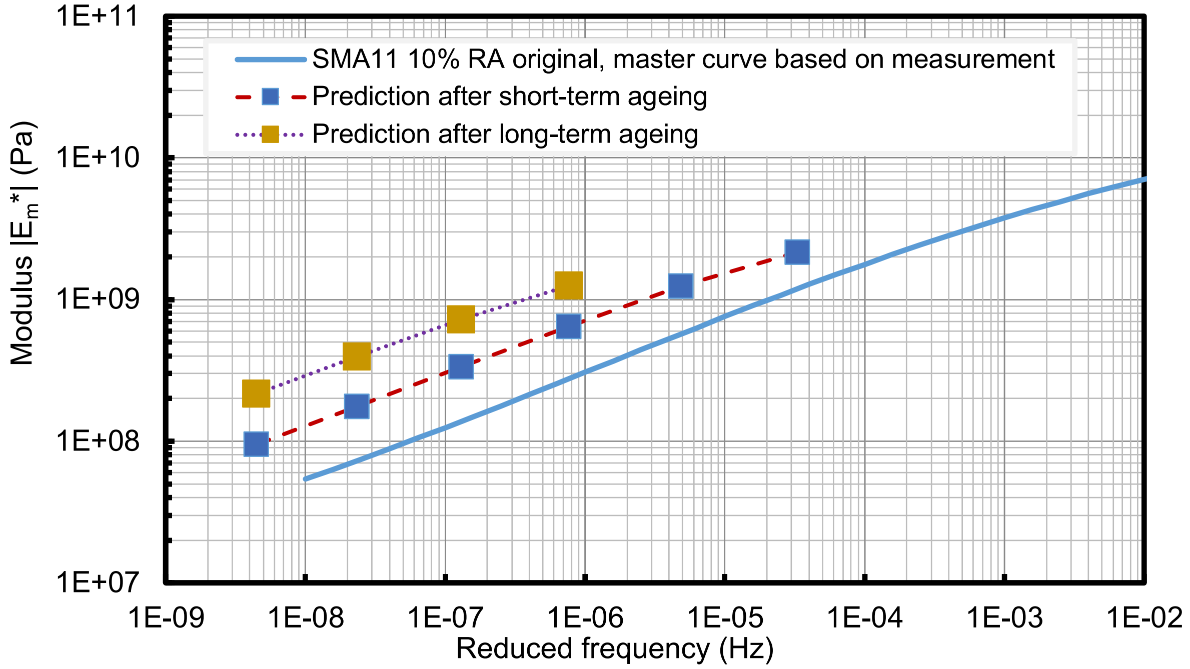

Figure B-2. Prediction of IDT dynamic modulus after ageing for asphalt mixture SMA11 10% RA, T_{ref}=10 °C.

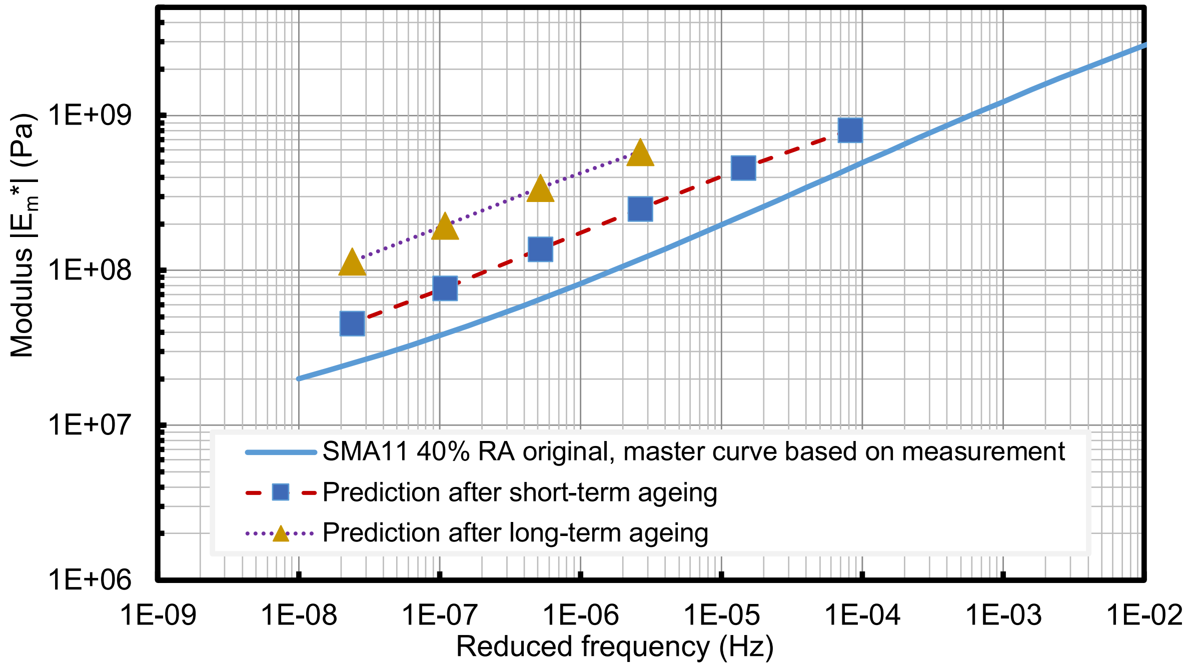

Figure B-3. Prediction of IDT dynamic modulus after ageing for asphalt mixture SMA11 40% RA, T_{ref}=10 °C.

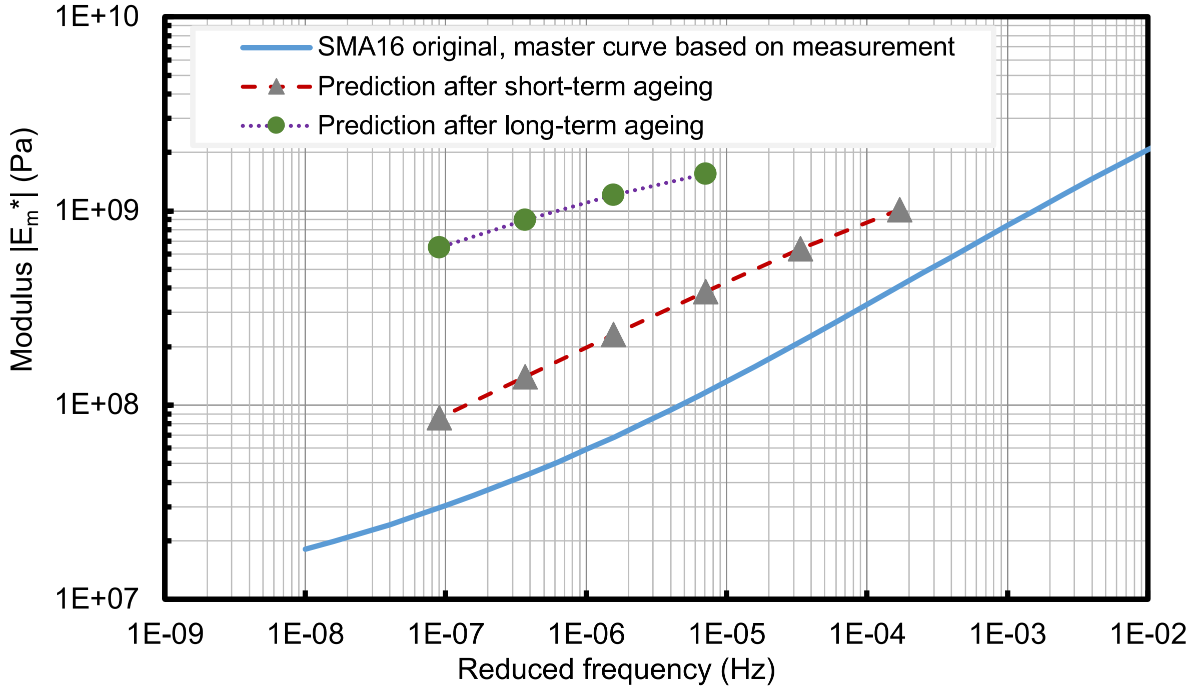

Figure B-4. Prediction of IDT dynamic modulus after ageing for asphalt mixture SMA16, T_{ref}=10°C.

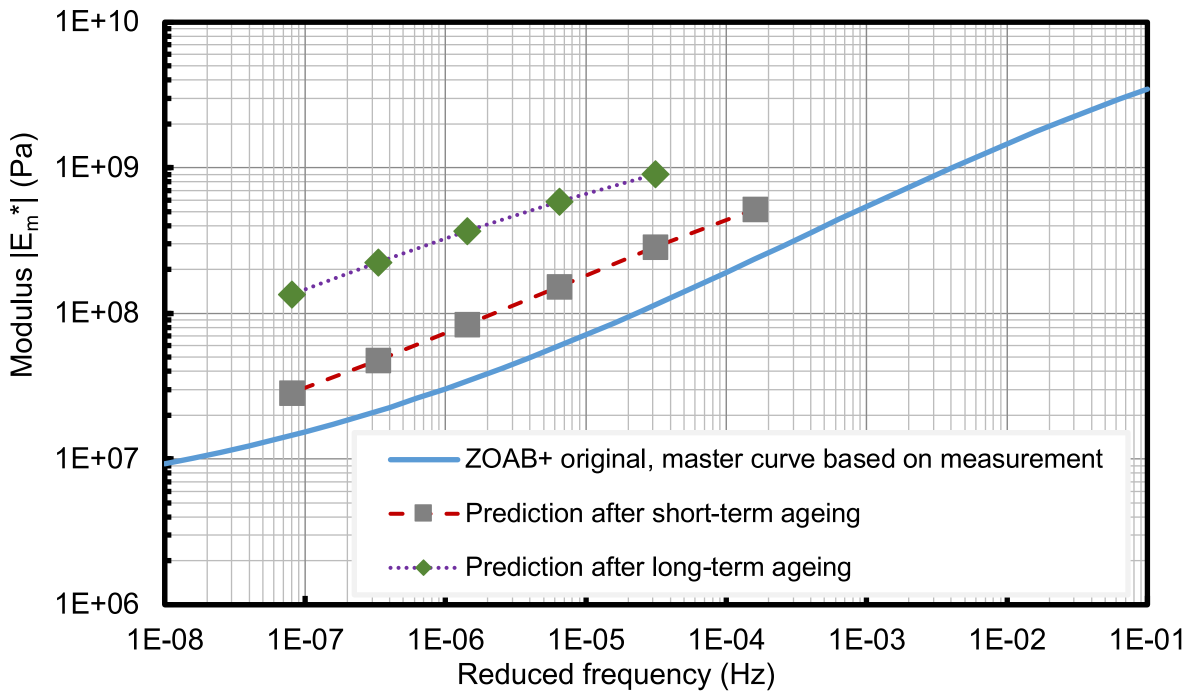

Figure B-5. Prediction of IDT dynamic modulus after ageing for asphalt mixture ZOAB+, T_{ref}=10°C.

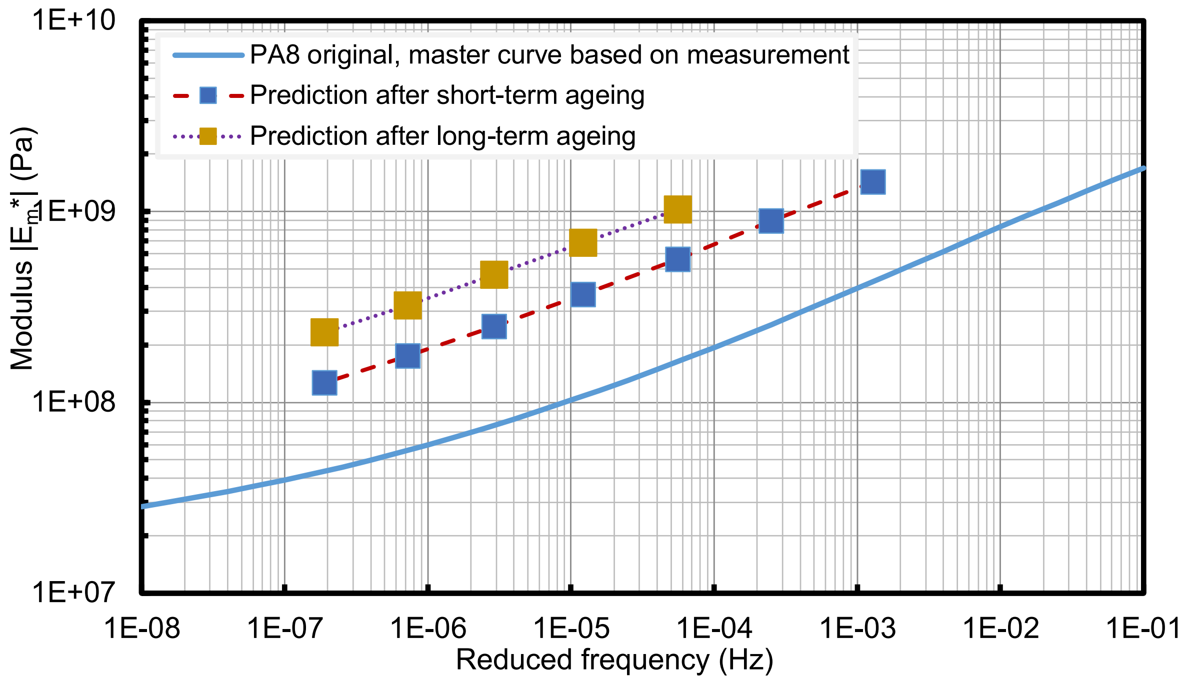

Figure B-6. Prediction of IDT dynamic modulus after ageing for asphalt mixture PA8, T_{ref}=10 °C.

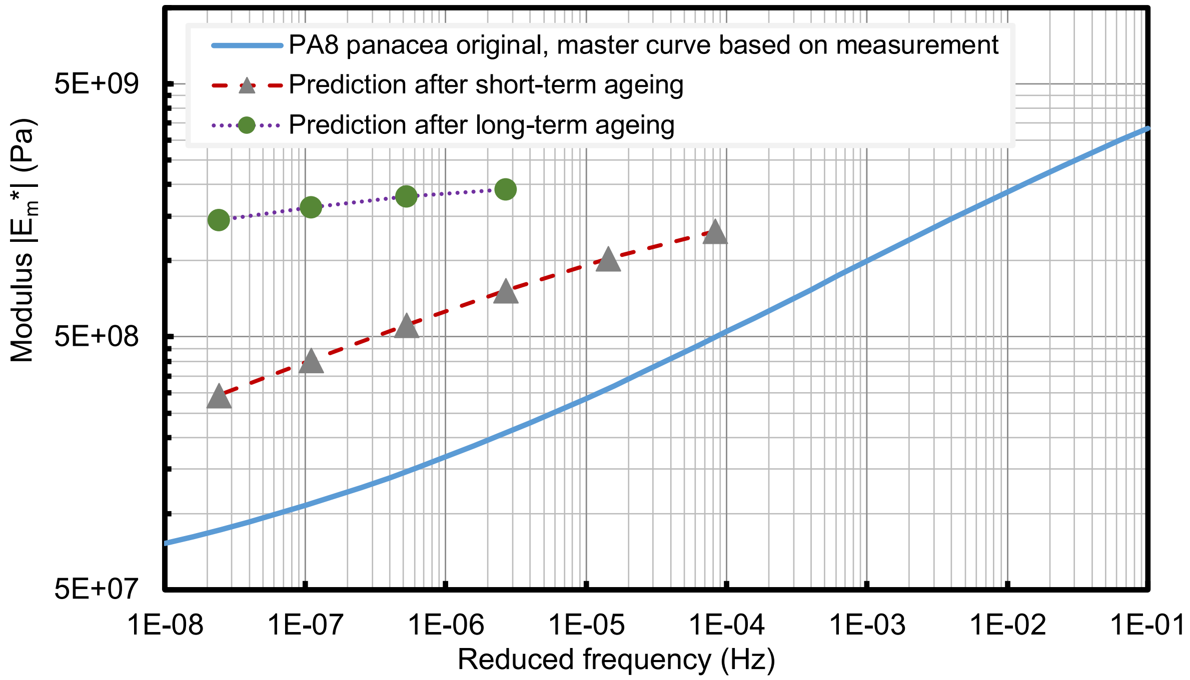

Figure B-7. Prediction of IDT dynamic modulus after ageing for asphalt mixture PA8 panacea, T_{ref}=10 °C.

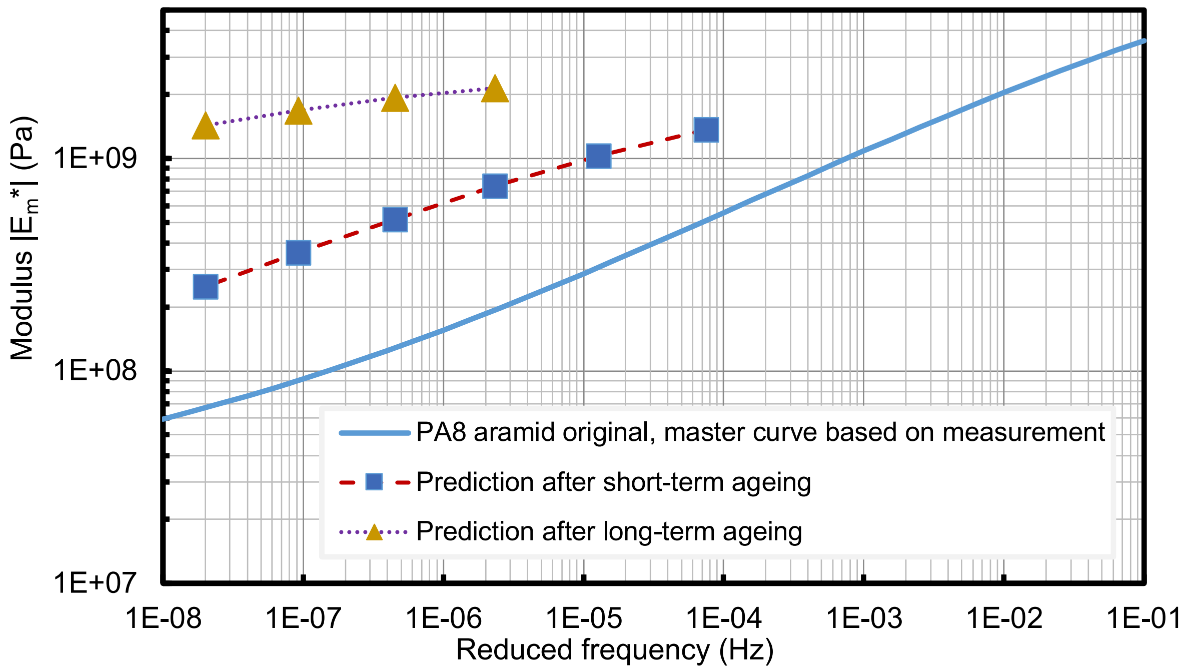

Figure B-8. Prediction of IDT dynamic modulus after ageing for asphalt mixture PA8 aramid, T_{ref}=10 °C.

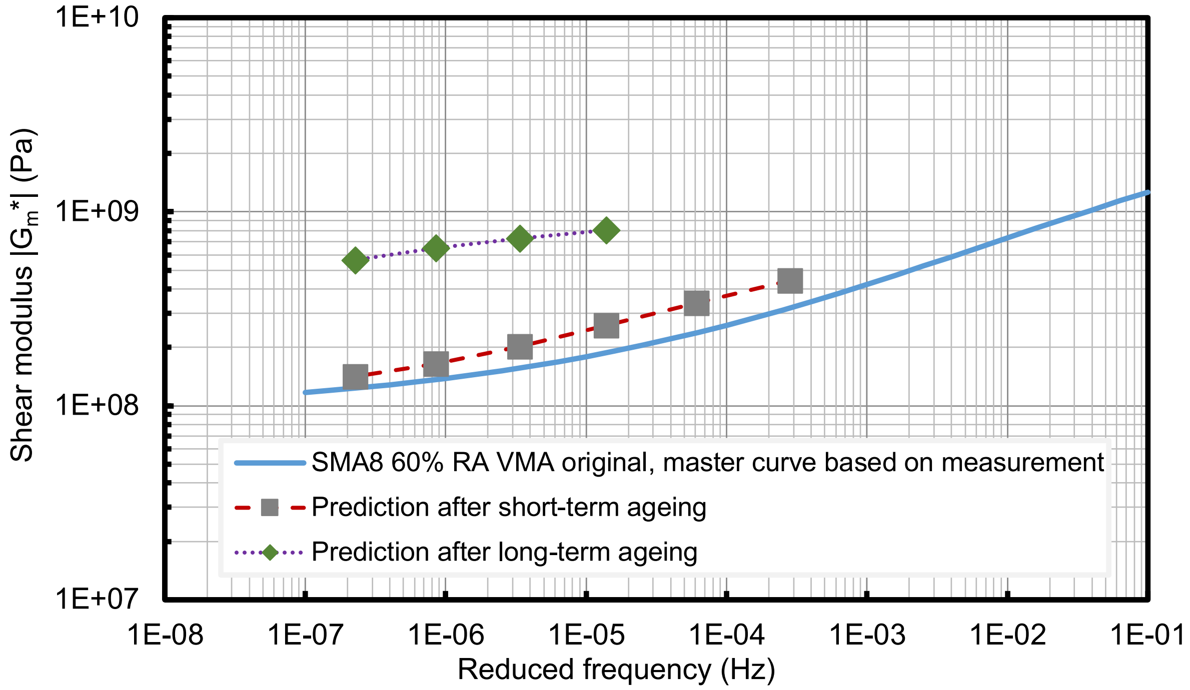

Figure B-9. Prediction of shear modulus after ageing for asphalt mixture SMA8 60% RA VMA, T_{ref}=10 °C.

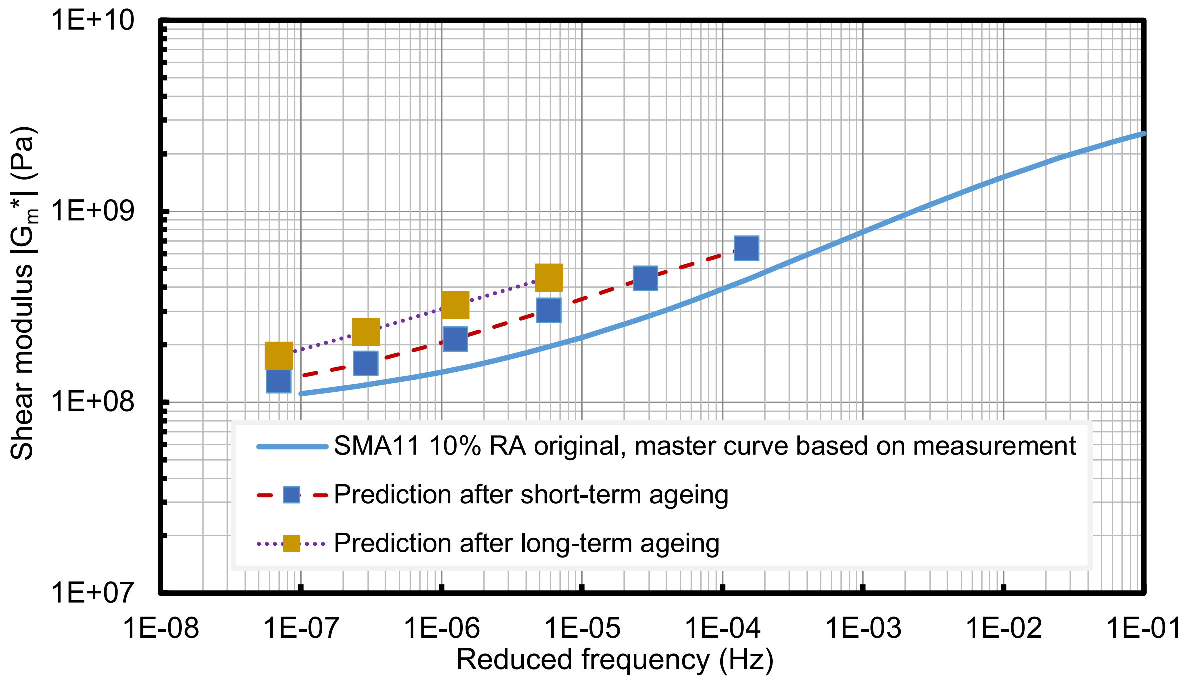

Figure B-10. Prediction of shear modulus after ageing for asphalt mixture SMA11 10% RA, T_{ref}=10°C.

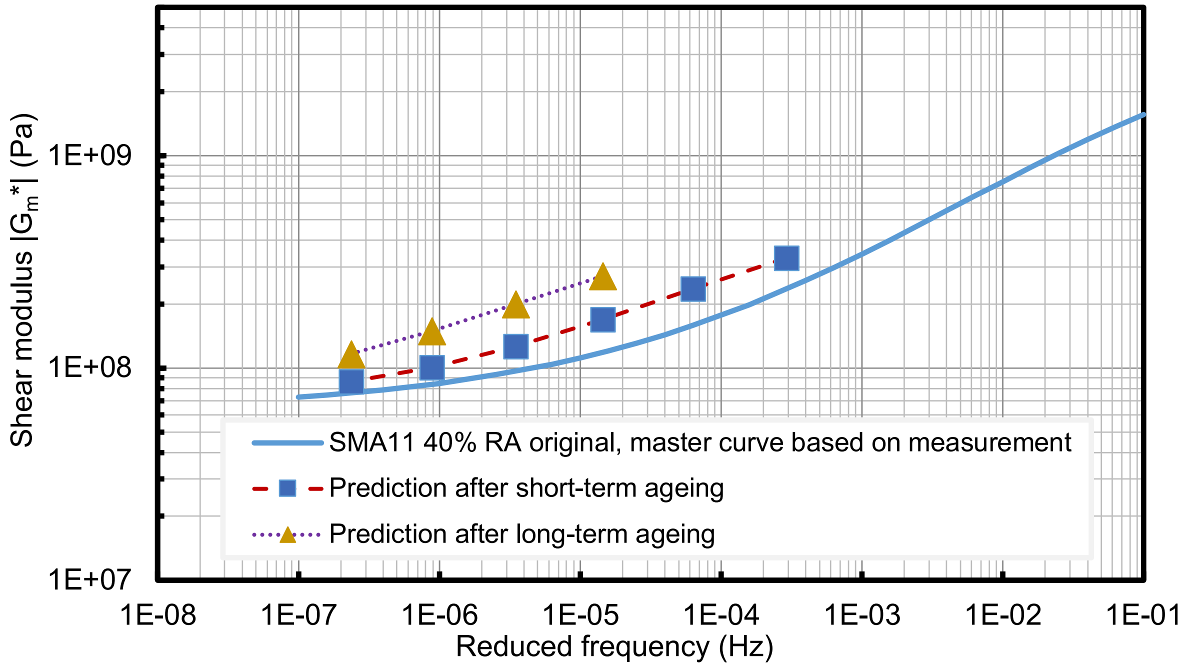

Figure B-11. Prediction of shear modulus after ageing for asphalt mixture SMA11 40% RA, T_{ref}=10°C.

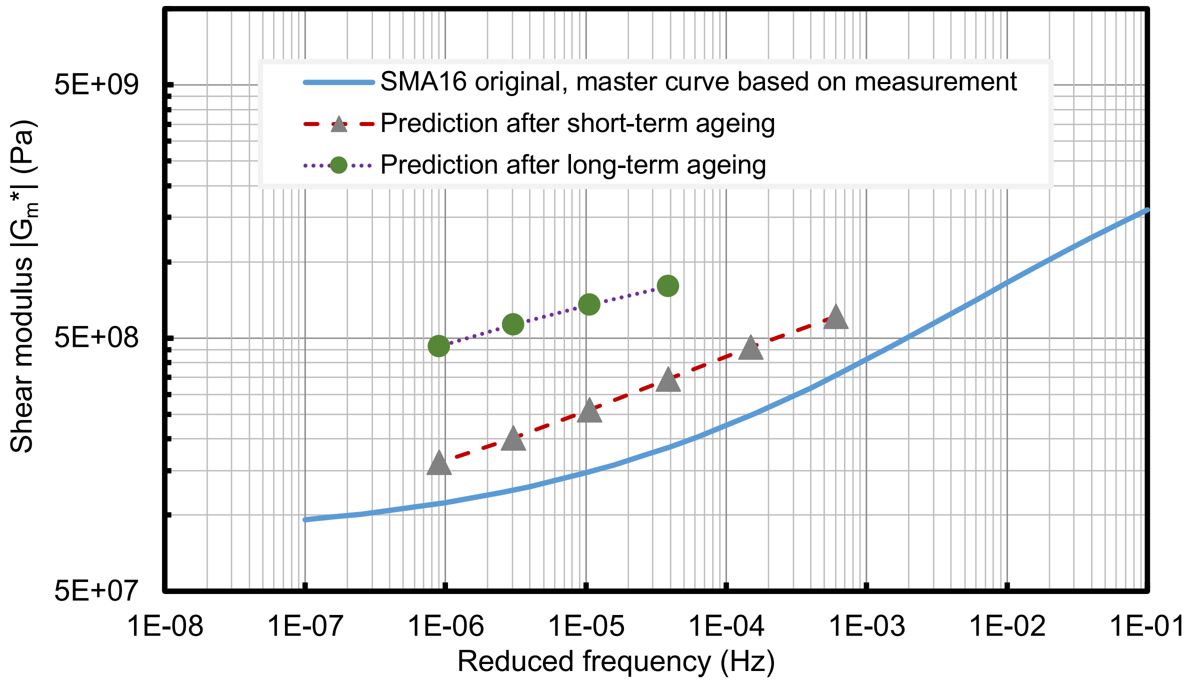

Figure B-12. Prediction of shear modulus after ageing for asphalt mixture SMA16, T_{ref}=10 °C.

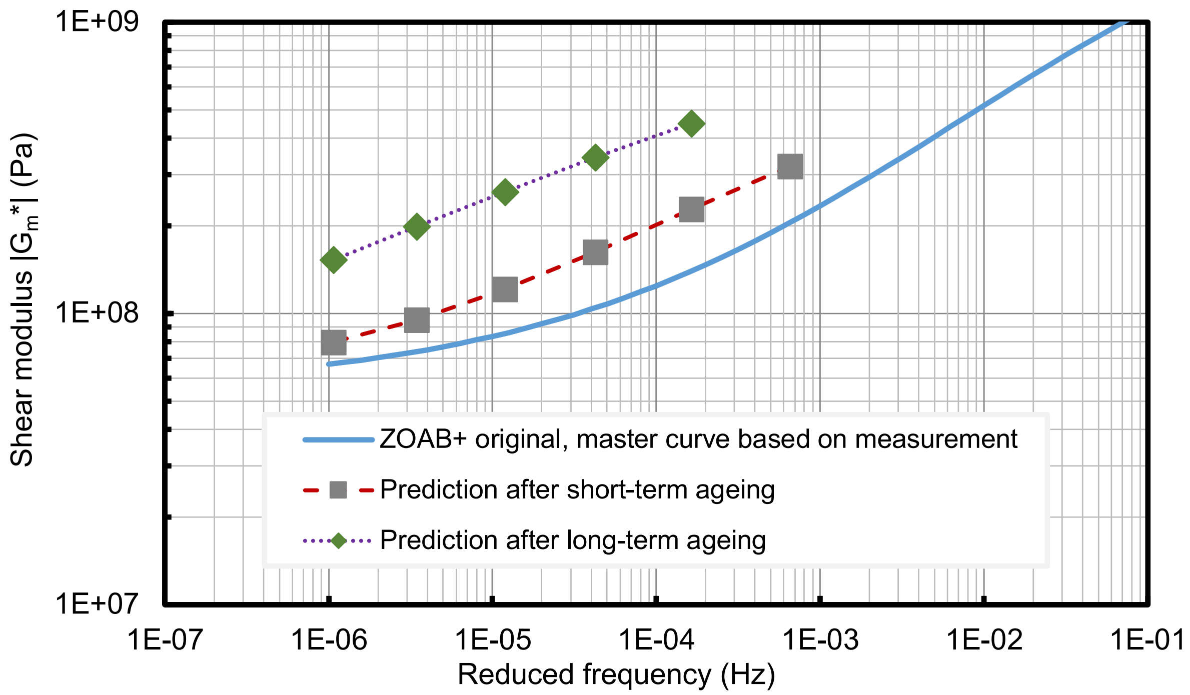

Figure B-13. Prediction of shear modulus after ageing for asphalt mixture ZOAB+, T_{ref}=10 °C.

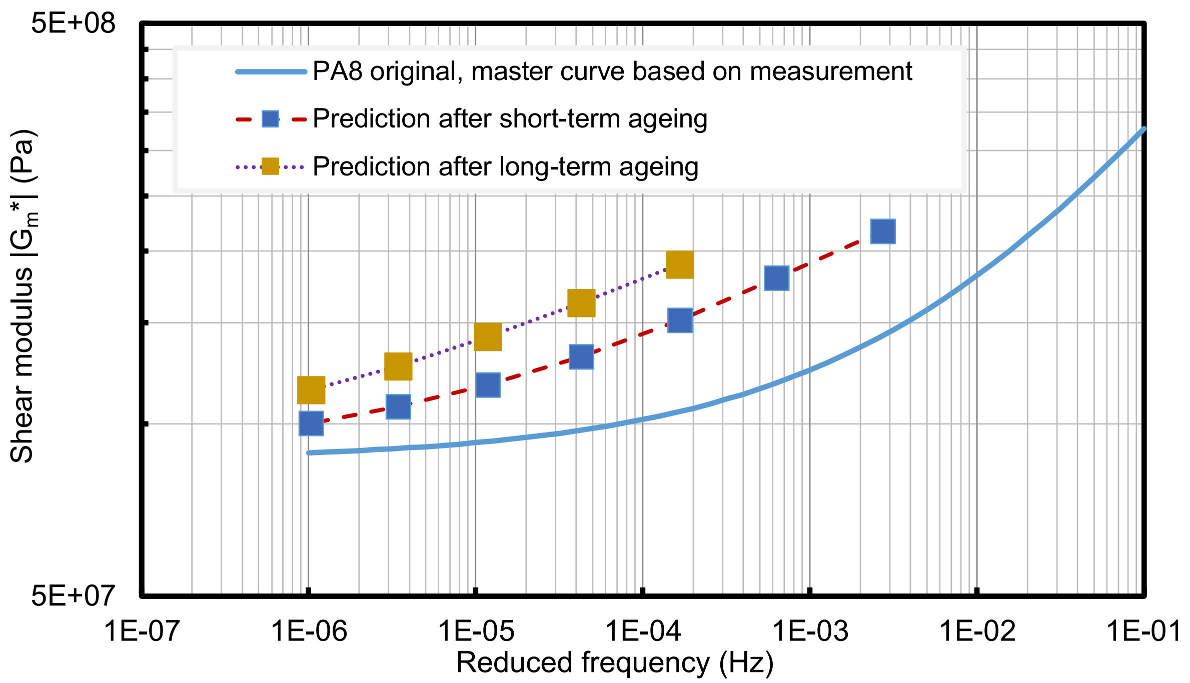

Figure B-14. Prediction of shear modulus after ageing for asphalt mixture PA8, T_{ref}=10 °C.

Conférence Européenne des Directeurs des Routes
Conference of European Directors of Roads

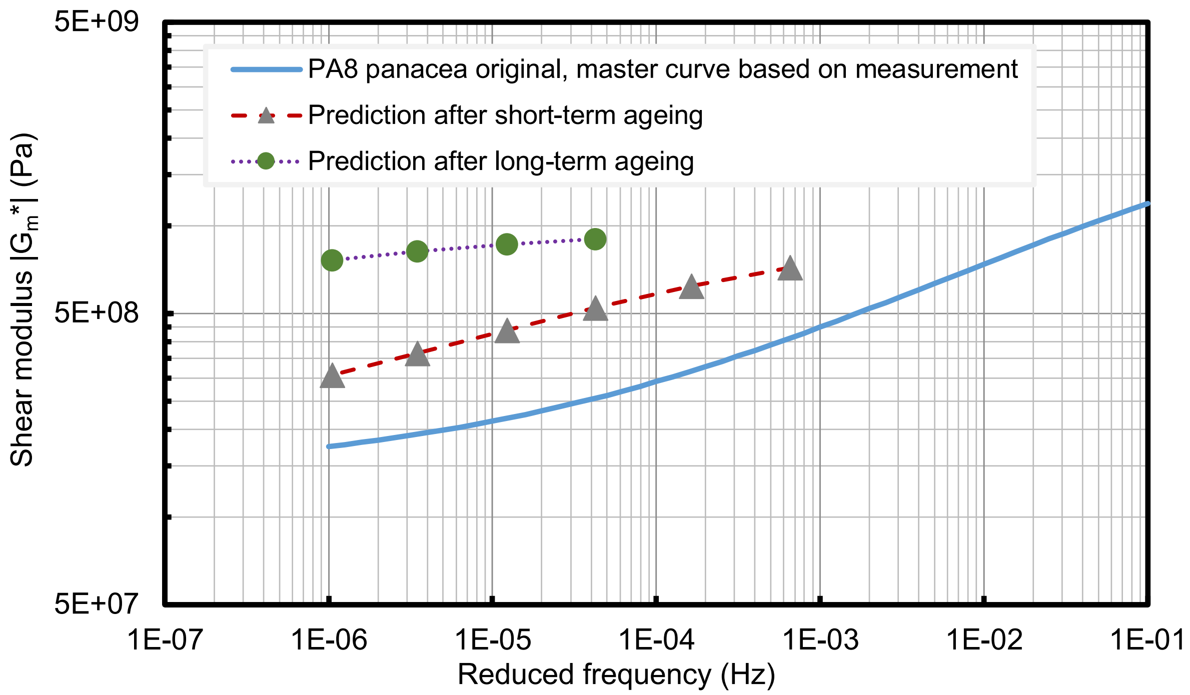

Figure B-15. Prediction of shear modulus after ageing for asphalt mixture PA8 panacea, T_{ref}=10°C.

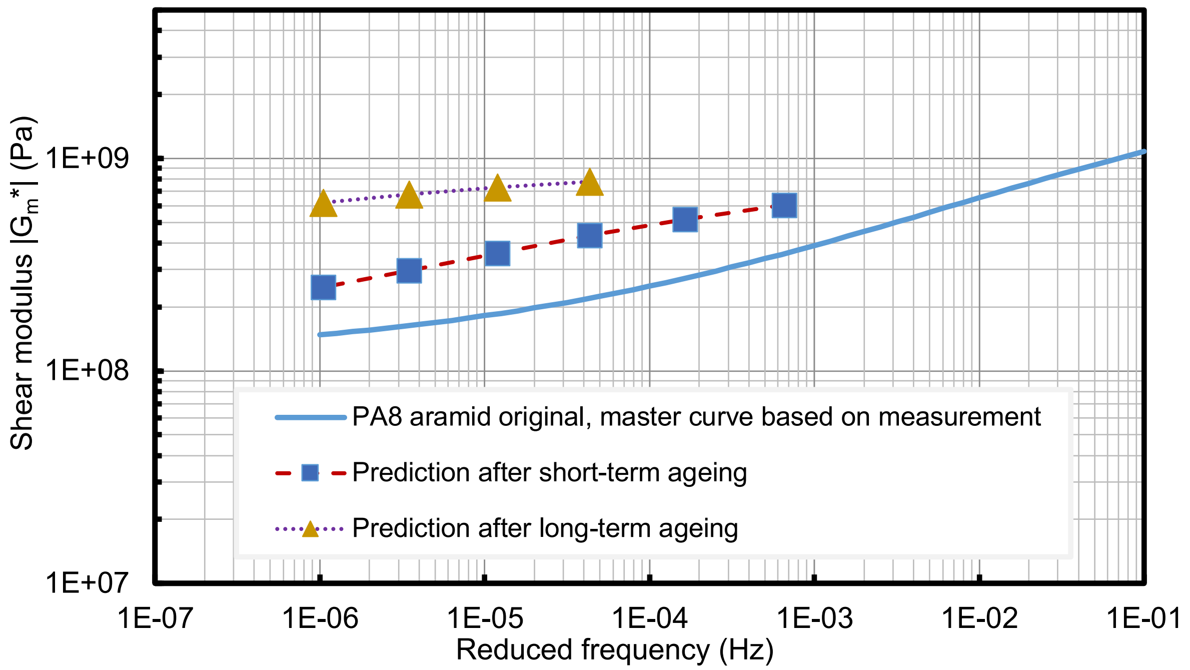

Figure B-16. Prediction of shear modulus after ageing for asphalt mixture PA8 aramid, T_{ref}=10 °C.

Appendix C. Asphalt mixture master curves after ageing by shift factor

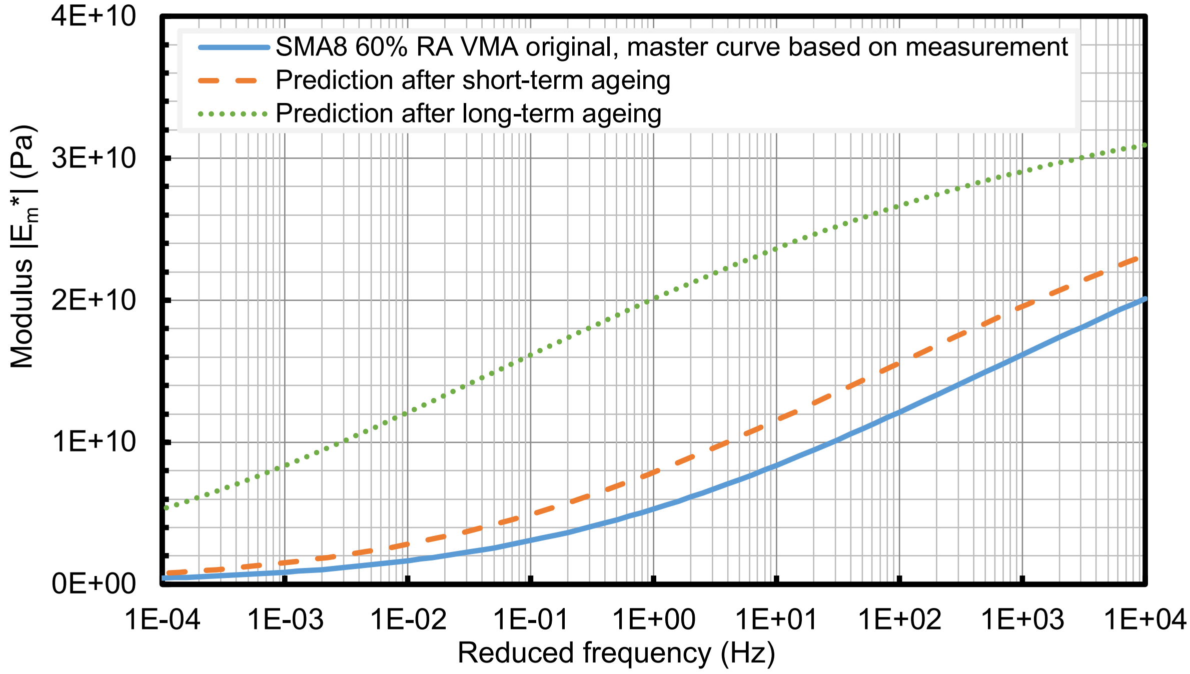

Figure C-1. IDT dynamic modulus master curves by shift factor due to ageing for asphalt mixture SMA8 60% RA VMA, T_{ref}=10 °C.

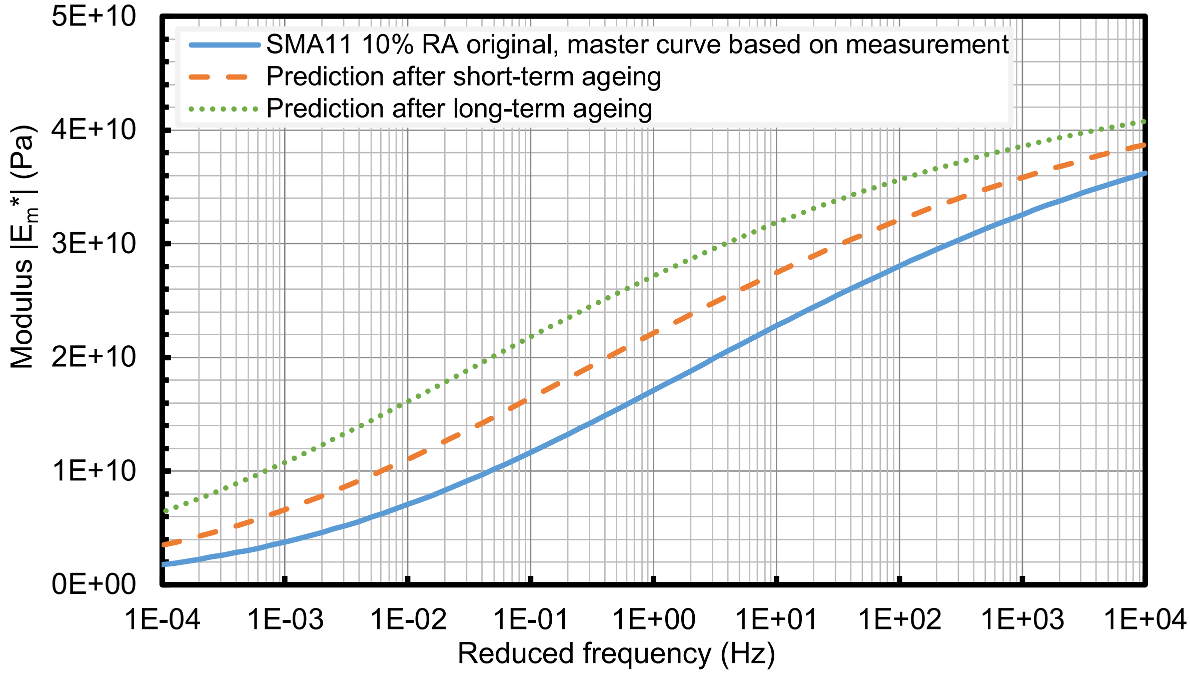

Figure C-2. IDT dynamic modulus master curves by shift factor due to ageing for asphalt mixture SMA11 10% RA, T_{ref}=10 °C.

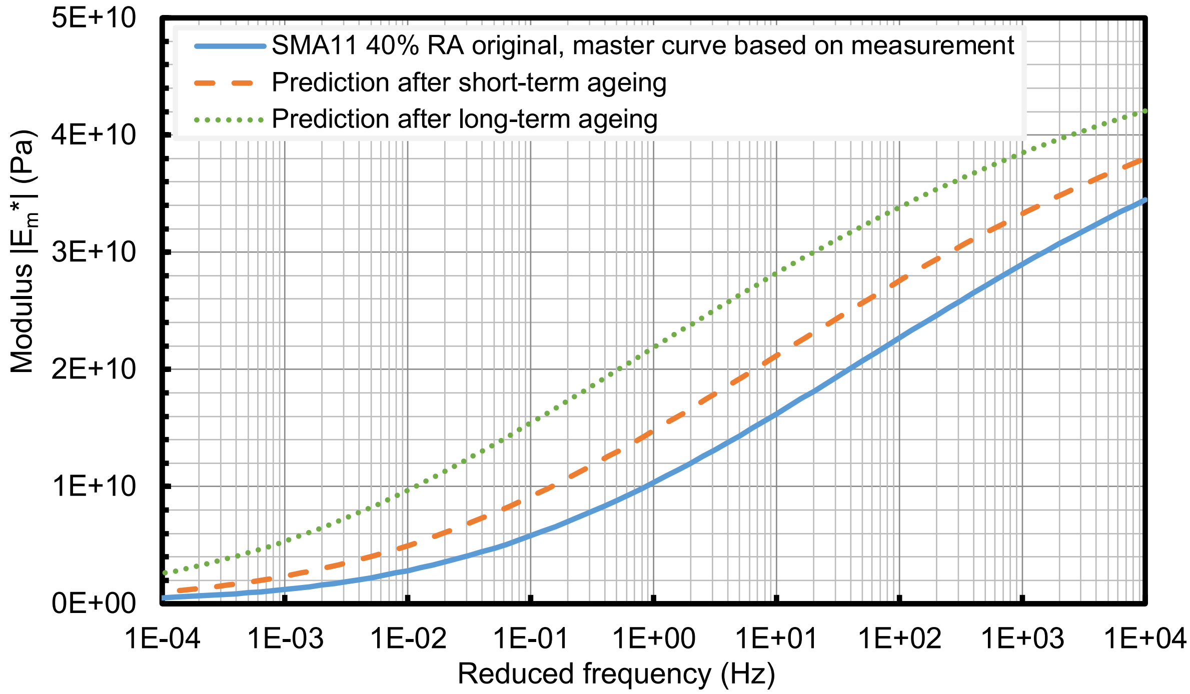

Figure C-3. IDT dynamic modulus master curves by shift factor due to ageing for asphalt mixture SMA11 40% RA, T_{ref}=10 °C.

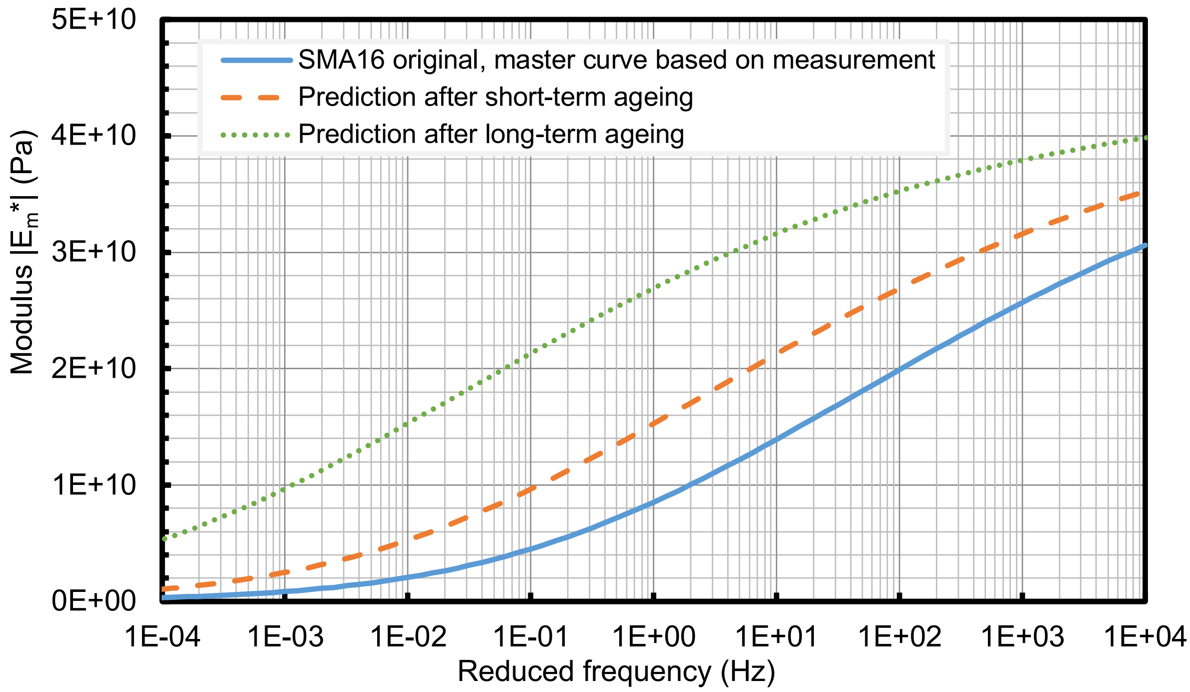

Figure C-4. IDT dynamic modulus master curves by shift factor due to ageing for asphalt mixture SMA16, T_{ref}=10 °C.

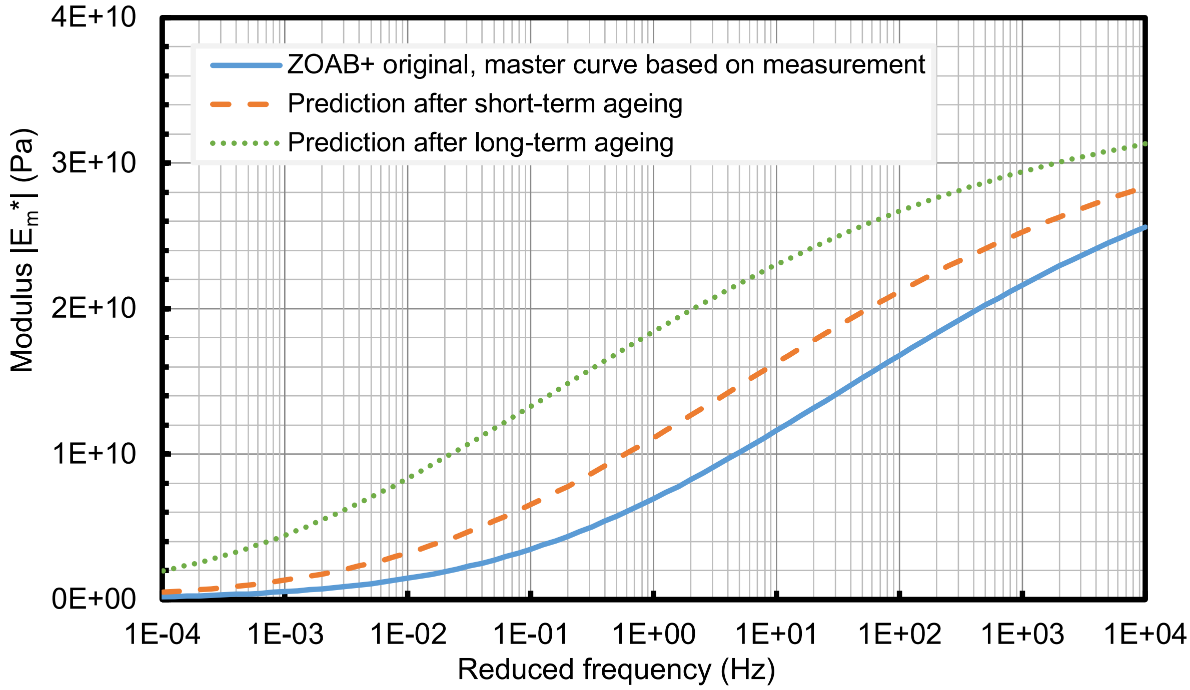

Figure C-5. IDT dynamic modulus master curves by shift factor due to ageing for asphalt mixture ZOAB+, T_{ref}=10 °C.

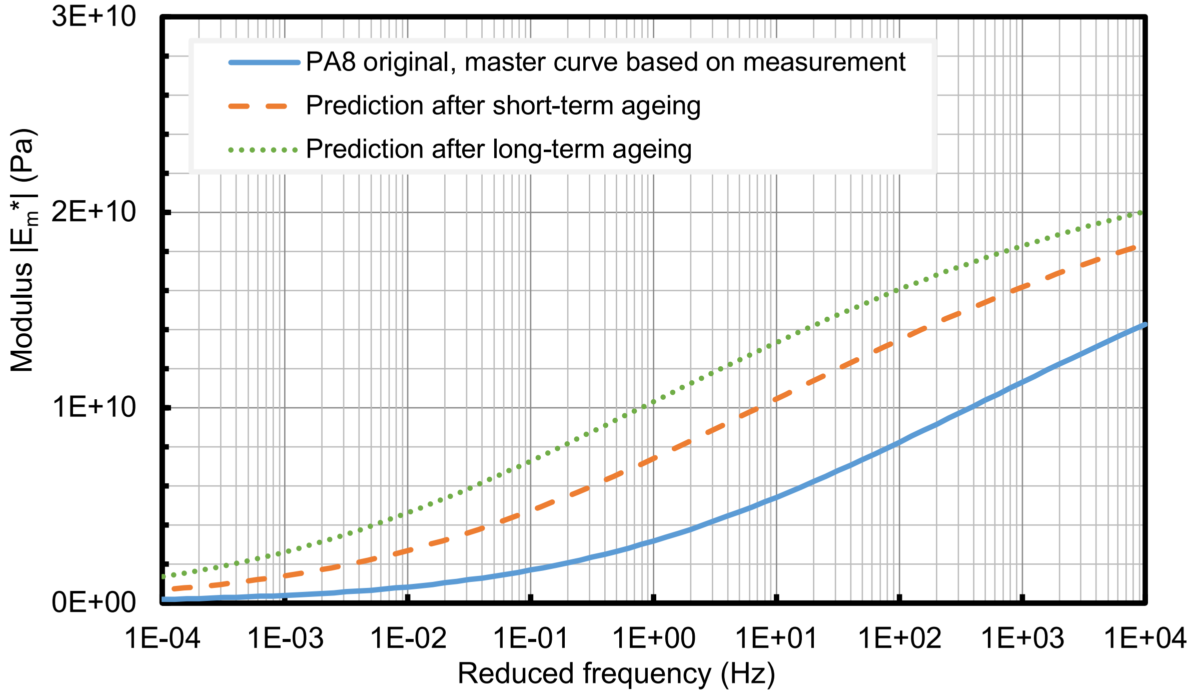

Figure C-6. IDT dynamic modulus master curves by shift factor due to ageing for asphalt mixture PA8, T_{ref}=10 °C.

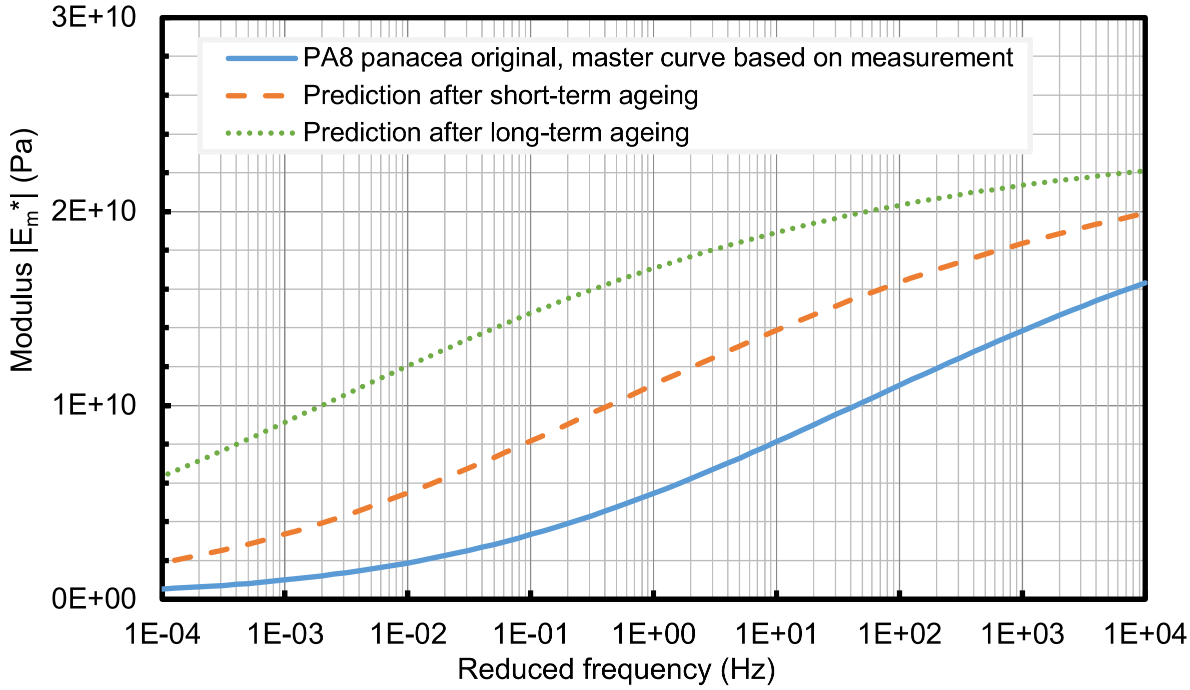

Figure C-7. IDT dynamic modulus master curves by shift factor due to ageing for asphalt mixture PA8 panacea, T_{ref}=10 °C.

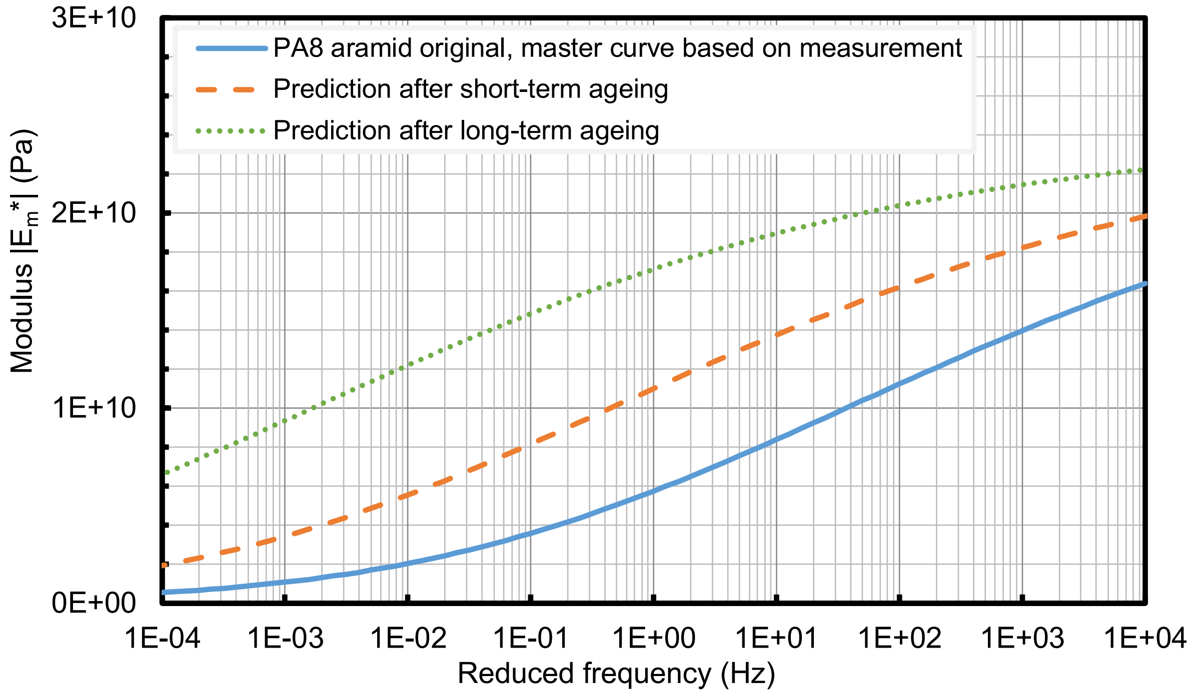

Figure C-8. IDT dynamic modulus master curves by shift factor due to ageing for asphalt mixture PA8 aramid, T_{ref}=10 °C.

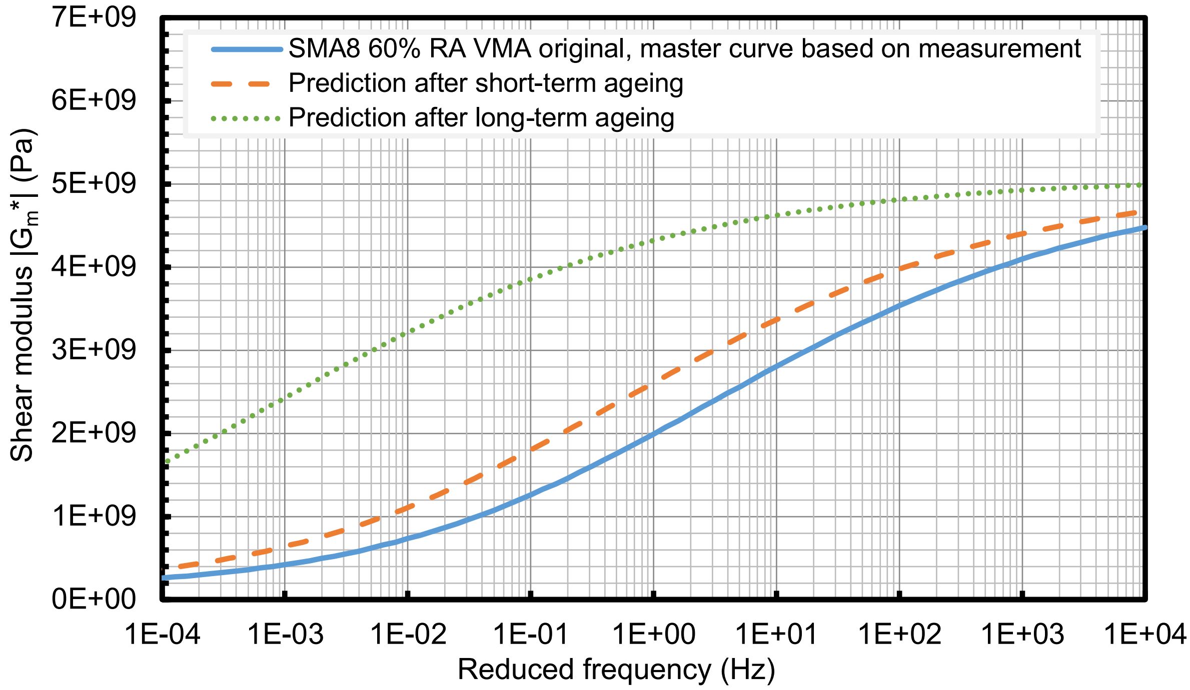

Figure C-9. Shear modulus master curves by shift factor due to ageing for asphalt mixture SMA8 60% RA VMA, T_{ref}=10 °C.

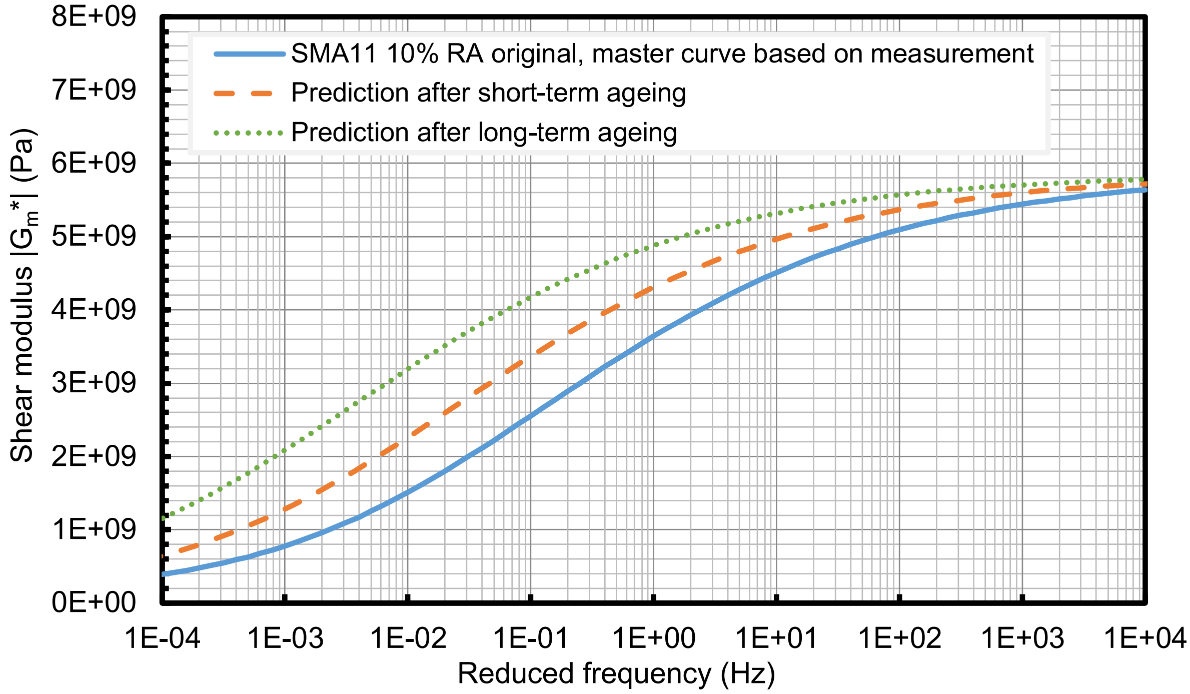

Figure C-10. Shear modulus master curves by shift factor due to ageing for asphalt mixture SMA11 10% RA, T_{ref}=10 °C.

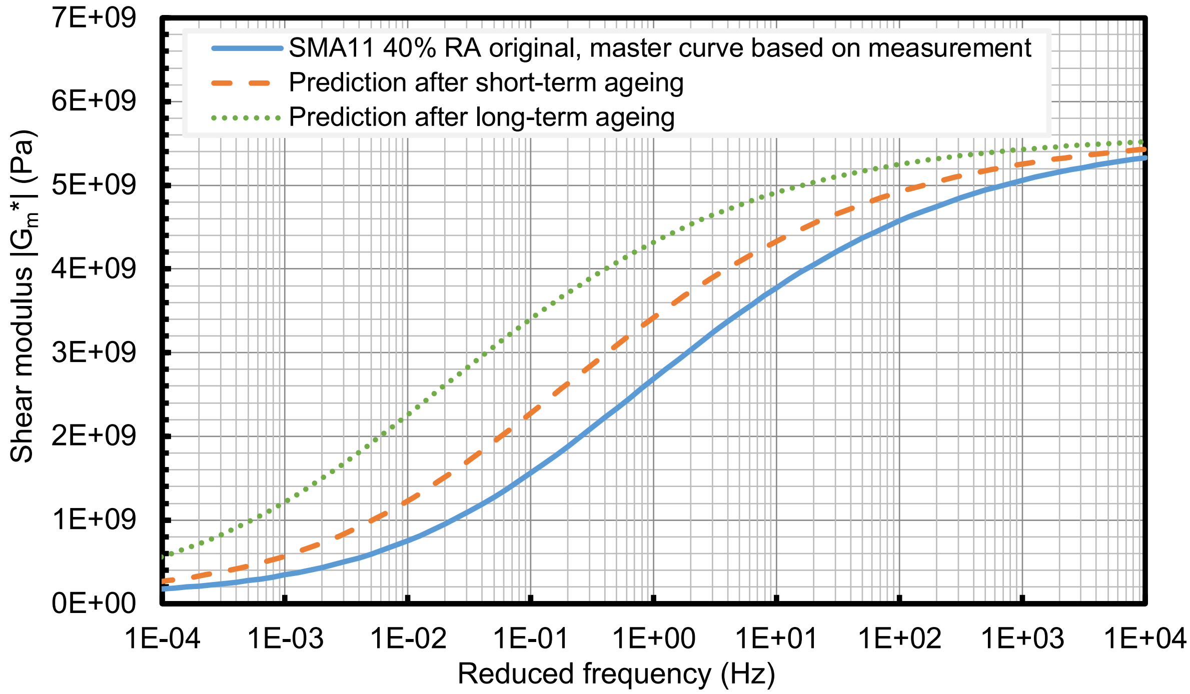

Figure C-11. Shear modulus master curves by shift factor due to ageing for asphalt mixture SMA11 40% RA, T_{ref}=10 °C.

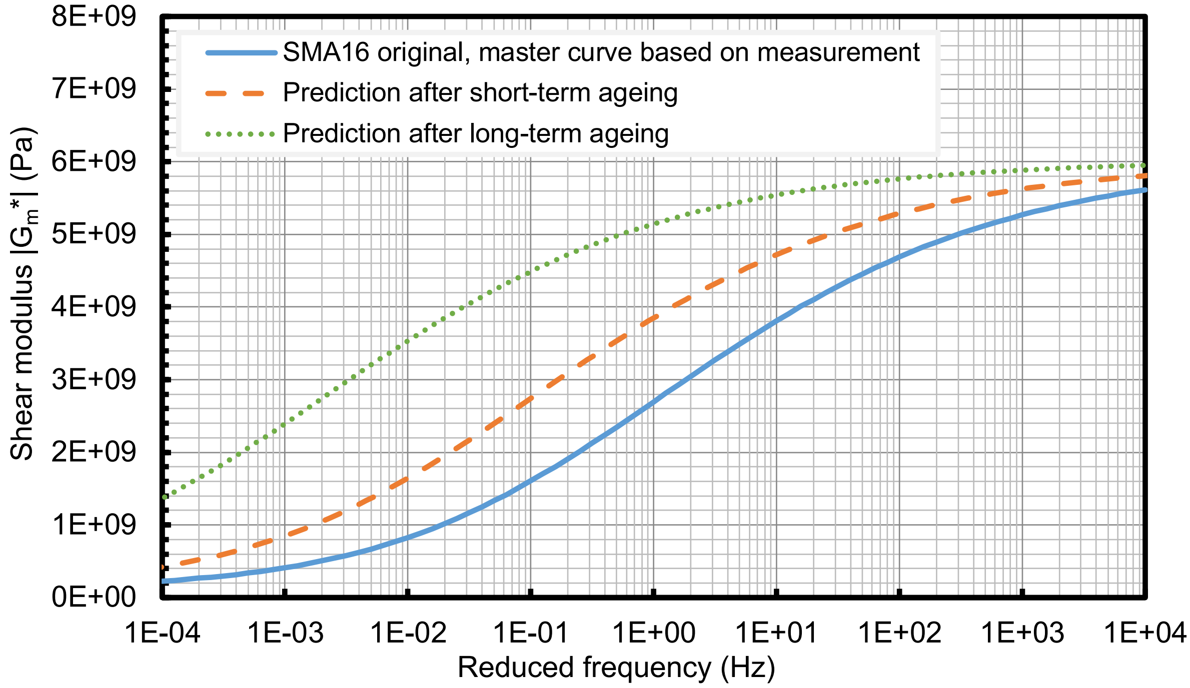

Figure C-12. Shear modulus master curves by shift factor due to ageing for asphalt mixture SMA16, T_{ref}=10 °C.

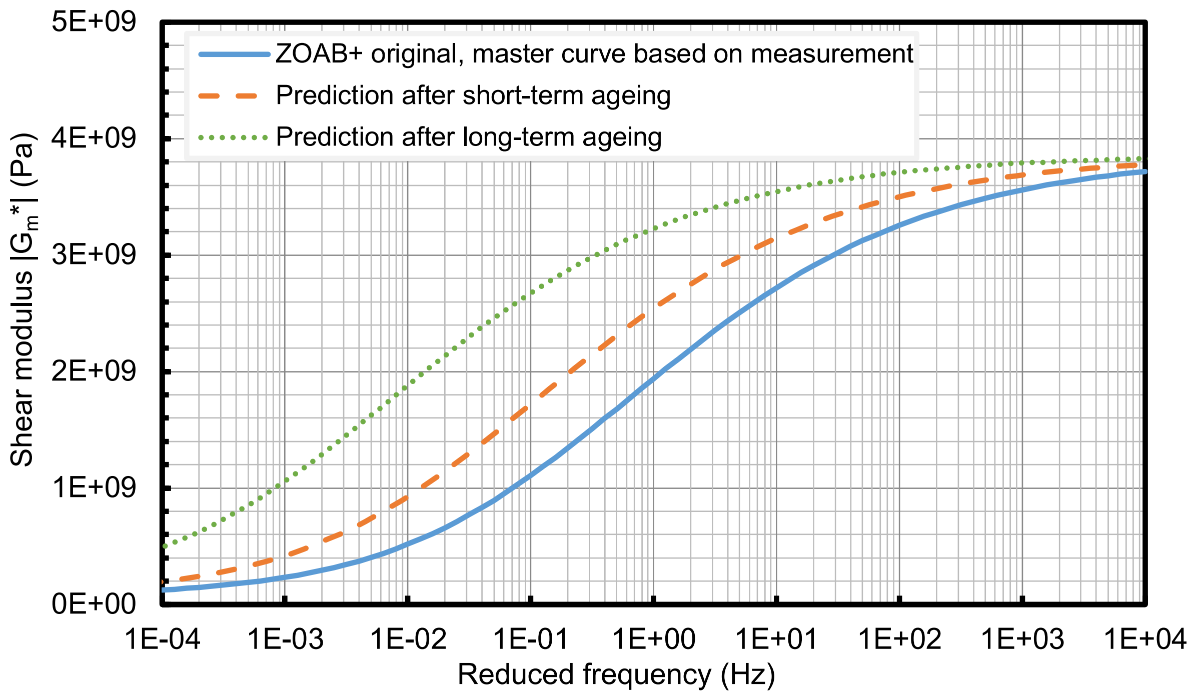

Figure C-13. Shear modulus master curves by shift factor due to ageing for asphalt mixture ZOAB+, T_{ref}=10 °C.

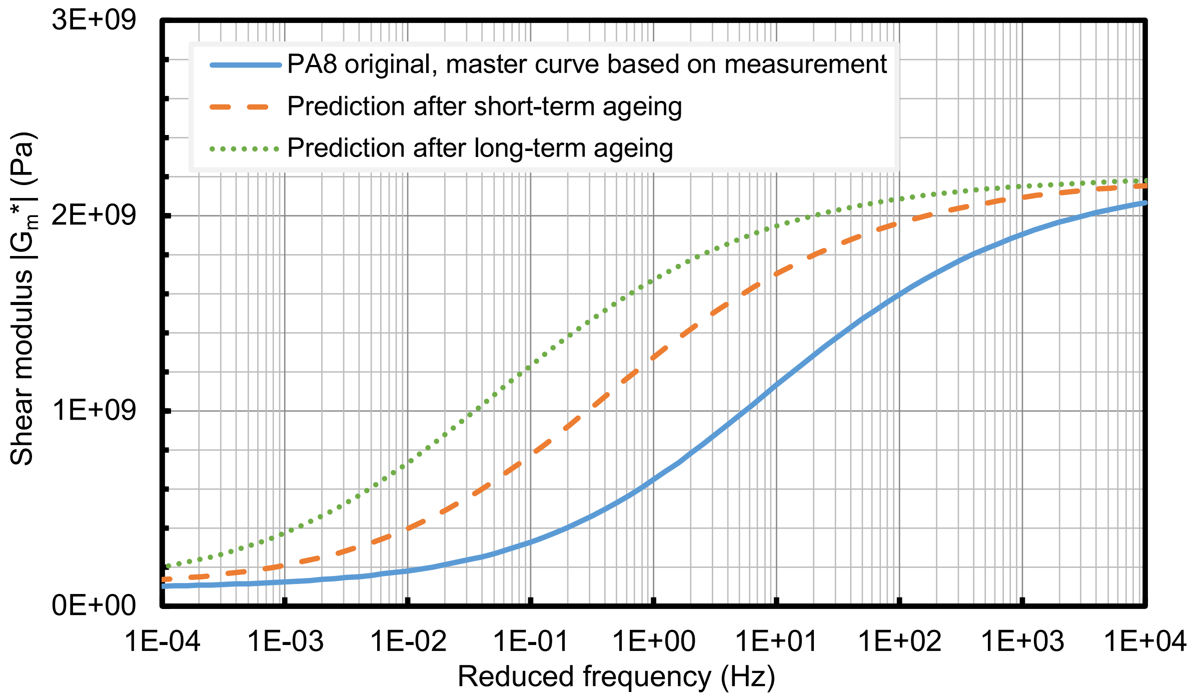

Figure C-14. Shear modulus master curves by shift factor due to ageing for asphalt mixture PA8, T_{ref}=10 °C.

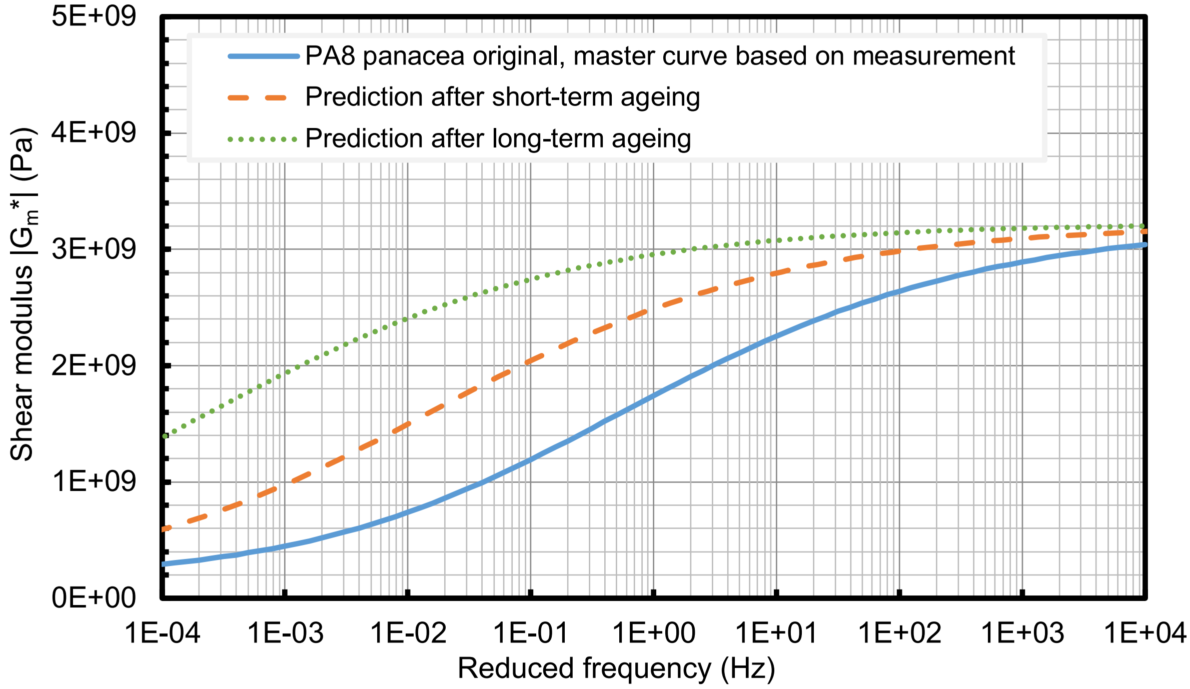

Figure C-15. Shear modulus master curves by shift factor due to ageing for asphalt mixture PA8 panacea, T_{ref}=10 °C.

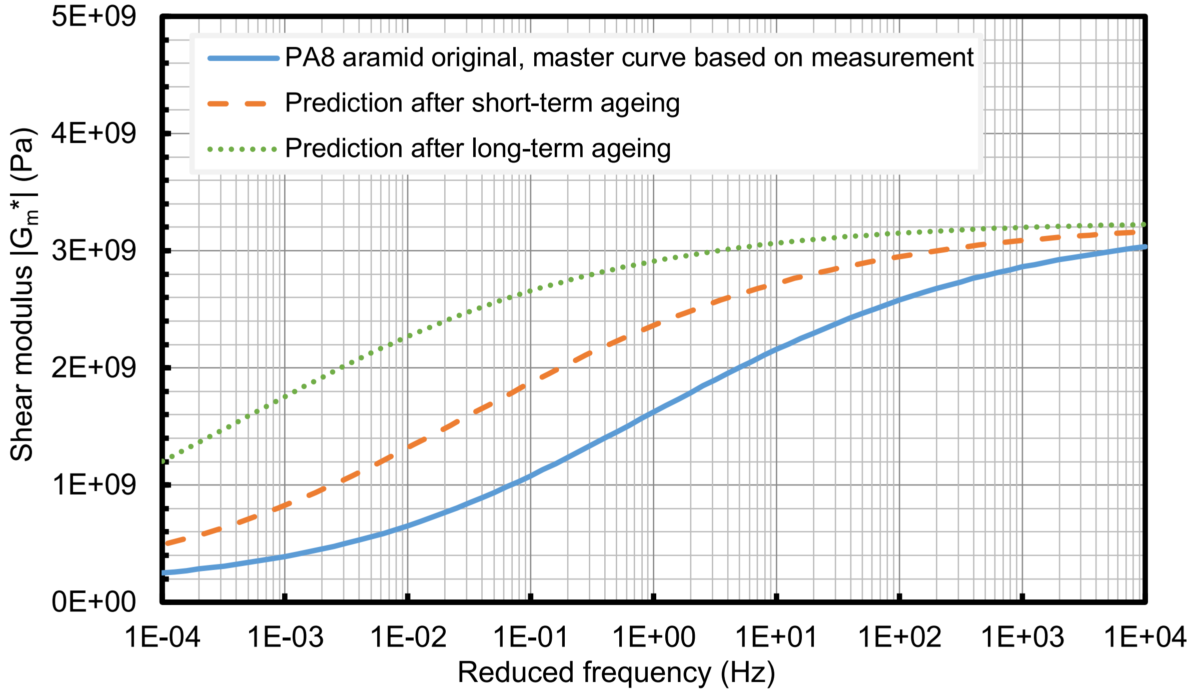

Figure C-16. Shear modulus master curves by shift factor due to ageing for asphalt mixture PA8 aramid, T_{ref}=10 °C.